AGEING ASTROCYTES

IMPLICATIONS FOR MOTONEURON DYSFUNCTION AND SARCOPENIA

Caitlin J. Arpel

Supervisor: Philip W. Sheard

A thesis submitted in fulfilment of the requirements for the degree Bachelor of Biomedical Sciences

Department of Physiology, Otago School of Biomedical Sciences, University of Otago, Dunedin, New Zealand

Acknowledgements

I would like to express my dearest gratitude to my supervisor, Dr. Phil Sheard. This year has been the most rewarding year of my academic life, and I can attribute that to Phil. Phil's kindness, guidance and support have been invaluable, and it has truly been a pleasure to work with him. Phil, I cannot thank you enough for your encouragement in all I have done this year, and also in my future endeavours. I can only hope to have gained some of the qualities which make you the great mentor you are.

To my lab mates, Ash and Nav; thank you for your constant lab banter, laughs and trips for 'shoffee'. Working with you has been a pleasure, and this year would not have been the same without you. Thank you for being patient with me, and always offering advice and help when I needed it. I consider you both dear friends and wish you both the best in your careers. I look forward to seeing you both do great things! To Katherine; thank you for your words of wisdom and advice, and keeping me grounded during some trying times this year.

Charlotte; I feel lucky to have completed this year with you, thanks for being my partner in crime - there really is no one I would rather be in the lab all night with!

Karlena; Thanks for the lunch time chats and always being ready with a smile and a heeeelloo - always made my day.

To my family, in particular my mother, Tracy; you have undoubtedly been my greatest supporter, and I wouldn't be where I am today without you. Thank you for always showing an interest in what I do, and reminding me how capable I am. I love you dearly.

A special thank you to my partner, Lewis; your support has been unwavering and your patience, admirable. This year has been challenging and very much rewarding, and you have stood by me through every second; I love you for it.

To the Department of Physiology and honours class of 2017, thank you to all the smiling faces who have been so welcoming this year, and those who have taken time to help me with my project. You have all played a small part in making this year a memorable one!

Abstract

Sarcopenia: The most conspicuous intractable feature of advancing age is the gradual loss of skeletal muscle mass and the resultant loss of strength and mobility, and this is a major driver of morbidity and mortality in our ageing population. Loss of muscle is accompanied by loss of motoneurons, however what causes the death of motoneurons with advancing age remains unknown. Astrocytes are the most numerous and diverse cell type in the central nervous system, and play a critical role in neuronal support. Recent research has revealed that *in-vitro,* ageing astrocytes become senescent and express a senescence-associated secretory phenotype (SASP) that confers a reduced neuroprotective capacity. However, culturing senescent astrocytes in Glial-Derived Neurotrophic Factor (GDNF), a trophic factor critical for survival and proliferation of neurons, reversed these effects. Whether any similar changes occur *in vivo* is unknown, which provides a need for further investigation.

This study aimed to investigate whether astrocytes in ageing mouse spinal cord become senescent, and whether the senescence phenotype can be reversed or attenuated by exercise - a known stimulus of GDNF production. The second aim was to investigate whether GDNF levels in the lumbar spinal cord reduce with age, and whether any decline is reversed by exercise. To inform the aims of this experiment, Semi-Quantitative Immunohistochemistry (SQI) was performed on sections of spinal cord from young, elderly, and elderly exercised mice. The levels of three proteins of interest were measured: Glial-Fibrillary Acidic Protein (GFAP) an intermediate filament protein and marker of astrogliosis; p16, a marker of senescence; and the trophic factor GDNF.

Here we report that levels of GFAP within astrocytes of the lumbar lateral motor column showed a trend of increasing with age, although this was not statistically significant ($p=0.052$). Exercise had no effect on GFAP levels. P16-positive cell nuclei were observed in sections of both elderly sedentary and elderly exercised, but these did not co-localise with GFAP

immunostaining of astrocytes. Instead, p16-positive nuclei appeared to be that of motoneurons, a novel finding. GDNF levels showed no change with age, but were increased significantly in exercised animals compared to sedentary ($p<0.0001$), indicating that exercise exerts neuroprotective effects by skeletal muscle-derived GDNF production.

These results indicate that astrocytes become reactive with age and as a result may show reduced neuroprotection of motoneurons, contributing to their demise associated with ageing and sarcopenia. Although exercise increased GDNF levels within spinal motoneurons, this did not correlate with a reduction in astrocyte reactivity or a reduction in the presence of p16-positive nuclei as hypothesized. Instead, GDNF may exert protective effects for motoneurons directly, attenuating their age-associated decline, and slowing the progression of sarcopenia.

Table of Contents

Figures

Tables

Terms & Abbreviations

1. ABTS

2,2'-azino-bis(3-ethylbenzothiazoline-6-sulphonic acid) 31

2. AD

Alzheimer's Disease 24

3. ALS

Amyotrophic Lateral sclerosis 24

4. ATM

Ataxia telangiectasia mutated 19

5. BDNF

Brain-Derived Neurotrophic Factor 31

6. BSA

Bovine Serum Albumin 46

7. CNS

Central nervous system 18

8. **DAPI**

4’,6-diamidino-2-phelylindole 101

9. DDR

DNA Damage Response 19

10. dH_2O

Distilled water 47

11. E2F

E2 Factor 81

12. ECL

Enhanced Chemiluminescence 49

13. ELISA

Enzyme Linked Immunosorbent Assay 31

14. FOXO4

Forkhead box protein O4 21

15. GDNF

Glial Derived Neurotrophic factor 17

16. GFAP

Glial Fibrillary Acidic Protein 23

17. GFR-alpha

GDNF Family Receptor Alpha 29

18. GLAST

glutamate-aspartate transporter 24

19. H_2O_2

Hydrogen peroxide 22

Hydrogen Peroxide 22

20. HDAC

Histone deacetylases 19

21. HIER

Heat-Induced Epitope Retrieval 41

22. IGF

Insulin-like Growth Factor 31

23. IHC

Immunohistochemistry 41

24. IL

Interleukin 20

25. LMM

Linear Mixed Model 70

26. NaCl

Sodium Chloride 100

27. NF-kB

Nuclear Factor Kappa-light-chain-enhancer of activated B cells 21

28. NMJ

Neuromuscular junction 17

29. PVDF

Polyvinylidene Difluoride 48

30. Rb

Retinoblastoma 19

31. RET

Rearranged during Transcription 29

32. RGB

Red, Green and Blue 50

33. RIPA

Radioimmunoprecipitation Assay 45

34. ROS

Reactive Oxygen Species 20

35. SASP

Introduction

1 Preface

1.1 The costly burden of ageing

We are fortunate enough to live in a 21st century society which has developed to be free of most diseases that once killed us in our youth. With the eradication of most infectious diseases in developed countries, we are surviving longer into old age, but unfortunately, with ageing comes a range of age-associated chronic conditions which we are yet to fully understand. One of those age-associated conditions is Sarcopenia.

Sarcopenia is defined as the deterioration of strength and mobility resulting from loss of muscle mass with age. In contrast to other diseases and pathological conditions, every person who lives to experience old age will experience the ravages of Sarcopenia, which makes it a high-impact area of research. The ageing population is the only demographic in New Zealand which is growing (Fig. 1). The aged 65+ demographic is continually increasing, and is projected to reach 21–26% by 2043, and 24–33% by 2068 (from 15% in 2016) (National Population Projections., 2016). The average life expectancy for a New Zealander born in 2015 is 90-95 years, and with chronic diseases becoming more prevalent in the aged population, there is an increasing burden on the healthcare system and on society (Janssen *et al.*, 2004; Tanimoto *et al.*, 2014; Dennison *et al.*, 2017).

The steady shift in age distribution in New Zealand is increasing the elderly dependency ratio: the number of dependents (age 65+) compared to the working population (tax payers) (Fig. 1). The projected change in population distribution predicts that by 2036, there will be only 2 tax payers for every person aged 65+ - a significant reduction from 7 in the 60's (National Population Projections., 2016). It is therefore critical to take measures to ensure the ever-increasing ageing population of New Zealand maintain their functional independence; strength, balance and overall vitality for as long as possible.

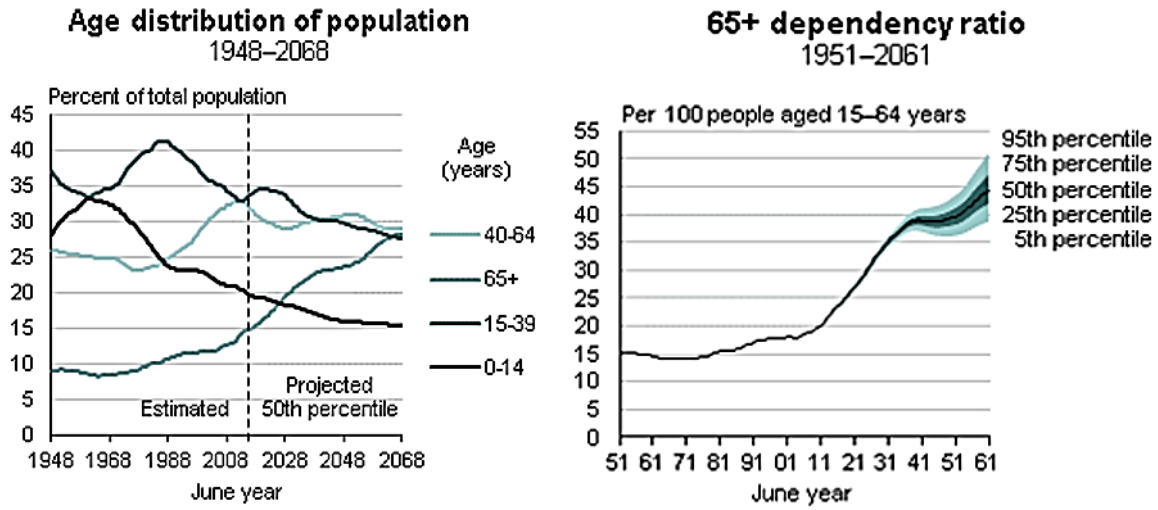

Figure 1: New Zealand population demographics and consequences for the dependency ratio

Left: The changing demographic age groups across time from 1948-2068 (projected). Right: The steadily increasing age dependency ratio: number of individuals aged 65+ per 100 working individuals (aged 15-64) (Statistics New Zealand., 2016)

Muscle deterioration leads to increased frailty and subsequent risk of falls and fractures (Waters *et al.*, 2010; Tanimoto *et al.*, 2014). The increased incidence of falls and fractures is a large contributor to both mortality and morbidity rates among the elderly population (Waters *et al.*, 2010; Tanimoto *et al.*, 2014); Of older people who fracture their hip, 27% will die within a year (Health Quality and Safety Commission New Zealand, 2014). Loss of the ability to live independently as a consequence of muscle weakness is costly not only to the individual who has lost the capacity to perform everyday tasks, but to society as a whole to support these individuals. It was estimated by Janssen et al. in 2004, that the annual cost of healthcare due to sarcopenia was US$18 billion in the United States. This expenditure was incurred by nursing home admission, hospitalisation and home-based health care (Janssen *et al.*, 2004).

Research into the etiology of Sarcopenia is critical to understanding how interventions may be used to attenuate its pathogenesis. Furthering our understanding of the progression of Sarcopenia is necessary not only for improving individual quality of life, but to minimise the economic and societal impacts of the increasing dependency ratio, which will otherwise become a costly burden to following generations.

2 Introduction

2.1 The pathogenesis of sarcopenia

The term sarcopenia (In Greek, 'sarx' meaning flesh and 'penia' meaning loss) was first proposed by Irwin Rosenberg in 1989, but even today, the etiology is not well-understood. (Waters *et al.*, 2010). Sarcopenia is the gradual deterioration of muscle mass with ageing. There are two ways by which muscle mass can be reduced; a decrease in muscle fiber number, or atrophy of individual fibers (Drachman, 1972; Edström *et al.*, 2007) (Fig. 2). These two processes are not independent of one another, but occur simultaneously, resulting in reduced muscle performance, strength and mobility (Aagaard et al., 2010).

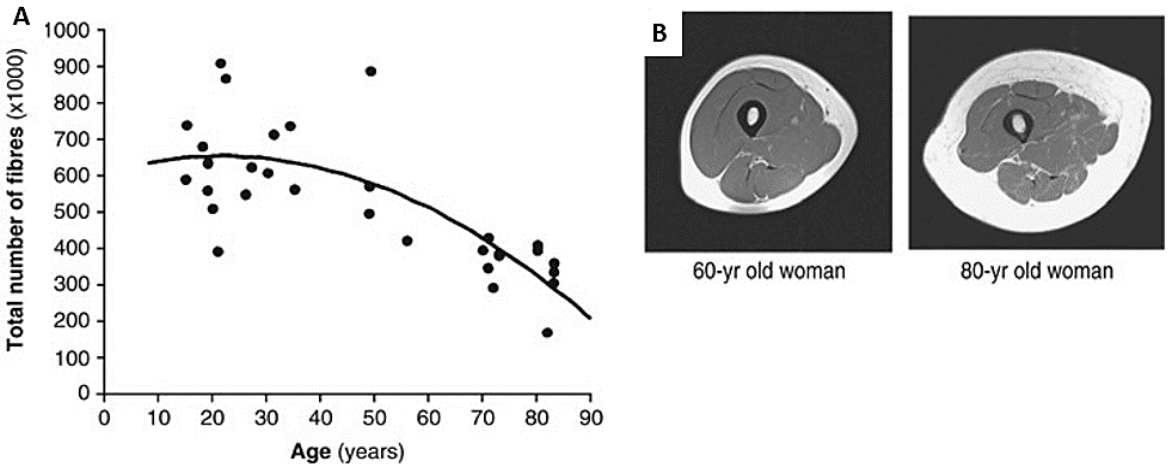

Figure 2: Reduction in muscle fiber number and cross sectional area.
Left: Data from autopsy studies demonstrates the accelerating reduction in muscle fiber number with age (m. quadriceps femoris; data from Lexell *et al.* (1988).Right: Decrease in muscle cross-sectional area (CSA) and infiltration of collagen and fat as a result of ageing (a)(Caserotti *et al.*, 2008). (Aagaard et al., 2010).

There have been various hypotheses proposing a cause of muscle fiber death or atrophy, the predominant being denervation (Rowan *et al.*, 2012). It is well documented that denervation, or retraction of the nerve terminal, induces orphaned muscle fibers to undergo disuse atrophy (Bongers *et al.*, 2013), yet there remains no complete mechanism underpinning this process. Two possible mechanisms for motoneuron terminal retraction (denervation) are the 'top-down' and the 'bottom-up' hypotheses. These hypotheses describe motoneuron dysfunction as a result

of either defects at the cell body causing downstream effects at the neuromuscular junction (NMJ) (top-down), or conversely, loss of trophic support from skeletal muscle at the NMJ may have detrimental consequences to motoneurons in the spinal cord (bottom-up).

Age-associated denervation not only implicates muscle fibers, but has upstream effects at the level of the spinal cord, via loss of skeletal muscle-derived trophic support for motoneurons (McCullough *et al.*, 2013). Glial-Derived Neurotrophic Factor (GDNF) is a trophic factor produced not only by glia, but also by skeletal muscle where it is then transported in a retrograde manner to the cell body of its motoneuron to exert its protective effects (McCullough *et al.*, 2013) (Fig. 3). Motoneurons depend on GDNF for maintenance and repair, therefore both denervation, and the subsequent death of muscle fibers would result in loss of this trophic support, and have detrimental consequences for motoneuron survival. An observed reduction in motoneuron number with age, particularly within the lumbar enlargement, has been documented for both humans and rodents (Tomlinson & Irving, 1977; Rowan *et al.*, 2012). A predominant hypothesis suggests the death of motoneurons to precede denervation, and consequently muscle fiber atrophy (Sacheck *et al.*, 2007; Rowan *et al.*, 2012). Taking a further step back, the question remains; what is it about ageing that causes motoneurons to die?

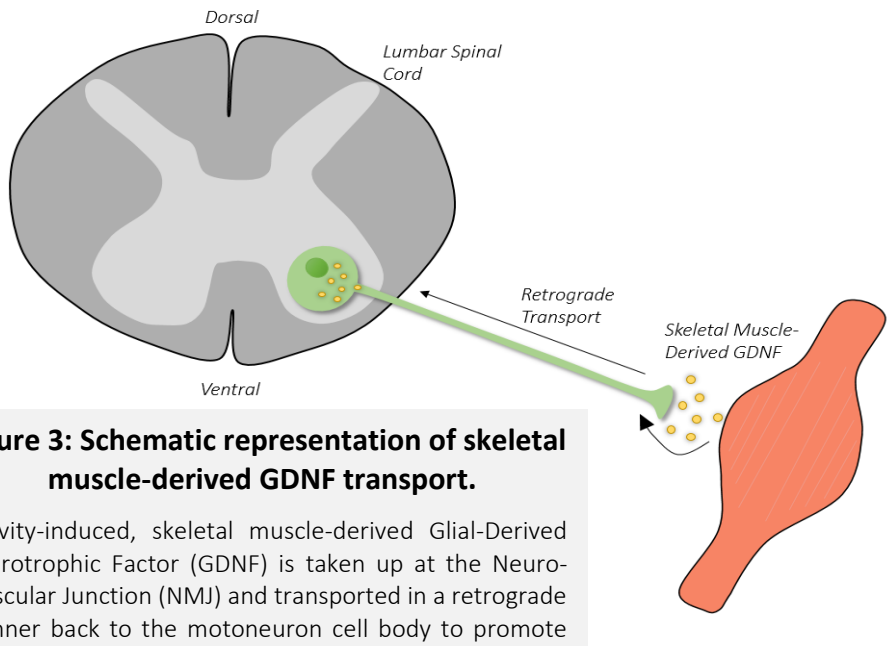

Figure 3: Schematic representation of skeletal muscle-derived GDNF transport.

Activity-induced, skeletal muscle-derived Glial-Derived Neurotrophic Factor (GDNF) is taken up at the Neuro-Muscular Junction (NMJ) and transported in a retrograde manner back to the motoneuron cell body to promote

2.2 Inflamm-ageing: Age-associated deterioration of the CNS

Ageing is the primary risk factor for a large majority of chronic diseases, yet the mechanisms which drive the ageing process are not well-understood. Our fundamental lack of understanding limits the development of interventions for age-associated diseases such as sarcopenia (Baker *et al.*, 2011). Age is associated with multifactorial changes in the metabolic and inflammatory status of the central nervous system (CNS) (Liu *et al.*, 2012). Reduced basal metabolic rate, chronic low level inflammation characterized by increased circulating cytokines, and oxidative stress (quantified by superoxide production, protein oxidation and lipoperoxidation) are all hallmarks of ageing (Salminen *et al.*, 2011). A combination of the metabolic and inflammatory changes occurring as a result of age may contribute to the complex pathogenesis of Sarcopenia.

It is becoming evident that chronic, low-level inflammation plays a particularly critical role in the dysfunction of the neuromuscular system with age (Cruz-Jentoft *et al.*, 2010; Liu *et al.*, 2012), but what is it about ageing that drives these alterations in the cellular microenvironment? A characteristic of ageing tissues is the accumulation of senescent cells, which are thought to contribute to the chronic inflammatory environment observed within these tissues and systems (Sasaki *et al.*, 2014; Childs *et al.*, 2015). Further investigation of these cells eludes to a cell-autonomous theory of ageing and age-associated inflammation.

2.2.1 Senescence: A cell autonomous theory of ageing

Replicative senescence was unheard of prior to 1961, when Hayflick and Moorehead observed that human fibroblasts did not replicate indefinitely in culture (Hayflick & Moorhead, 1961). They discovered that human fibroblasts in culture underwent a finite number of divisions before a state of senescence was reached. The term senescence has since been broadened to describe states of proliferative arrest induced by various stressors (Sharpless & Sherr, 2015). Senescent cells remain metabolically active whilst being held in an extremely stable form of cell-cycle arrest (Narita *et al.*, 2003). The discovery of replicative senescence overturned the previous

understanding that cells in culture could replicate infinitely, provided they were cultured with sufficient growth media. This discovery prompted speculation of a potential link between senescence and the ageing process - suggesting a 'cell-autonomous theory of ageing' (Childs *et al.*, 2015).

As cellular stresses accumulate during ageing, various signalling cascades are triggered, some of which drive cells into a state of senescence (Salminen *et al.*, 2011). Senescence is an in-built anti-tumour mechanism to prevent the proliferative expansion of damaged cells leading to tumour formation (Mombach *et al.*, 2015). There are a number of cumulative and acute cellular stresses which can drive cells to cease division and become senescent, including telomere erosion, oxidative stress such as lipoperoxidation, proteotoxic stress - for example β-amyloid protein aggregates - and oncogene activation (Kuilman *et al.*, 2008; Bhat *et al.*, 2012).

Replicative senescence is thought to be induced by progressive telomere erosion (Hewitt *et al.*, 2012). Telomere erosion is a process which occurs progressively with age; with each mitotic division a fragment of DNA is lost from the extreme ends of the chromosomes (Narita *et al.*, 2003). Over time, this telomere erosion becomes significant enough to initiate a permanent DNA Damage Response (DDR) which directs the cell toward a fate of senescence (Hewitt *et al.*, 2012; Olivieri *et al.*, 2015). Following this initiation, damage sensor ataxia telangiectasia mutated (ATM) is recruited to the site of erosion and stabilizes the tumour suppressor p53, which upregulates p21 (Childs *et al.*, 2015). It is the cyclin-dependent kinase inhibitors p21 and p16 which then inhibit CDK2/4/6 and in turn, disinhibit Retinoblastoma (Rb) activity on E2F target genes which are essential for cell cycle progression (Narita *et al.*, 2003). The Rb family of proteins recruit histone deacetylases (HDACs) which ultimately repress gene expression at their site of action (Narita *et al.*, 2003). This cascade of events results in cells which are irreversibly halted in the G1 phase of the cell cycle (Ohanna *et al.*, 2011; Demaria *et al.*, 2014) (Fig. 4).

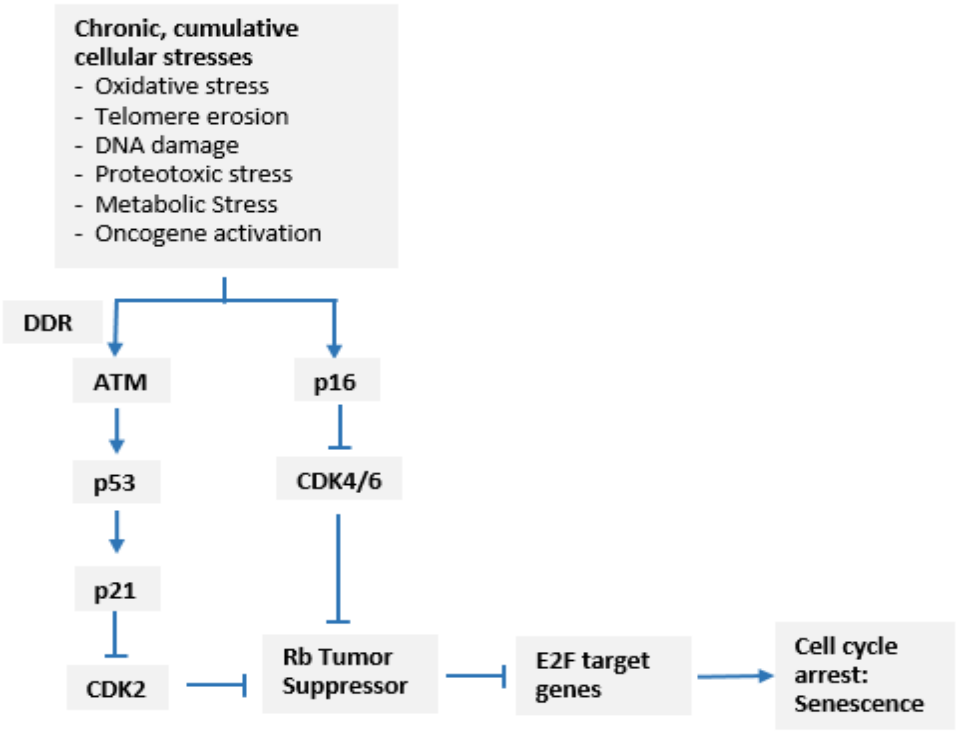

Figure 4: The cascade of events leading to cell cycle arrest.

Cumulative stresses activate p16 and the DNA-Damage Response (DDR) which then recruits Ataxia-Telangiectasia Mutated (ATM) and p53 is stabilised. P16 is also directly upregulated following cellular stresses and with p21, acts to inhibit cyclin-dependent kinase activity. Rb is disinhibited and can then inhibit E2F target genes, leading to permanent cell cycle arrest (Ohanna *et al.*, 2011).

2.2.2 Senescence Associated Secretory Phenotype

Senescent cells express a chronic inflammatory phenotype which was first described by Judith Campisi as the Senescence Associated Secretory Phenotype (SASP) (Krtolica & Campisi, 2002). Markers of the SASP include increased senescence-associated (SA)-β-galactosidase activity and upregulated p53, p16 and p21 (discussed above) (Bitto et al., 2010). As well as intrinsic markers of cell cycle arrest, senescent cells actively secrete a series of pro-inflammatory cytokines such a TNFα, interleukins such as IL-6, IL-8 and IL-15, matrix metalloproteinases (MMPs), reactive oxygen species (ROS) and growth factors (Demaria *et al.*, 2014; Das & Svendsen, 2015). It is these factors which generate the chronically damaging microenvironment within ageing tissues.

The SASP is induced via a separate pathway to cell-cycle arrest. The transcription factors NF-kB and C/EBPβ are involved in producing this inflammatory secretory phenotype, with C/EBPβ

being essential for the production of interleukins such as IL-8 (Olivieri *et al.*, 2015). The secretion of such factors exerts paracrine effects to induce senescence in neighbouring cells, resulting in an inflammatory microenvironment within whole tissues (Salminen *et al.*, 2012; Olivieri *et al.*, 2015). The SASP has an important short-term role for wound healing which was demonstrated by generating a p21 and p16 double knockout mouse (Demaria *et al.*, 2014). The knockout mouse showed significantly delayed cutaneous wound closure following a dorsal skin puncture, demonstrating a transient role of for the SASP in tissue repair following injury (Demaria *et al.*, 2014). Despite this transient role, the chronic nature of the inflammatory environment generated by senescent cells with ageing is damaging to surrounding cells and tissues over a long period of time (Salminen *et al.*, 2011; Das & Svendsen, 2015).

2.2.3 The SASP as a therapeutic target

A hallmark of ageing is the accumulation of senescent cells, and the nature of their inflammatory phenotype is implicated in various age-associated diseases (Das & Svendsen, 2015). Due to the damaging nature of the SASP, it is an attractive target for delaying the progression of these age-associated diseases and overall tissue degeneration. Therapeutic targeting of the NF-kB and C/EBPβ pathways has shown promising results in reversing senescence-induced changes in cell morphology and the SASP (Walters *et al.*, 2016).

The complete removal of p16-positive senescent cells in late-life attenuated the progression of various age-associated disorders including sarcopenia (measured by lordokyphosis and muscle diameter) (Baker *et al.*, 2011), suggesting a role for cellular senescence in the pathogenesis of sarcopenia. The therapeutic benefit of removal of senescent cells was also demonstrated in a study which used a Forkhead box protein O4 (FOXO4) peptide to competitively inhibit FOXO4 activity on p53. Inhibition of FOXO4 induced apoptosis of senescent cells, effectively restoring renal function, fitness and fur density in aged mice (Baar *et al.*). These findings outline the detrimental effects of the SASP, and its potential as a therapeutic target to restore homeostasis in aged tissues.

There is strong evidence that senescence is a potential therapeutic target to reverse the effects of cellular ageing. To relate these findings to sarcopenic etiology, we must determine which cells involved in the chain of command for motor function are affected by senescence. Motoneurons and muscle fibers are the most obvious candidates for understanding degeneration of motor function. Nonetheless, by taking a step back one can acknowledge that these cells do not function in isolation, but rely on various other support cells for maintenance, repair and general function. It is these support cells which must be investigated to put together the story of Sarcopenia and neuromuscular ageing.

2.3 Astrocytes are critical support cells

Astrocytes are the most numerous cell in the CNS and have several roles in maintaining neuronal homeostasis (Bitto *et al.*, 2010; Rodríguez-Arellano *et al.*, 2016) These include processing excess neurotransmitter via tripartite synapses (synapses between neurons which can be modulated by astrocyte-neuron interaction), ion homeostasis, inflammatory defence, antioxidant response and establishment of the blood-brain barrier (Bellaver *et al.*, 2017) (Fig. 5). Their broad functionality can partly be attributed to their cytoskeletal organization, abundant in Glial-Fibrillary Acidic Protein (GFAP), an intermediate filament protein specific to astrocytes (Nakagawa & Schwartz, 2004; Souza *et al.*, 2015). Astrocytes are characterized by highly ramified processes which extend out to interact with vasculature, neurons and neighbouring astrocytes simultaneously (Bushong *et al.*, 2004) (Fig. 5). Due to the diverse nature of the role of astrocytes, their demise is implicated in various pathological diseases and disorders of the CNS and potentially Sarcopenia.

2.3.1 Astrocyte senescence and neuroinflammation

The senescent state and resulting SASP of astrocytes was defined in a study which exposed astrocytic cultures to sub-lethal hydrogen peroxide (H_2O_2) concentrations and analysed resulting changes in the transcriptome (Crowe *et al.*, 2016). Astrocytes are particularly sensitive

to low levels of H_2O_2, making them more susceptible to the cellular stresses that accumulate with age (Mombach *et al.*, 2015). Senescent astrocytes express a characteristic SASP, as well as an enlarged morphology due to actin reorganization, and increased Glial Fibrillary Acidic Protein (GFAP) a well-known marker of astrogliosis and astrocyte reactivity (Salminen et al., 2011).

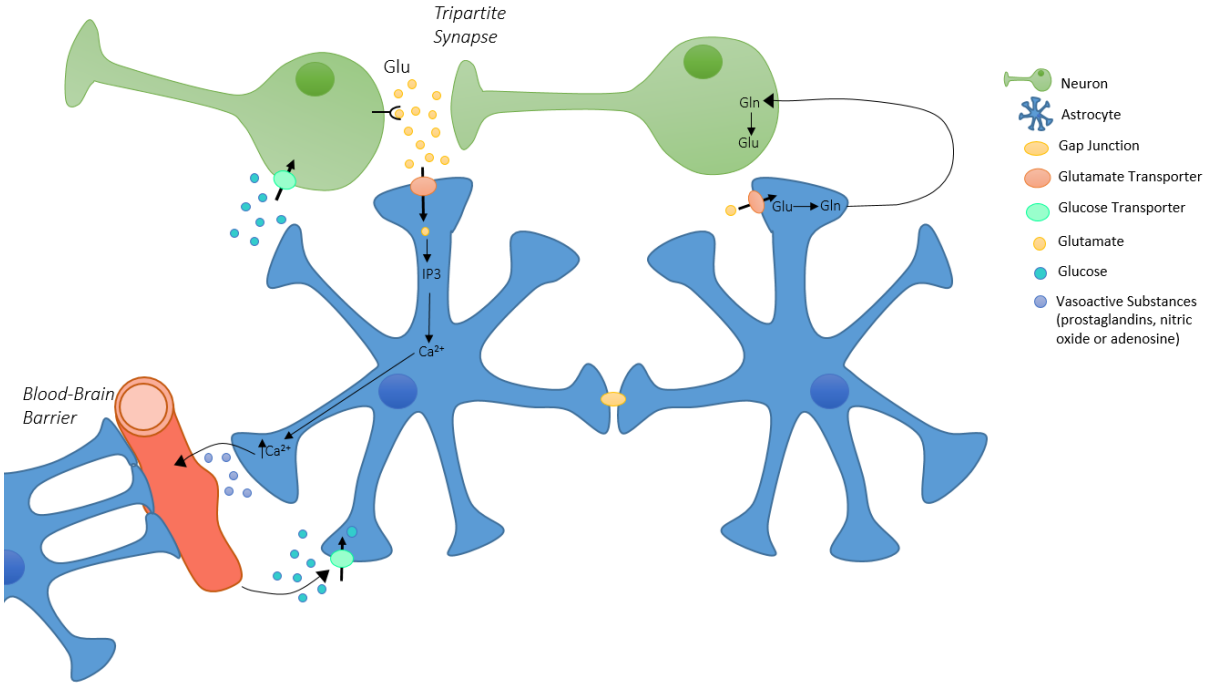

Figure 5: Schematic of astrocytic roles and interactions in the central nervous system.

Schematic shows astrocytes taking part in tripartite synapses, interacting with blood vessels to maintain the blood brain barrier, processing metabolites and releasing vasoactive substances into the blood. Figure adapted from (Maragakis & Rothstein, 2006).(Glu = Glutamate).

The literature regarding astrocytes and the SASP is largely based on diseases of the brain, such as Alzheimer's and Parkinson's diseases, where their secretory phenotype is shown to contribute to the pro-inflammatory status observed (Mombach *et al.*, 2015). The presence of β-amyloid protein aggregates triggers the senescent pathway in astrocytes, and results in increased IL-6 production - a characteristic of the SASP (Bhat *et al.*, 2012). This secretory phenotype is what gave Alzheimer's Disease its term 'inflamm-aging' disease - resulting from ageing with associated inflammation (Mombach *et al.*, 2015). The disease state of Alzheimer's implicates

the significant role of astrocytes in maintaining the microenvironment of the CNS, and the consequences when this role is disrupted (Rodríguez-Arellano *et al.*, 2016).

A study investigating the changes in astrocytic markers in an AD rodent model saw a reduction in GLAST (glutamate-aspartate transporter) immunoreactivity and Glutamine Synthetase (Bitto *et al.*, 2010). There was also a significant increase in the presence of ROS, RNA oxidation and an age-dependent reduction in Superoxide Dismutase activity (Bellaver *et al.*, 2017). All these features indicate an overall reduced ability of astrocytes to process neurotransmitter and reactive oxygen species (ROS) in the diseased and senescent state. These findings reiterate the diversity in astrocytic function within the CNS, and thus the complex, multifactorial pathology associated with astrocytic dysfunction.

A large proportion of studies which address the role of astrocytes in the spinal cord direct their focus on motoneuron diseases such as Amyotrophic Lateral Sclerosis (ALS) and Spinal Muscular Atrophy (SMA) (Das & Svendsen, 2015; Zhou *et al.*, 2016). ALS is of particular interest in relation to sarcopenia, as it is associated with an accelerated ageing phenotype characterised by the accelerated loss of spinal motoneurons (Pirooznia *et al.*, 2014).

2.3.2 Astrocytes play a role in motoneuron dysfunction: ALS

Astrocytes have been implicated in various neurodegenerative disorders via their reduced neuroprotective capacity in the senescent state, one of which is ALS (Bitto *et al.*, 2010).

ALS is characterized by exaggerated levels of oxidative stress - a hallmark of normal ageing (Das & Svendsen, 2015). Twenty percent of familial ALS cases are characterized by a mutation in the SOD1 enzyme, resulting in the rapid progressive loss of both upper and lower motoneurons, followed by muscle atrophy and paralysis (Das & Svendsen, 2015). SOD1 is responsible for processing and destroying superoxide free radicals in neurons, therefore the mutation results in detrimental levels of oxidative stress. Wild-type astrocytes, due to their antioxidant capability, show a protective effect on SOD1 mutant motoneurons in the lumbar

spinal cords of mice (Das & Svendsen, 2015). Conversely, SOD1 mutant (150 day-old) and senescent astrocytes (300 day old) both caused wild-type motoneurons to die (Das & Svendsen, 2015). This study, published in 2015, is one of the first to demonstrate a link between senescent astrocytes and their reduced neuroprotective capacity for motoneurons. No study has yet explored the effects of ageing alone on astrocyte neuroprotective capability, and the mechanism by which senescence impairs their homeostatic role in health or disease remains unknown (Das & Svendsen, 2015).

As previously discussed, ageing is associated with increased cellular stress (oxidative and metabolic stress) (Salminen *et al.*, 2011). It is the multifactorial stresses of ageing that drive cells into a state of senescence (Fig. 6). Astrocytes are of particular interest with regard to the SASP, as they are sensitive to low levels of free radicals due to their high metabolic rate and oxygen consumption (Crowe *et al.*, 2016). This makes them susceptible to the ravages of ageing, and thus more likely to enter a state of senescence (García-Matas *et al.*, 2008; Bitto *et al.*, 2010). Although astrocytes have antioxidant defence systems such as glutathione, glutathione transferase and SOD, these defences are compromised with age (García-Matas *et al.*, 2008). Due to the critical functions served by astrocytes in the CNS, disruption of their neuroprotective capacity has multiple implications which must be further investigated in relation to motoneurons, which are dependent on astrocytes for survival.

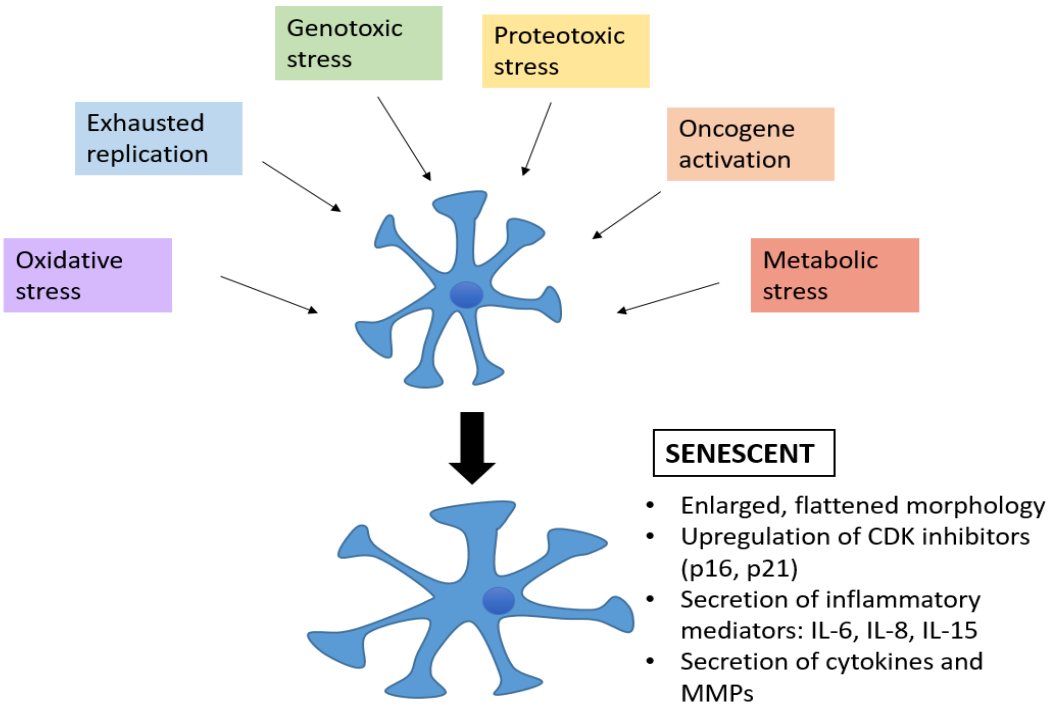

Figure 6: Various triggers of senescence and the resulting senescence phenotype of astrocytes.

Schematic representation showing the various stressors which induce astrocytes to become senescent, and the various markers of cell-cycle arrest and the Senescence-Associated SecretoryPhenotype (SASP).

2.4 Glial-Derived Neurotrophic Factor (GDNF)

2.4.1 Protective role for motoneurons

Trophic factors such as Glial-Derived Neurotrophic Factor (GDNF) are required to enhance survival and proliferation of neurons (Bellaver *et al.*, 2017). GDNF plays an integral role in maintaining the neuromuscular system and promoting neuronal plasticity (Gyorkos *et al.*, 2014). GDNF is produced by both glial cells and skeletal muscle, where it can be taken up at the NMJ and be transported in a retrograde manner to the cell body (Li *et al.*, 2007) (Fig. 3). A continuous supply of neurotrophic factors is essential for the maintenance of mature motoneurons and repair following injury (Gyorkos *et al.*, 2014).

GDNF was first discovered in dopaminergic neurons of the midbrain (Lin *et al.*, 1993), but has since been identified in Schwann cells, skeletal muscle and motoneuron axons and cell bodies

(Gyorkos *et al.*, 2014). GDNF acts on target cells via its receptor GFR-alpha which interacts with RET tyrosine kinase receptors (Gyorkos *et al.*, 2014). GDNF has protective and regenerative roles, therefore an age-dependent reduction within the CNS may contribute to various neuropathological conditions (Li *et al.*, 2007; Bellaver *et al.*, 2017). It has been proposed that a contributing factor to loss of motoneurons with age is a reduction in neurotrophic support from skeletal muscle (McCullough *et al.*, 2013).

GDNF is the most potent neurotrophic factor associated with motoneuron survival (McCullough et al., 2013). Knockout of GDNF protein production or its receptor GFRα1 resulted in a 24-25% loss in lumbar spinal motoneurons and a reduction in ventral root diameter (Gould *et al.*, 2008; McCullough *et al.*, 2013). The role of GDNF has also been established in the motoneuron survival of ALS patients. Exogenous delivery of GDNF, or genetic engineering of neural progenitors to secrete GDNF substantially improved survival of Superoxide Dismutase (SOD1) mutant rats, and showed a protective effect on their motoneurons (Das & Svendsen, 2015). These findings provide an insight into the critical role of GDNF in motoneuron maintenance and survival, and the therapeutic potential for GDNF in the treatment of ALS and the also for motoneuron loss associated with ageing (Das & Svendsen, 2015).

2.4.2 Skeletal muscle vs astrocyte-derived GDNF

There are two sources by which motoneurons receive GDNF; astrocyte-derived and skeletal muscle-derived (Li *et al.*, 2007). Motoneurons have the capacity to transport GDNF in both an anterograde and retrograde directions depending on both the source and site of action required - either the cell body or nerve terminal (Ortega-de San Luis & Pascual, 2016). It is for this reason the neurotrophic factor was considered as a potential therapy for motoneuron diseases such as ALS (Ortega-de San Luis & Pascual, 2016).

Various studies have looked at the two sources of GDNF in the context of motoneuron survival in SOD1-mutant mouse models. One such study cultured astrocytes in medium containing

exogenous GDNF for 7 days. GDNF completely reversed the increase in p21 in aged astrocytes, as well as IL-6 and IL-8, two pro-inflammatory markers of the SASP (Das & Svendsen, 2015). This study also demonstrated that short-term priming of aged astrocytes in GDNF increases their neuroprotective capacity, with motoneurons showing increased survival following culture with GDNF-primed astrocytes (Das & Svendsen, 2015). Whether this effect leads to a reduction in other damaging factors of the SASP or stimulates production of protective factors is yet to be investigated, in both ageing and disease.

While astrocyte-derived GDNF can act directly on the motoneuron cell body, skeletal muscle-derived GDNF is transported along the axon in a retrograde manner to exert its effects at the cell body (McCullough *et al.*, 2013). A study by Liu *et al.* (2012) used a transgenic approach to overexpress GDNF in either skeletal muscle (Myo-GDNF) or in astrocytes (GFAP-GDNF). They measured motoneuron survival, disease-onset, muscle innervation, axonal degeneration and locomotor performance (Liu *et al.*, 2012). In contrast to the previous study, GFAP-GDNF overexpression showed no neuroprotective effects in SOD1-mutant mice, but Myo-GDNF resulted in improvement of all parameters (Li *et al.*, 2007). These findings suggest that skeletal muscle-derived GDNF exerts potent effects on motoneurons as well as acting on astrocytes to increase their neuroprotective capacity, proposing a mechanism for exercise to have neuroprotective benefits.

2.4.3 GDNF can modulate astrocytes

Not only do astrocytes produce endogenous GDNF, but they retain the receptors, GFR-alpha and RET during ageing, therefore maintain the ability to be modulated by GDNF (Das & Svendsen, 2015). This means any detrimental effects of reduced GDNF signalling via astrocytes may be reversible via an exogenous source of GDNF - such as skeletal muscle-derived (Gyorkos *et al.*, 2014) (Fig. 7).

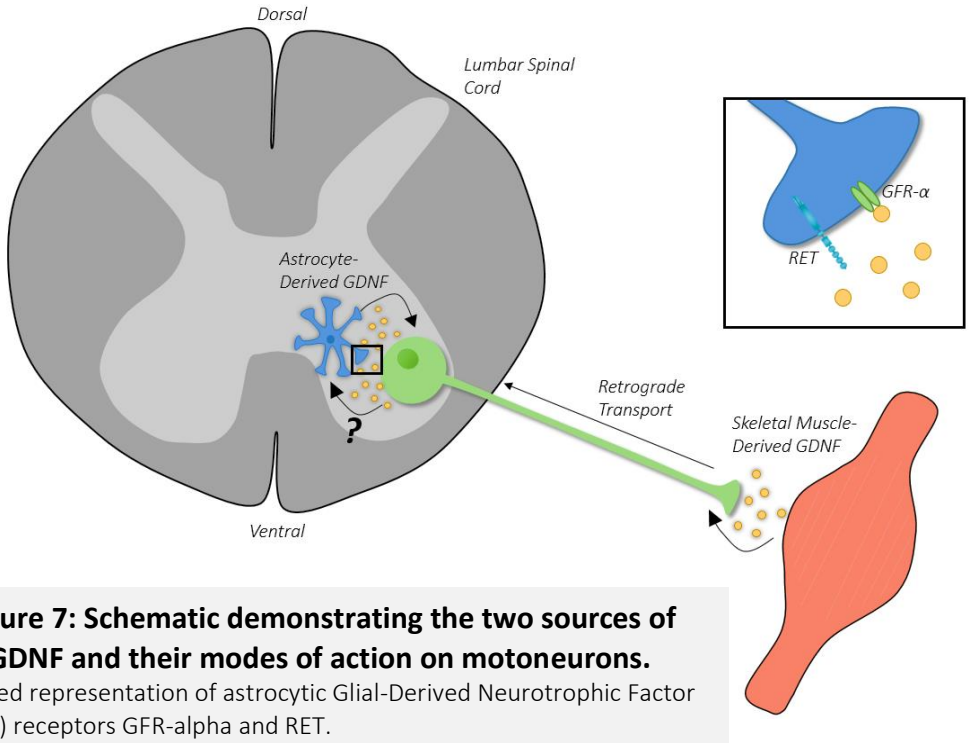

Figure 7: Schematic demonstrating the two sources of GDNF and their modes of action on motoneurons.
Enlarged representation of astrocytic Glial-Derived Neurotrophic Factor (GDNF) receptors GFR-alpha and RET.

GDNF expression is increased in the L1-L3 region of the spinal cord following exercise, and causes axonal branching and a subsequent increase in motor unit size (McCullough *et al.*, 2013). The benefits for increased GDNF within motoneurons are direct, but it remains to be seen whether skeletal muscle-derived GDNF can act on astrocytes via their receptors GFR-alpha and RET, subsequently increasing their neuroprotective ability. Exogenous GDNF was able to reduce the SASP and accordingly, restore the neuroprotective capacity of astrocytes in culture (Das & Svendsen, 2015). These findings support the hypothesis that exercise may have protective effects on astrocytes via activity-dependent, skeletal muscle-derived GDNF, but the mechanism by which this may occur *in vivo* remain unknown.

There is extensive research into the therapeutic benefits of GDNF for neurodegenerative conditions, yet the mode of action on neuronal circuits is poorly characterized (Ortega-de San Luis & Pascual, 2016). How the role of GDNF is impeded with age and whether this disruption is via an indirect mechanism through astrocytes remains unknown. GDNF reduced markers of the SASP in culture (Das & Svendsen, 2015), but it is yet to be investigated whether this occurs

in vivo. It also remains unknown whether exercise plays a role in restoring astrocyte vitality and neuroprotective capacity via GDNF activity, or an alternative mechanism in the spinal cord.

2.5 Exercise as an intervention for neuromuscular deterioration

2.5.1 Exercise reduces the senescence phenotype

Due to the nature of the cellular stresses which induce cellular senescence, it can be hypothesized that premature cellular senescence may be attenuated by reducing metabolic dysfunction. It is well-established that physical activity provides many benefits on the metabolic status of the body and reduces the risk of numerous age-related diseases (Schafer *et al.*, 2016). The molecular mechanisms by which exercise attenuates these age-related physiological changes are poorly characterized, specifically how exercise may attenuate senescence.

In terms of astrocyte senescence, it is known that senescent astrocytes display an enlarged, hypertrophied morphology characterised by increased GFAP expression: a hallmark of the ageing brain (Diana *et al.*, 2010; Latimer *et al.*, 2011). It was demonstrated that aerobic exercise reduced astrocyte hypertrophy in the hippocampus of middle-aged mice (Latimer *et al.*, 2011). This reduction in hypertrophy was accompanied by improved vascular function measured by vascular corrosion casting visualised under a scanning electron microscope (Latimer *et al.*, 2011). Astrocytes play an integral role in vascular function and neurovascular coupling, therefore these findings demonstrate that exercise may exert indirect protective effects for the CNS by improving astrocytic function (Latimer *et al.*, 2011).

Exercise has been shown to reduce triggers of cellular senescence, preventing the pathway altogether. (Soares *et al.*, 2015) conducted a study in 2015 which evaluated the effects of a combined exercise protocol (strength and aerobic training) on DNA damage and oxidative stress, measured by lipoperoxidation in human lymphocytes. Both parameters were significantly reduced following 16 weeks of exercise, and this was supported by a significant

increase antioxidant capacity, measured by ABTS radical-scavenging activity (Soares *et al.*, 2015). This data suggests a role for exercise in reducing oxidative stress - a well-established trigger for the senescent pathway (Bitto *et al.*, 2010; Das & Svendsen, 2015). As well as oxidative stress, telomere erosion is a well-understood trigger for cellular senescence, and long term vigorous exercise was shown to conserve telomere length in older athletes (Werner *et al.*, 2009). These findings demonstrate the potential mechanisms by which exercise may reduce the observed accumulation of senescent cells with ageing, and therefore the senescence-induced inflammatory microenvironment of aged tissues.

2.5.2 Exercise increases neurotrophin production

Exercise not only has a role in reducing markers of cellular senescence and improving astrocyte functionality, but also results in increased production of GDNF, BDNF, IGF and NT4 (Funakoshi *et al.*, 1995; Park & Höke, 2014). Protein levels in both skeletal muscle and serum were significantly increased following exercise (Park & Höke, 2014). The proposed explanation for the observed increase of trophic factors in the distal nerves of exercised mice is not only the changes in serum level, but also increased blood flow to the region which occurs as a result of increased exertion (Park & Höke, 2014). Exercise is known to increase vascularization of muscle tissue, which could in-turn improve supply of trophic factors to their sites of action, including Schwann cells of peripheral nerves (Park & Höke, 2014). Most importantly, it is skeletal muscle-derived GDNF which has been shown to increase with exercise and exert the most potent effects on motoneuron survival (Li *et al.*, 2007; McCullough *et al.*, 2013; Park & Höke, 2014).

GDNF protein levels measured by an Enzyme-linked Immunosorbent Assay (ELISA) were increased significantly in the lumbar region of the spinal cords of exercised mice (McCullough *et al.*, 2013). A significant increase in spinal GDNF was observed in both 6 month old and 24 month old exercised mice, demonstrating that exercise can increase trophic levels, even into old age (McCullough *et al.*, 2013). Increased GDNF protein content was correlated with

motoneurons double the size of those in the sedentary controls (McCullough *et al.*, 2013). It can be interpreted from these results that exercise results in increased skeletal muscle-derived GDNF which is transported in a retrograde manner to exert effects at the motor end plate and the motoneuron cell body (Li *et al.*, 2007; Gyorkos *et al.*, 2014; Park & Höke, 2014) (Fig. 7).

2.6 Astrocytes, GDNF and the SASP

Understanding the fundamental processes causing astrocytic dysfunction associated with ageing, is integral to finding therapeutic strategies to target motoneuron dysfunction associated with both ageing and disease. Reduced neuroprotective capacity of astrocytes in the senescent state was recently been demonstrated in a study by Das & Svendsen (2014). The use of SOD1 mutant animals proved to be effective at demonstrating the functional alterations of senescent astrocytes due to the similarities observed in the molecular profile of aged wild-type (300-day old) and end-stage (150-day old) SOD1 mutants (Das & Svendsen, 2015). Both of these animal models showed a reduced protective capacity of motoneurons which was restored following culture in GDNF.

The literature regarding astrocyte senescence and their neuroprotective capacity in the senescent state remains limited in the context of normal ageing. The literature is also largely based on astrocytes in culture, which may not be directly translatable to *in vivo* conditions. There remains to be established a complete mechanism by which astrocyte senescence affects motoneurons, and furthermore, how skeletal muscle-derived GDNF may act on astrocytes to restore their neuroprotective capacity.

Das and Svendsen are the only authors thus far who have shown a link between senescent astrocytes, GDNF and motoneuron viability. They demonstrate the ability of GDNF to directly reduce components of the SASP, but it remains to be seen whether this effect can occur in-*vivo*. The significance of understanding these mechanisms lies in understanding sarcopenic etiology. Astrocyte dysfunction and resulting motoneuron death may be contributing to muscle wastage

with age, via denervation of muscle fibers inducing disuse atrophy and overall reduced muscle mass (section 2.1). The protective effects of GDNF may for both motoneurons and astrocytes may prove to be useful in counteracting age-associated frailty and sarcopenia. The current literature provides a need for further investigation on how GDNF may exert its effects *in-vivo*, and whether exercise may reduce the SASP of astrocytes via skeletal-muscle derived GDNF (Fig. 8).

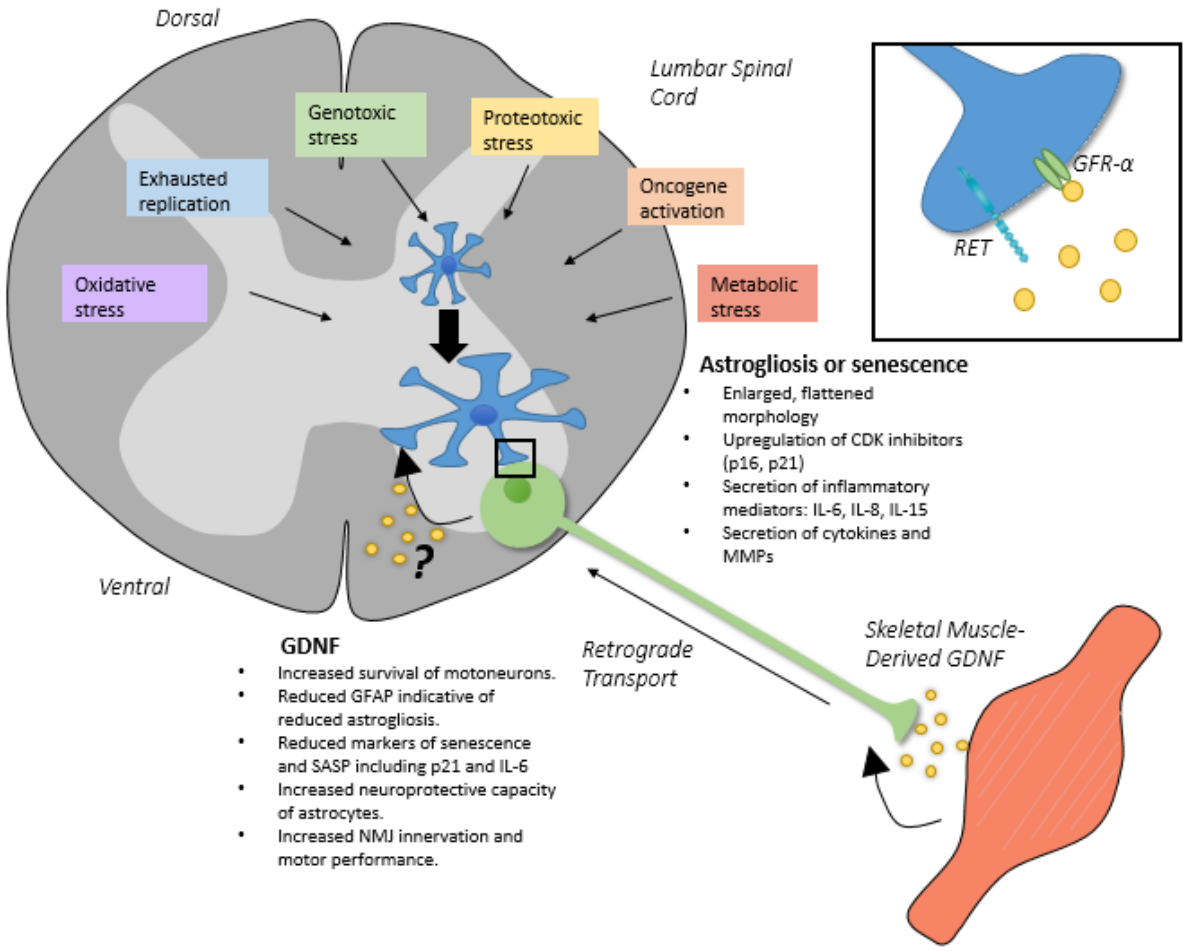

Figure 8: Schematic representation of the proposed interactions between skeletal-muscle derived GDNF, motoneurons and astrocytes.

This schematic shows the proposed relationship between skeletal muscle-derived GDNF which is taken up at the Neuromuscular Junction (NMJ), transported in a retrograde manner and exerts effects at the motoneuron cell body, as well as acting on astrocytes to reduce their reactive phenotype.

3 Aims and hypotheses

Aim one: To determine whether astrocytes in the lateral lumbar column of mice become senescent or reactive with age, and whether this is reversed or attenuated by exercise.

Hypothesis: I hypothesize that the abundance of both p16 and GFAP within astrocytes of the lateral lumbar column will increase with age, and exercise will attenuate or reverse this increase.

Aim two: Determine if the amount of GDNF in motoneurons of the lateral lumbar column reduces with age, and whether exercise can reverse or attenuate this reduction.

Hypothesis: I hypothesize that the amount of GDNF will be reduced within motoneurons of the lateral lumbar column with age, and this will be reversed or attenuated with exercise.

Aim three: To determine if there is a correlation between changes in amount of GFAP and p16 expression and changes in amount of GDNF in the lateral lumbar column with age.

Hypothesis: I hypothesise that with age, there will be an increase in p16 expression and a subsequent reduction in GDNF within the same cells. I also hypothesise that with exercise, there will be an increase in GDNF levels within motoneurons and a subsequent reduction in p16 expression.

Methods

4 Methods

4.1 Overview

The first aim of this experiment was to determine whether astrocytes in the lateral lumbar enlargement of the spinal cord become senescent with age, and show signs of astrogliosis. The second aim was to find out whether exercise could reverse or attenuate these effects by increasing levels of the trophic factor, GDNF. To inform the aims of this experiment, I used semi-quantitative immunohistochemistry (SQI) to fluorescently label the proteins of interest on sections of mouse spinal cord, and use staining intensity as an indicator of relative protein amount.

A total of 15 female C57B6 mice were used; 5 young animals (6 weeks), 5 elderly sedentary (24 months) and 5 elderly exercised mice (24 months with exposure to a running wheel for the final 4 months of life). Goat anti-Glial-Fibrillary Acidic Protein (GFAP) was used to mark astrocytes and indicate astrogliosis, rabbit anti-p16Ink4a was used as a marker of senescence and cell-cycle arrest, and sheep anti-Glial-Derived Neurotrophic (GDNF) factor was used to label GDNF. GDNF was co-stained with Choline-Acetyltransferase (ChAT), a specific marker of spinal motoneurons, to allow measurement of GDNF within motoneurons specifically. All proteins of interest proteins were labelled with Alexa Fluor® conjugated secondary antibodies.

Western blotting was used to attempt to measure relative amounts of p16 protein levels in young and elderly sedentary mouse spinal cord tissue.

4.2 Ethics

Ethical consent for the experiments documented in this thesis was obtained from the University of Otago Animal Ethics Committee.

4.3 Animals

The data obtained was derived from female C57B6 mice sourced from the University of Otago breeding colony at the Hercus Taieri Resource Unit. This strain was chosen as it shows several age-related musculoskeletal changes (reduction in muscle mass, force generating capacity and reduction in myofiber number) that are similar to those observed in humans, in both degree and relative age of onset (Ballak *et al.*, 2014). For this study, mice were compared by both age and activity level; young (1-3 months old), elderly sedentary (24 months old) and elderly exercised (24 months old with exposure to a running wheel for the final 4 months of life). The young and elderly groups are equivalent to approximately 15 and 70 years old respectively (The Jackson Laboratory, 2017). A total of 5 animals per group (listed above) were used for data collection.

Animals were group housed to minimize levels of stress, with the exception of the elderly exercised mice. The exercise protocol involved exposure to a running wheel fitted with a device to track the distance each mouse run per day. The cages for these animals were designed to prevent climbing, ensuring the only exercise undertaken was on the running wheel. For the duration of the exercise protocol, the solitary housed animals were caged near to one another to allow verbal communication and smell, both shown to reduce stress (National Research Council, 2008). Mice had access to food (standard chow) and water *ad libitum*, as well as enrichment toys. The mice were housed with a 12:12 hour light/dark cycle.

4.4 Anesthesia and transcardial perfusion

Animals were euthanized with an intra-peritoneal (IP) injection of sodium pentobarbital at a dilution of 15mg/ml. The toe-pinch reflex was used to determine deep anesthesia prior to beginning surgery. Following loss of the toe-pinch reflex, the mouse was taped down with its hind limbs and forelimbs spread to expose the anterior torso. An incision was made in the inferior abdomen along the midline, and the skin was cut in the rostral direction, ensuring the abdomen wall remained intact. The skin was peeled back to expose the ribcage, and two cuts

were made lateral to the sternum in a V-shape. The ribcage was then deflected to expose the mediastinum and the right atrium was cut to allow venous blood to drain out. The left ventricle was perfused with a 23 gauge needle, injecting heparinised phosphate buffered saline at 37°C, at a rate of 6ml/min using a peristaltic pump. Heparin prevents blood clot formation during perfusion. Next, the fixative (1% paraformaldehyde in 0.1M phosphate-buffered saline), also at 37°C, was perfused for 5 minutes and the rate of perfusion was gradually increased to 10ml/min in a step-wise manner. (Appendix C).

4.5 Spinal cord dissection

The animals were skinned and eviscerated prior to the tissues of interest being removed. The animals were decapitated below the brainstem to expose the spinal cord. The vertebral column was dissected ventrally, by cutting one single vertebra at a time and deflecting it backwards to gradually expose the cord. The cauda equina was severed, and the cord was gradually lifted with forceps, severing the dorsal and ventral roots to gradually release it. (Appendix C).

4.6 Techniques to reduce Freezing Artifact

The spinal cord was stored in a 20% sucrose/TBS solution for a minimum of 24 hours prior to freezing for cryoprotection. The cord was cut to isolate the lumbar enlargement and the tissue was blotted dry and transferred to a 1:1 solution of 20% sucrose and OCT overnight. This was found to prevent the cord from separating from the OCT in the freezer or during sectioning. The cord was embedded in OCT in small, hand-made foil capsules. The foil capsules were partially submerged in isopentane which had been cooled to -170°C with liquid nitrogen. Partial immersion is essential to allow for expansion and prevent cracking as the OCT freezes. Isopentane is used for freezing as it has a higher boiling point than nitrogen, and does not vaporize upon contact with the foil capsule. The use of isopentane allows for a freezing time of <10 seconds to be achieved. Frozen tissue was stored in the -80°C freezer until required.

4.7 Sectioning

Tissue was sectioned transversely using an upright Leica CM1850 cryostat at -22°C. The tissue was mounted onto a tissue mounting stud using OCT, and then sectioned at 16µm and picked up onto slides treated with poly-L-lysine (Sigma-Aldrich, AKL, NZ). Poly-L-lysine is polycationic in nature, and interacts with anionic sites in the tissue sections, adhering them to the slide (Huang *et al.*, 1983). The slides were left to dry for approximately 30 minutes prior to being stored in the -80°C freezer until required.

Sectioning was performed systematically to allow each protein of interest to be assessed regularly along the entire length of the lumbar enlargement (Fig. 9). For each spinal cord, sections were cut in sets of 10 slides beginning at the rostral end of the enlargement. One section was cut per slide, for 10 slides, and this was repeated until each slide had 10 sections. The next 1.6mm of the cord was sectioned and used for spare slides, and this method was repeated for the middle and caudal regions of the lumbar enlargement.

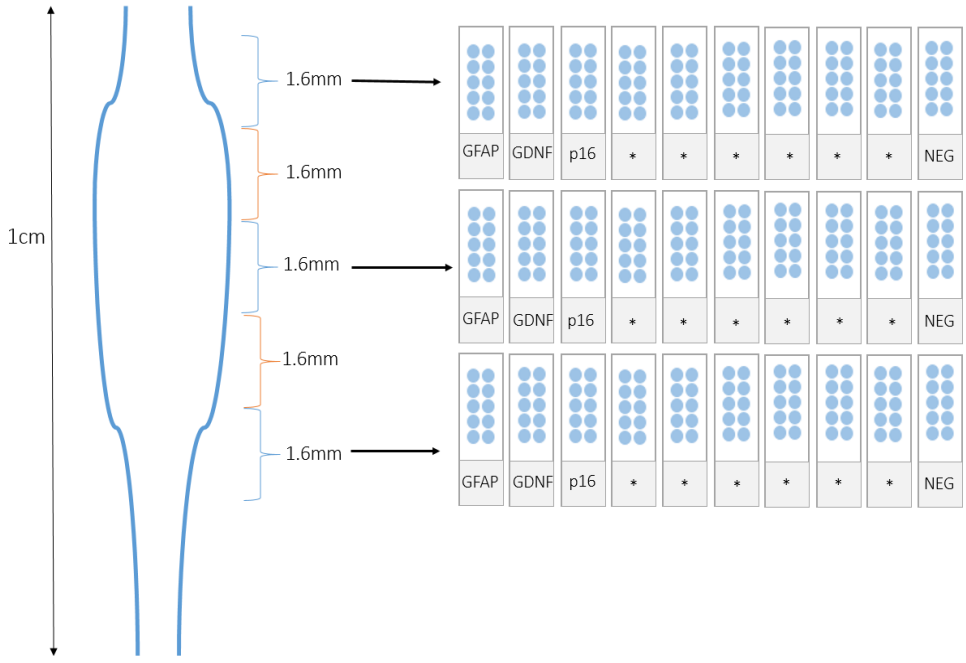

Figure 9: Sectioning schematic
The systematic method used to section along the entire length of the lumbar enlargement and acquire sections from the rostral, middle and caudal regions.* Indicates slides used for other experiments not a part of this project.

4.8 Semi-Quantitative Immunohistochemistry

The use of semi-quantitative immunohistochemistry (SQI) allows intensity of a stained tissue specimen to be used as an arbitrary indicator of protein content within a sample. It is assumed that as protein content increases, this will be reflected in an increase in fluorescence intensity of the staining. SQI relies on the assumption that variables which may affect immunostaining intensity such as primary antibody concentration, temperature and incubation time have equal impact on comparable samples. This method has been tested in the Sheard Laboratory through the development of a reference standard containing a known amount of the protein of interest. The reference standard was then stained alongside the tissue of interest and used to demonstrate the linear relationship between protein amount and brightness of staining.

For a standard to be reliably comparable to the tissue specimens, it must be equally affected by variables known to affect staining of tissue samples, including protein amount and antibody concentration. To validate the standard, sequential dilutions of the protein of interest were suspended in agarose gel and sectioned on a vibratome. The sections were then mounted onto microscope slides alongside sections of the tissue samples. The standards were treated with primary and secondary antibodies under identical conditions as the tissue samples and viewed under a fluorescence microscope. The fluorescence intensity of the standards was proportional to amount of protein present (Appendix D) (Brady, 2015). Next, a single known amount of protein was suspended in the agarose gel, and the concentration of primary antibody was varied (1:100, 1:300 and 1:900). The resulting staining intensity was proportional to the antibody concentration (Brady, 2015) (Appendix D). These results indicate that staining intensity may be used as an indicator of protein content, as long as the tissue specimens to be compared are treated under identical conditions.

4.9 Protocol optimisation

Immunohistochemistry (IHC) was used to stain the four proteins of interest in this experiment. The primary antibodies used were rabbit polyclonal anti-p16INK4a, goat polyclonal anti-GFAP, sheep polyclonal GDNF and rabbit anti-Choline Acetyltransferase (ChAT) (Table 1). The three secondary antibodies used were donkey anti-goat (Alexa Fluor® 405 or 488), goat anti-rabbit (Alexa Fluor® 568), and donkey anti-sheep (Alexa Fluor® 488) (Table 1). All antibodies used in this study were diluted using an immunodiluent which has been optimised in the Sheard lab to give the highest quality immunofluorescent staining (appendix A). Each antibody was optimised by performing serial dilutions of 1:50, 1:100, 1:200, 1:400 and 1:800, and selecting the dilution which produced the optimal signal: noise ratio. For this optimisation, sections were processed together under identical conditions so the only variable was antibody dilution.

For some proteins of interest, antigen retrieval is required to expose the antibody binding site which becomes obstructed during fixation. There are multiple methods for antigen retrieval, but for this experiment three methods were trialled: sodium dodecyl sulphate (SDS), Heat-Induced Epitope Retrieval (HIER) with citrate buffer (pH 6) and HIER with tris buffer (pH 10) (appendix A). The HIER protocol involved heating the buffer to 90°C, then fully submerging the slides and maintaining a temperature between 80-90°C for 20 minutes. The buffer was then left to cool gradually until the temperature was below 40°C, at which point the slides were washed three times for five minutes in 1x TBS before primary antibody incubation.

For the experiments listed below, all slides were submerged in a glycine solution (appendix A) following rehydration, to quench any excess aldehyde from the fixation. All antibodies were washed off as follows: 3x5 minutes in 1xTBS, 3x5 minutes in 2xTBS and finally 3x5 minutes in 1xTBS (appendix A). Prior to mounting, all sections were treated with TrueBlack™ autofluorescence quencher (Biotium, CA, USA) diluted 1:20 in 70% ethanol, to reduce

visibility of lipofuscin autofluorescence common in aged tissues. Slides were mounted with glycerol/TBS mounting medium with DAPI to stain nuclei (appendix A).

Table 1. Antibodies used for this study.

Antibody against	Animal raised in	Conjugate	Antibody specificity	Catalogue number	Dilution
p16INK4a	Rabbit	N/A	This antibody is against CDKN2A/p16INK4a (aa50-150) and recognises mouse and human antigen. It has been validated for western blot, IHC (fixed and frozen), immunocytochemistry and ELISA	LifeSpan Biosciences LS-C49180-100	1:100
GDNF	Sheep	N/A	This antibody reacts with GDNF in its mature form and pro-form, so multiple bands may be observed in western blot. Both forms have been shown to be present in elderly spinal cord (McCullough *et al.*, 2013)	Abcam ab6206	1:400
GFAP	Goat	N/A	This antibody binds to GFAP aa 417-430 (C terminal cysteine residue). Western blot data from the supplier of mouse brain lysate shows a single band at 50kDa.	Abcam ab53554	1:200
ChAT	Rabbit	N/A	Antibody against Choline Acetyltransferase (ChAT). Validated for use in IHC for frozen and paraffin embedded sections.	EMD Millipore AB143	1:400
Rabbit	Goat	AlexaFluor® 568			1:500
Sheep	Donkey	Alexa Fluor® 488	Cross-Adsorbed secondary antibody reacts with heavy and light chains of gamma immunoglobulins.	ThermoFisher A-11015	1:500
Goat	Donkey	Alexa Fluor® 488			1:500

4.10 Glial Fibrillary Acidic Protein

Glial Fibrillary Acidic Protein (GFAP) is an intermediate filament protein specific to astrocytes (Nakagawa & Schwartz, 2004; Khakh & Sofroniew, 2015), it is the most widely used astrocytic marker.

The optimum dilution of the primary antibody, goat anti-GFAP, was determined to be 1:200 based on optimal signal: noise ratio. Incubation times were optimised to overnight at 4°C for the primary antibody, and 3 hours at room temperature for the secondary antibody. Sections were cut at serial thicknesses: 6, 8, 10, 12 and 16μm and optimised at 16μm. Although thinner sections result in lower background due to more area outside of the focal plane, astrocytic processes are extensive and a single cell may span 40μm in its entirety (Cirillo *et al.*, 2012), therefore 16μm allowed for distinction of single astrocytes and their associated processes.

A solution (appendix A) containing glycine, which quenches any residual paraformaldehyde, and two permeabilising agents: tween-20 and triton, was found to improve quality of staining of the extensive astrocytic projections. Slides were incubated in this solution for 4 mins, followed by 2x5 minute washes in 1xTBS prior to primary antibody incubation.

4.11 P16

4.11.1 Immunohistochemistry

The primary antibody, rabbit anti-p16Ink4a, was run under standard conditions at serial dilutions of 1:50, 1:100, 1:200, 1:400 and 1:800, as well as the various permutations of antigen retrieval listed in section 1.8. The signal was optimal in tissue processed without antigen retrieval at a dilution of 1:200. Incubation time was optimised to overnight at 4°C for the primary antibody, and 4 hours at room temperature for the secondary antibody, goat anti-rabbit Alexa Fluor® 568.

To validate the positive signal attained in the spinal cord, sections of positive control tissue (paraffin embedded mouse lung carcinoma tissue) known to express high amounts of p16

(Witkiewicz *et al.*, 2011) were acquired from the Department of Pathology, University of Otago. Prior to staining, the control sections were de-paraffinised by immersion in xylene for two minutes, three times. The slides were then transferred to 100% ethanol for two minutes, twice, then 95% ethanol for one minute, 70% ethanol for one minute, and finally distilled water for two minutes. The sections were run with anti-p16Ink4a at a 1:200 dilution under standard conditions, with SDS treatment and HIER with citrate buffer (pH 6) and tris buffer (pH 10). A signal was acquired following HIER with tris buffer (pH 10).

To establish whether p16 is located in nuclei of either astrocytes or motoneurons, p16 was co-stained with antibodies to both GFAP to label astrocytes, and ChAT to label motoneurons. Negative control slides had both primary antibodies omitted. The slides were all run the optimised staining protocol as described above. The anti-GFAP protocol was run as described in section 1.9. Prior to the anti-ChAT primary incubation, the slides were incubated with goat anti-rabbit $F(ab')_2$ fragment (Jackson ImmunoResearch Laboratories Inc., PA, USA), as this primary antibody was also raised in rabbit. Rabbit anti-ChAT (1:400) was incubated overnight at 4°C, and then the secondary, goat anti-rabbit Alexa Fluor® 488 was incubated for 4 hours at room temperature. All slides were washed, treated with TrueBlack™ (Biotium, CA, USA) and mounted as described in section 1.8.

4.11.2 Western blotting

Western blotting is used to separate out proteins based on molecular weight and then label proteins of interest with antibodies to detect them on a membrane. For this experiment, western blotting was used to attempt to measure the fold change in amount of p16 in young versus elderly spinal cord homogenate. The protocol for western blotting is described below, and the optimisation procedure can be found in appendix E.

4.11.2.1 Tissue preparation

Spinal cords removed from euthanised animals (section 1.4) were placed in cold 1x TBS and kept on ice. The cord was then cut to remove the lumbar enlargement which was post-fixed in 1% paraformaldehyde overnight. The rest of the cord was cut into small pieces and placed in a 1.5ml Eppendorf tube maintained on ice. An equal amount of 0.9-2mm RNAse-free, stainless steel beads (Lab Supply, NZ) were added to the tube, followed by 400ul of Radioimmunoprecipitation Assay (RIPA) buffer (appendix B) resulting in a 1:1:2 ratio of beads, tissue and buffer. The tissue was then homogenised in the bullet blender® (Next Advance Storm 24) for 4 minutes on level 10. The homogenate was centrifuged for 15 mins at 15000rcf, at 4°C, and the supernatant was removed and put in a separate tube on ice.

4.11.2.2 Tissue sample analysis

The protein amount in each sample was calculated to ensure an equal amount of protein was loaded into each well of the gel. Protein amount was initially determined using a µDrop™ plate (ThermoFisher Scientific, MA, USA), and measuring absorbance with SkanIt software version 4.1 (ThermoFisher Scientific, MA, USA). First, 1µl of RIPA buffer was added to each 'blank' plate, this is the standard which will be subtracted from the total absorbance reading. The supernatant was vortexed to ensure protein was equally dispersed in the tube, then 1µl of the sample was added to each of the two plates in the second row. Absorbance was measured using a wavelength of 280nm and subtracting the absorbance readings of the RIPA buffer alone (blanks). The Beer-Lambert Law is the linear relationship between concentration and absorbance of a substance. A simple equation of absorbance (A) multiplied by path-length of light (l) gives protein concentration in mg/ml (µg/µl) (C):

$$C = A \, x \, l$$

Due to the large variance observed using the µDrop™ Plate technique, a BSA Protein Assay was performed to generate a standard curve of absorbance and calculate protein amount of each

sample based on individual absorbance readings. 5µl of 8 serial amounts of BSA were added to the first 8 wells of a 96-well plate. The next 10 wells were loaded with 5µl of each of the 10 tissue samples. 1mL of reagent A (DC™ Protein Assay, BioRad, NZ) and 20µl of reagent S was then added to the wells. 200µl of reagent B was added to the wells last, and the plate was left on an agitating table for 15 mins before being read using the microplate reader. The standard curve was generated and protein amount in each sample was determined. The samples were aliquoted out into appropriate amounts required for blots, and snap frozen in liquid nitrogen before being stored in the -80°C freezer.

4.11.2.3 Gel electrophoresis

Sodium Dodecyl Sulphate Poly-Acrylamide Gel Electrophoresis (SDS-PAGE) was used to separate proteins based on their molecular weights. The result is bands of protein at various levels down the gel which can then be visualised using antibodies. Gel electrophoresis utilises the principle that opposites attract, i.e. negatively charged proteins move toward a positively charged region of an electrical field. For an SDS-PAGE gel, the negative charge on the proteins is acquired from the SDS; this causes them to migrate from the negatively charged cathode to the positively charged anode. Large proteins take longer to move through the gel, and consequently the end result is a protein ladder with large proteins closer to the cathode, and small proteins nearest the anode. A marker ladder composed of dyed proteins of known molecular weight was used to indicate molecular weight of the bands formed by the sample.

The percentage of acrylamide used in the resolving gel is important to consider. Acrylamide is the component of the gel which polymerises and forms a matrix which acts like a sieve in separating the proteins based on their molecular weights. A high percentage gel forms a denser matrix and thus is more effective at separating small proteins, and a low percentage gel contains a less-dense matrix of polyacrylamide, and thus small proteins move rapidly through the gel and out the other side, leaving large proteins separated out along the gel. For this study a 15%

gel was used (table 2) which was appropriate for visualising my protein of interest which is 16kDa.

The resolving gel was made by adding all of the reagents to a beaker with a magnetic spinner. The TEMED and acrylamide are added last as they initiate setting of the gel. 9ml of resolving gel was pipetted into the cassette, followed by a small volume of methanol which smooths the surface of the gel and prevents evaporation. The gel was left to set for an hour at room temperature. Once set, the methanol was washed off with dH_2O, and 3mL of stacking gel (table 2) was pipetted on top of the resolving gel. A comb was inserted on top (Fig. 10) and this was left to set for an hour before the comb was removed and the wells rinsed with distilled water.

Table 2: Ingredients for gels for running an SDS-PAGE gel electrophoresis.

	Resolving Gel (15%)	**Stacking Gel (4%)**
dH_2O (mL)	3.7	4.766
Lower Tris (pH 8.8) (mL)	4	-
Upper Tris (pH 6.8) (mL)	-	2
10% SDS (µl)	160	80
30% AA:MBA(mL)	8	1.066
10% Ammonium persulfate (µl)	160	80
TEMED (µl)	16	8

The set gel was put into a running frame inside a gel tank filled with running buffer (Appendix B). 4µl of the protein ladder (Precision Plus Protein™, BioRad, NZ) was loaded into the first well, followed by the first five samples. An initial gel was run with serial protein amounts: 10, 20, 40 and 80µg, and optimised at 20µg. 20µl was loaded into each well, containing 1µg/µl of protein (appendix B); by keeping the amount of protein the same within each well, this ensures the samples are directly comparable with respect to the loading control, β-actin. The gels were run at 100V for 120 minutes which allowed the proteins to separate out completely.

4.11.2.4 Protein transfer to membrane

Proteins from the gel were transferred onto a polyvinylidene difluoride (PVDF) membrane for detection with antibodies. The PVDF membrane was cut to size and soaked in methanol for 1 minute to activate it, and then washed in transfer buffer for 3 minutes. As the stack was assembled (Fig. 10), transfer buffer was poured over the layers, and a small roller was used following the addition of each layer to roll out any bubbles which could disrupt the electrical current and quality of transfer.

The transfer sandwich was placed in a transfer cassette and clamped shut. The cassette was placed in the transfer box and the box was filled with cold transfer buffer. A magnetic stirrer was placed at the bottom of the tank and ice packs were placed inside the tank to keep the buffer cold. The whole tank was placed in a box packed with ice and the transfer was run at 100V for 100 minutes. As the electricity flows between the electrodes, the negatively charged proteins move from the gel to the membrane where they can be detected with antibodies. Prior to protein detection with antibodies, the PVDF membrane was submerged in Ponceau S red, which stains all protein on the membrane to ensure the transfer was successful before continuing. The Ponceau S stain was washed off thoroughly in TBST until all the pink was removed.

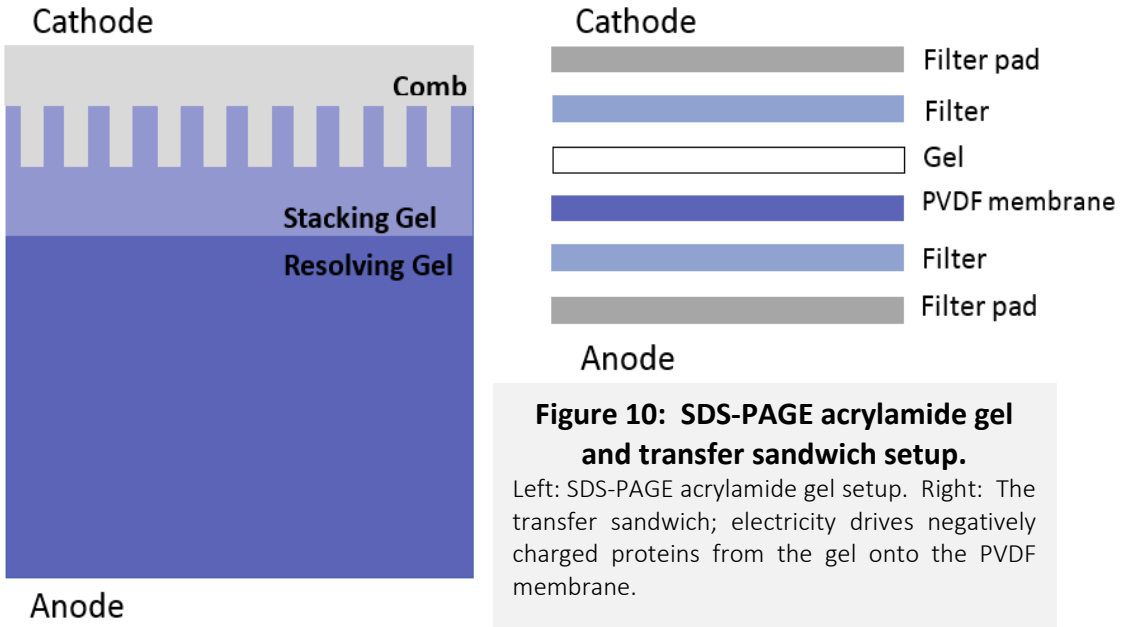

Figure 10: SDS-PAGE acrylamide gel and transfer sandwich setup.
Left: SDS-PAGE acrylamide gel setup. Right: The transfer sandwich; electricity drives negatively charged proteins from the gel onto the PVDF membrane.

4.11.2.5 Protein detection with antibodies

The protocol to stain the protein of interest with antibodies was run with several permutations as summarised in appendix E. The PVDF membrane was blocked in 5% BSA in TBST on an agitating table for 2 hours at room temperature. The membrane was washed three times for five minutes in TBST before the primary antibody was added. Rabbit anti-p16Ink4a was made up in immunodiluent to a dilution of 1:1000, and incubated at 4°C overnight on an agitating table. The membrane underwent 4x5 minute washes in TBST before being incubated with the secondary antibody (anti-Rabbit HRP) diluted to 1:10 000 in TBST, for 2 hours at room temperature. The membrane was washed for 10 minutes, four times in TBST, and the Enhanced Chemiluminescence (ECL) substrate reagents were added at a 1:1 ratio (200µl of each substrate) for 5 minutes. The membrane was placed between two sheets of thin clear plastic, and viewed under the Syngene PXi Gel Imaging System (Syngene, A Division of Synoptics Ltd., MD, USA).

4.12 Glial-Derived Neurotrophic Factor

Neurotrophins such as glial-derived neurotrophic factor (GDNF) are held within intracellular vesicles therefore antigen retrieval or permeabilisation steps are often required to allow the primary antibody to bind. Several antigen retrieval methods were tested to establish a protocol which gave optimal staining (best signal: noise ratio).

The primary antibody, sheep anti-GDNF, was optimised by performing serial dilutions of 1:50, 1:100, 1:200, 1:400 and 1:800, which were then applied to serial sections from the same tissue. The sections were all processed together under identical conditions so that the only variable was the primary antibody concentration. The dilution 1:400 was selected based on optimal signal: noise ratio. Incubation time was also optimised to overnight at 4°C for the primary antibody, and to 4 hours on the bench for the secondary antibody, donkey anti-sheep Alexa Fluor® 488.

Sections of the same cord were cut at 16µm, and processed under standard conditions (no antigen retrieval), as well as with each of the following antigen retrieval methods: SDS (1% and 0.5%) for 30s, 1 minute and 3 minutes, heat-induced epitope retrieval with citrate buffer (pH 6) and heat-induced epitope retrieval with tris buffer (pH 10). From these steps it was concluded that the signal was not improved following any antigen retrieval protocols, therefore future sections were processed without antigen retrieval.

A co-staining protocol was developed to view the co-localisation of GDNF with Choline Acetyltransferase (ChAT) - a specific marker of motoneurons within the spinal cord (Barber *et al.*, 1984). The ChAT antibody used for this experiment was rabbit anti-ChAT. For this protocol, GDNF was stained as described above, followed by rabbit anti-ChAT which had previously been optimised at a 1:400 dilution, overnight in the fridge (4°C). The secondary, goat anti-rabbit Alexa Fluor® 568 was incubated for 4 hours at room temperature. Following the washes, the slides were treated with TrueBlack™ (Biotium, CA, USA) and mounted as described in section 1.8.

4.13 Microscopy

Stained specimens were viewed using an Olympus BX-50 upright compound microscope (Olympus® Corporation, Tokyo, Japan) fitted with a coolLED fluorescence illuminator (pE-1 excitation system, coolLED Ltd, NY, USA). Images were acquired using a SPOT-RT™ Slider microscope camera (Diagnostic Instruments Inc., MI, USA). The microscope has three dichroic filters which restrict the wavelengths of excitation and emitted light; the Wide Band Interference (WBI) red filter (excited at 515-700nm), WBI green (580-700nm) and the UV narrow band filter (360-370nm) which passes blue light. The images were photographed in RGB (red, green and blue) using the 40x objective oil immersion lens. The exposure time, LED illumination and gain were set using the sample with the brightest staining for each antibody and the exposure and illumination parameters were then kept constant across all images taken

for each antibody. This ensured the images were comparable, and that relative fluorescence intensity could be used as an indicator of protein amount within the tissue.

4.14 Analysis and statistics

Protein immunostaining was quantified by acquiring mean greyscale values of images of stained areas. All images were taken in RGB to allow non-specific fluorescence to be eliminated, therefore images were initially loaded onto ImageJ and split into the three respective channels. The data from the two channels not of interest was discarded, and the data from the channel of interest was analysed.

4.14.1 GFAP

The green channel data was loaded into Ilastik, an Interactive Learning and Segmentation software (Heidelberg Collaboratory for Image Processing (HCI), Germany). Ilastik was trained using pixel classification to identify GFAP immunofluorescence and exclude background. Once Ilastik was trained on six images and could reliably separate staining from background, the parameters obtained by the program were applied to all images using batch processing. The use of Ilastik to batch process all images eliminates subjectivity, as the same selection criteria are applied to all images. A mask was generated for each image and used to identify the area for

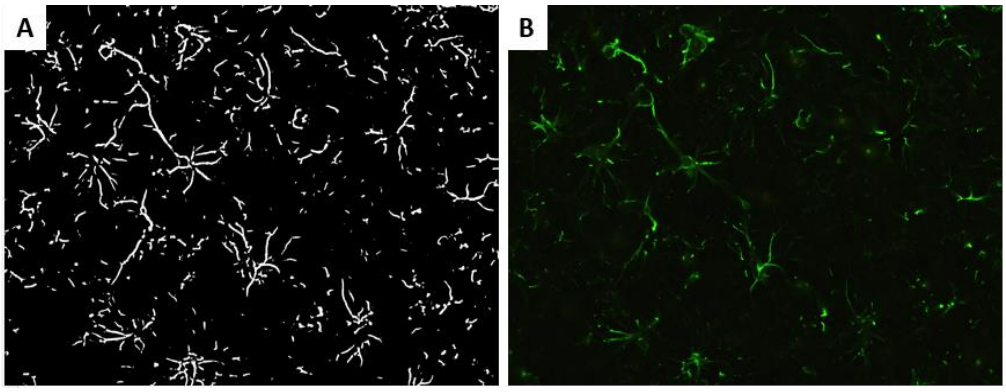

Figure 11: Mask of GFAP immunostaining generated by Ilastik.
A) Binary image produced by Ilastik showing a mask of white astrocytic staining on a black background. B) Original image showing AlexaFluor™ 488 staining of Glial Fibrillary Acidic Protein (GFAP).

analysis (Fig. 11). The mask and green channel data were loaded into Fiji software (Schindelin *et al*., 2012), and mean fluorescence intensity within the mask was measured as an average grayscale value.

GFAP average greyscale values were statistically analysed using a linear mixed-model (LMM) on RStudio (R Core Team, 2013) which analyses both the fixed effects such as age and exercise, and random effects such as intra-individual variation. P values were acquired by calculating standard error from the two groups to be compared, and then calculating the Z statistic by dividing the difference in the two averages by the standard error (Altman & Bland, 2011). The Z statistic was then inserted into the following equation:

$$0.717xZ - 0.416Z2$$

4.14.1 P16

Ten images were acquired from the lumbar lateral motor column per animal (n=5). Images of DAPI immunostaining of nuclei (blue channel), p16 immunostaining (red channel) and GFAP immunostaining (green channel) were merged using Adobe® Photoshop® (Adobe Systems Inc., CA, USA) to allow the identification of co-localisation of p16 immunostaining within astrocyte nuclei. Co-staining with GFAP was analysed qualitatively, as the total number of individual astrocytes could not be determined due to the nature of the GFAP immunostaining in relation to the size and shape of astrocytes.

P16 co-localisation with ChAT immunostaining was not analysed due to the incompatibility of the ChAT and p16Ink4a antibodies causing the staining to be indistinguishable between the two proteins. In view of this limitation, ImageJ was used to measure the diameter of cells with cytoplasmic anti-p16 staining present. Both the longest axis of the cell, and perpendicular to that axis (orthogonal axis) were measured and the two values averaged to obtain a final diameter. Unpublished data from the Sheard lab found that because a cell body is not a sphere,

taking the longest axis may confound the results by over-estimating cell size, and the shortest axis may underestimate the cell size.

4.14.2 GDNF

Images of GDNF/ChAT co-stained tissues were analysed by acquiring the mean grayscale value of GDNF immunostaining within the boundaries of the anti-ChAT stained motoneurons. First, the RGB images were split into the respective channels, and the red channel data (ChAT staining) was loaded into ImageJ software to generate a mask for motoneurons. An appropriate threshold was chosen which most accurately distinguished motoneurons from background, and a minimum size threshold was established to exclude small areas of background that the mask had selected. This mask was then loaded into Fiji software (Schindelin *et al.*, 2012) with the green channel data (GDNF staining), and the mean grayscale value of the GDNF immunofluorescence within the boundaries of the mask was measured.

Due to the appearance of bright staining within the nucleus of the young and elderly exercised animals which is abnormal for both ChAT and GDNF, analysis was repeated to measure only cytoplasmic GDNF levels, eliminating the potentially artefactual bright nuclei which may confound the results. To do this, GDNF images were loaded into ImageJ and the channels were split, disregarding the blue and red channel data. The motoneurons were circled by hand, followed by the nuclei. The area between these two circles was then analysed for mean greyscale value (Fig. 13).

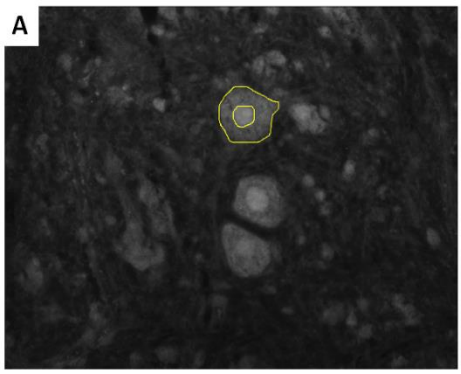

B

	Area	Mean	Min	Max
1	24883	42.930	10	84
2	19855	37.818	10	63

Figure 12: Analysis of cytoplasmic GDNF levels

Once the channels were split, the green channel image was analysed by circling the cell soma, followed by the nucleus, and measuring the greyscale value of only the cytoplasm (area between the two circles). B) Data in line 1represents the mean greyscale value within the whole cell, line 2 represents only the cytoplasm which is notably lower.

Statistical analysis was performed as described for GFAP (Section 1.14.1) using mean greyscale values from each cell cytoplasm and performing a linear mixed model (LMM) using RStudio (R Core Team, 2013).

Results

5 Results

5.1 Elimination of technical and processing artefacts

5.1.1 Freezing artefact

Optimisation of tissue freezing was crucial for allowing quality immunohistochemistry to be performed on tissue sections. The following results are images of GFAP-labelled, 16um sections of mouse spinal cord, within the lateral lumbar column. If the spinal cords are not frozen adequately, ice crystals may pierce holes through the tissue, or the innermost parts of the tissue may begin to degrade in the freezer, resulting in little-to-no immunostaining of these regions. Below are images of GFAP-labelled sections, which contain freezing artefact.

Spinal cords were frozen using specific techniques to avoid formation of ice crystals during freezing (Section 2.6). Quality freezing techniques provide the basis for optimal immunostaining of proteins within the tissue.

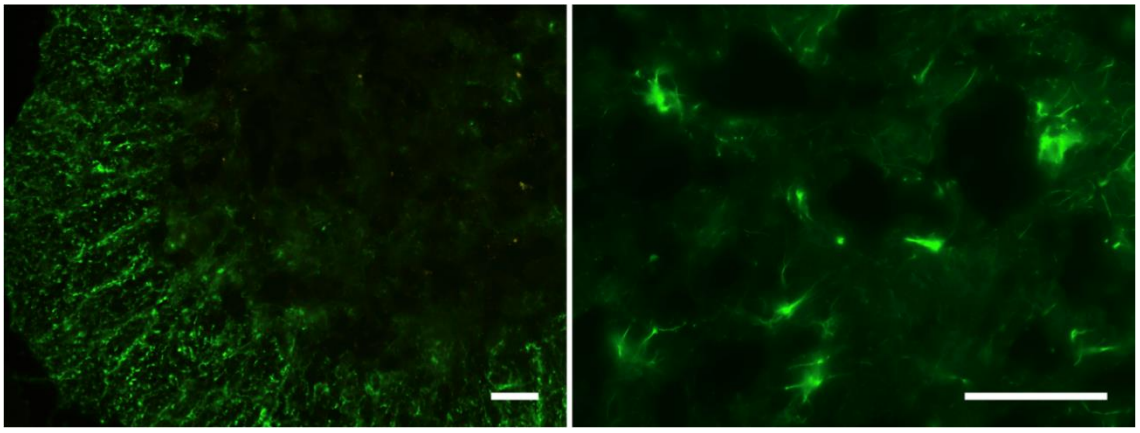

Figure 13: Freezing artefact
Images of anti-GFAP-immunostained sections of elderly spinal cord show the grey matter has degraded, and holes have been pierced through the tissue during freezing. (Scale bars = 50µm).

5.1.2 Lipofuscin granules and tissue autofluorescence

Due to the increasing presence of lipofuscin in aged tissues, all images were taken in RGB to allow the channels to be split, and only the data from the desired channel to be analysed, disregarding non-specific fluorescence. This is particularly important as lipofuscin granules are autofluorescent and appear yellow or orange under the microscope. Figure 14 shows the same image taken in RGB and then fluorescence green, demonstrating how lipofuscin is no longer distinguishable from AlexaFluor™488 staining when imaged in green. TrueBlack™ (Biotium, CA, USA) was used to reduce the visibility of lipofuscin and tissue autofluorescence for all tissue sections from all age groups following the immunohistochemistry protocol, prior to mounting (Fig. 15).

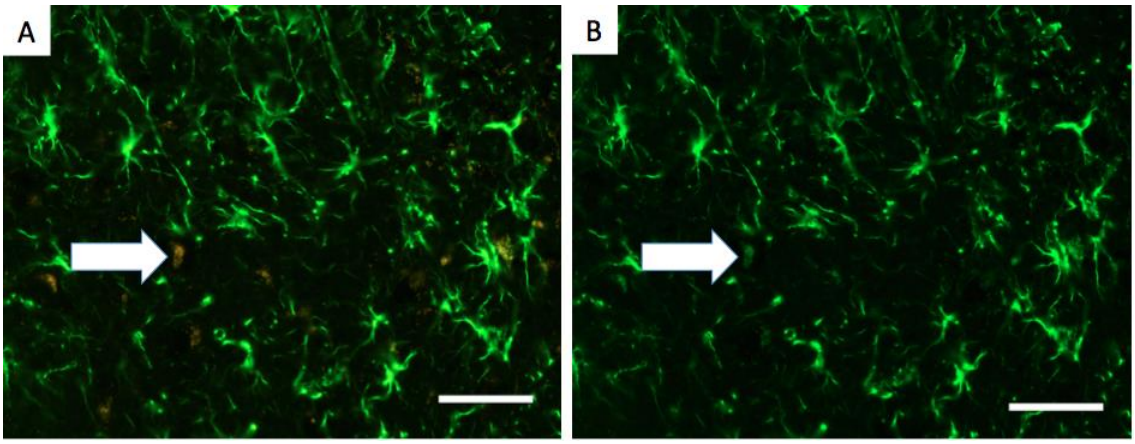

Figure 14: Images of GFAP immunostaining containing lipofuscin granules
A) Image of GFAP-immunostained elderly spinal cord taken in RGB with lipofuscin granules (indicated by arrows) appears a dark orange colour. B) The same area imaged in fluorescence green; the same lipofuscin granule (indicated by arrow) appears green. (Scale bars = 50µm).

5.2 Glial Fibrillary Acidic Protein

5.2.1 Immunohistochemistry

As described in the methods section, each antibody was optimized via various permutations of the protocol to ensure optimal signal to noise ratio was achieved. Due to the extensive nature of astrocytic projections - a single astrocyte can span up to 40μm (Cirillo *et al.*, 2012) - section thickness was optimized for GFAP immunostaining to achieve low background fluorescence, but allow visualization of single astrocyte profiles. Figure 15 shows GFAP immunostaining of sections cut at 6μm (A), 16μm (B), and 16μm imaged at 6 planes of focus and assembled as a focus composite (C). By compiling the images as a stack, it allows for visualization of extensive astrocytic projections through multiple focal planes. By overlaying the stacked image with DAPI staining of nuclei, it allowed distinction of astrocyte cell bodies and their associated projections. Images B-D were acquired from elderly tissues which were treated with TrueBlack™.

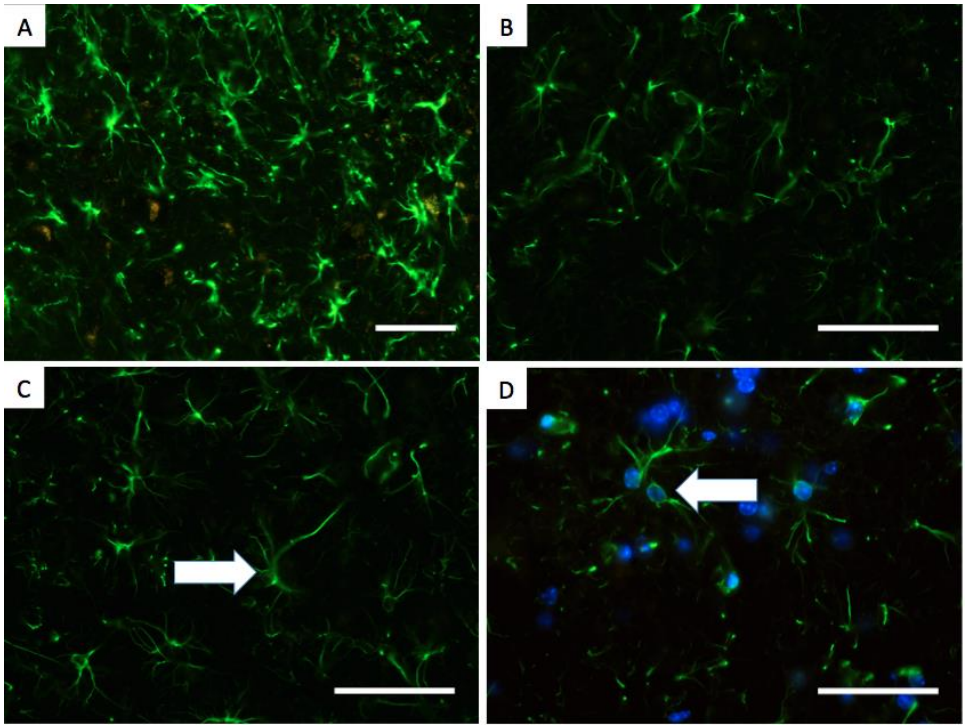

Figure 15: Anti-GFAP immunostaining of sections of multiple thicknesses
A) 6μm thick section showing astrocytic staining with little distinction of whole astrocytic profiles. B) 16μm thick section showing astrocytic profiles. C) Pseudo-confocal stack of 6 planes of focus showing astrocytes and their projections (example indicated by arrow). D) Focus composite stack of 6 planes of focus showing astrocyte cell bodies with DAPI staining of nuclei (indicated by arrow). Scale bars = 50μm

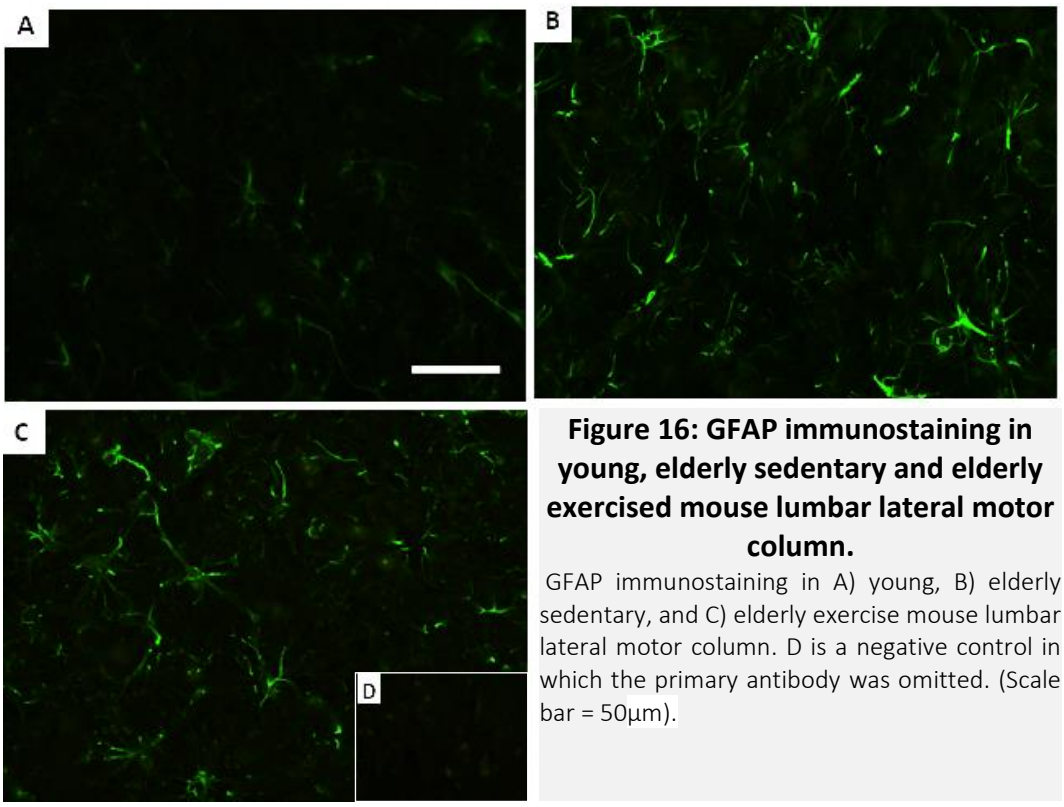

Figure 16: GFAP immunostaining in young, elderly sedentary and elderly exercised mouse lumbar lateral motor column.

GFAP immunostaining in A) young, B) elderly sedentary, and C) elderly exercise mouse lumbar lateral motor column. D is a negative control in which the primary antibody was omitted. (Scale bar = 50µm).

Figure 16 demonstrates anti-GFAP staining in sections of spinal cord from young, elderly sedentary and elderly exercised animals. There appears to be a higher quantity of anti-GFAP staining within each astrocyte visible in an image and more astrocytic projections are visible in both elderly and elderly exercised lumbar lateral motor column compared to that of young animals.

5.2.2 Statistical analysis of GFAP immunostaining

Statistical analysis was performed using a linear mixed model (LMM) on R software (R Core Team, 2013). There was a strong trend toward an increase in GFAP levels between young and elderly sedentary groups, but this was not statistically significant (p=0.052). In addition to this, there was no difference in GFAP levels between elderly sedentary and elderly exercised animals (p=0.12) (Fig. 18).

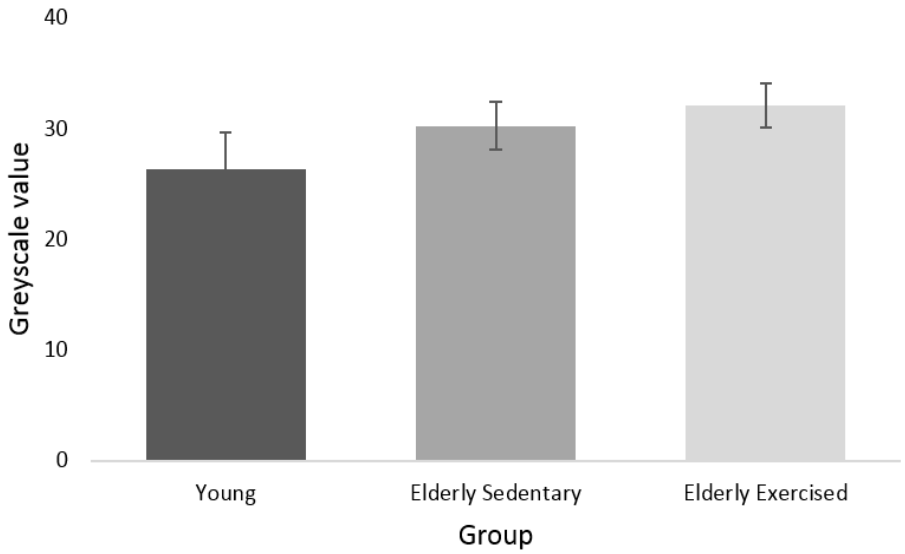

Figure 17: Changes in GFAP staining levels with age and exercise.
The above graph shows average greyscale value of GFAP immunostaining in young, elderly sedentary and elderly exercised spinal cord. A linear mixed model was used to calculate statistical values. There was a trend toward an increase between young and elderly sedentary which was not statistically significant (p=0.052), and no difference between elderly sedentary and exercised (p=0.12). Data expressed as mean ± SEM.

5.2.3 GFAP staining intensity and average distance run by exercised animals

The two data sets of GFAP immunostaining and average distance travelled per day for each animal were plotted together to establish if there was an observed correlation between the two data sets. The results show no observable trend between distance travelled and GFAP levels (Fig. 18).

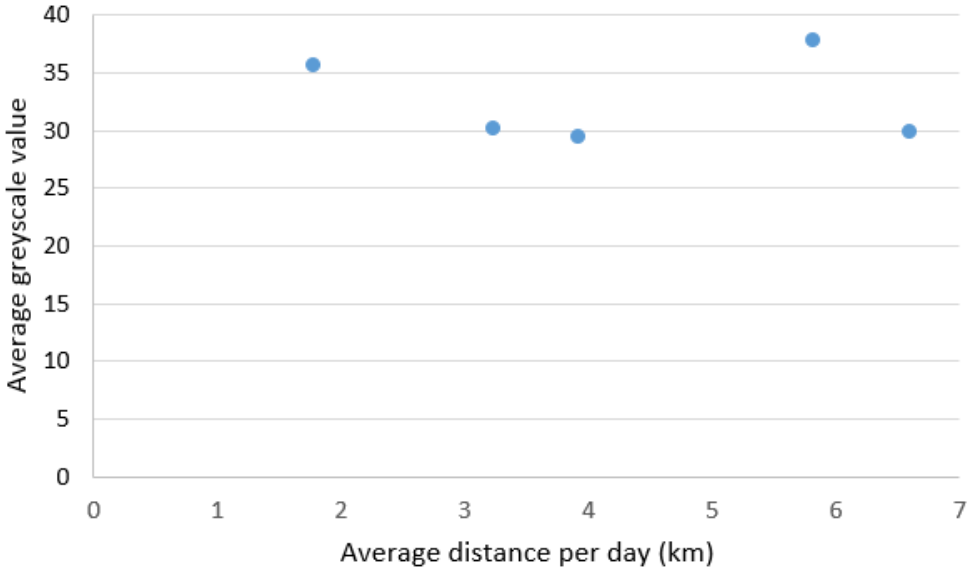

Figure 18: Changes in GFAP staining plotted with average distance run per day.

The above graph shows average greyscale value of GFAP immunostaining elderly exercised animals, plotted with the average distance in kilometres run by each animal. The results demonstrate no relationship between distance travelled and GFAP immunostaining.

5.3 P16

P16 is a cyclin-dependent kinase inhibitor and marker of cell-cycle arrest (Baker *et al.*, 2008). P16 was chosen for this study as is the most widely used senescence marker in the literature, but there is low availability of well-established antibodies against p16 for use with fluorescence immunohistochemistry. Due to initial difficulties in visualizing p16 immunostaining in mouse lumbar lateral motor column, the rabbit anti-p16Ink4a antibody was run on sections of positive control tissue provided by the Department of Pathology, University of Otago, to establish the reliability for future use as a senescence marker in sections of spinal cord.

5.3.1 Positive control

Mouse lung carcinoma tissue was used as the positive control for p16 immunostaining as tumours are known to have high expression of p16 (Shapiro *et al.*, 1995; Shapiro *et al.*, 1995)(Witkiewicz *et al.*, 2011). Figure 19 shows tumour cells which are positive for p16 with diffuse cytoplasmic staining which is described in the literature as a characteristic of various cancers including lung carcinoma (Shapiro *et al.*, 1995; Evangelou *et al.*, 2004). Images were mounted with DAPI mounting medium (appendix A) to allow overlay of the nuclear stain.

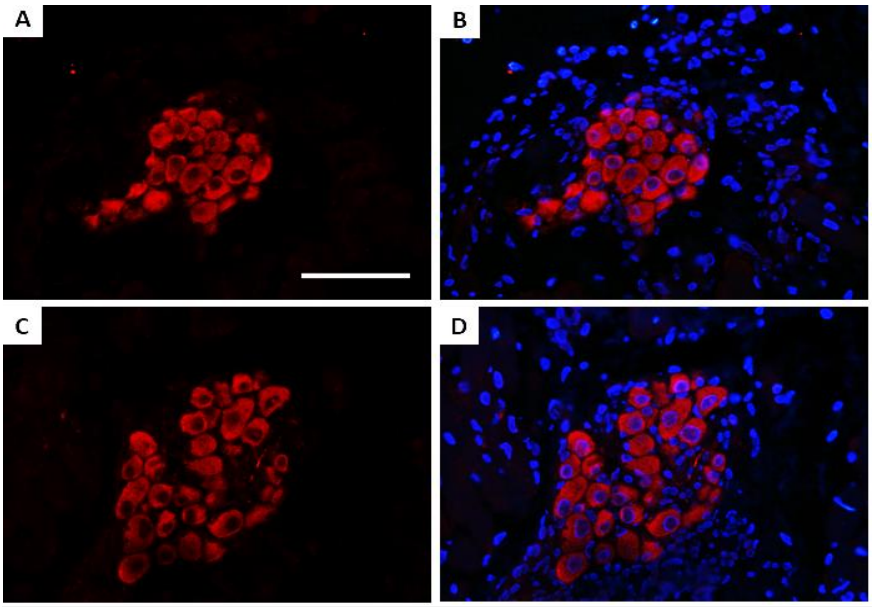

Figure 19: Positive control staining for p16
P16 positive staining of mouse lung carcinoma tissue. A and C show clusters of cells with diffuse cytoplasmic anti-p16 staining. B and C show DAPI staining of cell nuclei within the p16-positive cells. (Scale bar = 50µm)

5.3.2 P16 and GFAP

To inform the aim of investigating whether astrocytes become senescent in the lumbar lateral motor column with age, a co-staining protocol was established for p16 and GFAP.

A staining protocol was established to allow the visualisation of co-localisation of p16 with anti-GFAP staining of astrocytes, and DAPI to identify cell nuclei. Figure 20 is a representative image showing the three staining components (A, B and C), and then the final combined image (D). Images were qualitatively analysed based on observations of p16 co-localisation with GFAP immunostaining. It was observed that p16 does not co-localise with astrocyte nuclei (indicated by arrows), as no astrocyte nuclei were positive for p16 immunostaining. Anti-P16 staining appears within nuclei of another cell type within the lumbar lateral motor column.

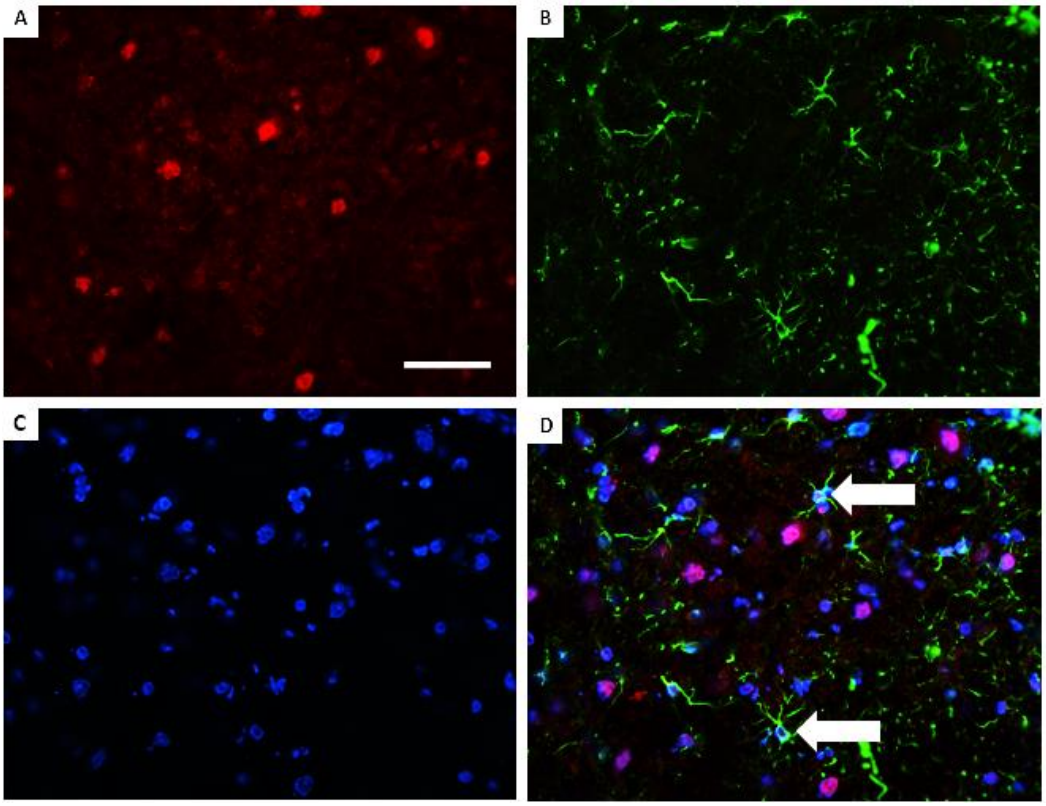

Figure 20: P16 co-staining with GFAP and DAPI.
The above figure shows triple-immunolabelling of A) p16, B) GFAP and C) DAPI staining of nuclei. Image C shows the first three images combined. Astrocyte nuclei indicated by arrows. (Scale bar = 50µm).

Figure 21 shows the appearance of p16-positive nuclei within the lumbar lateral motor column of elderly mice. Exercise did not have a visible effect on reducing the number of p16-positive nuclei although this was not quantified.

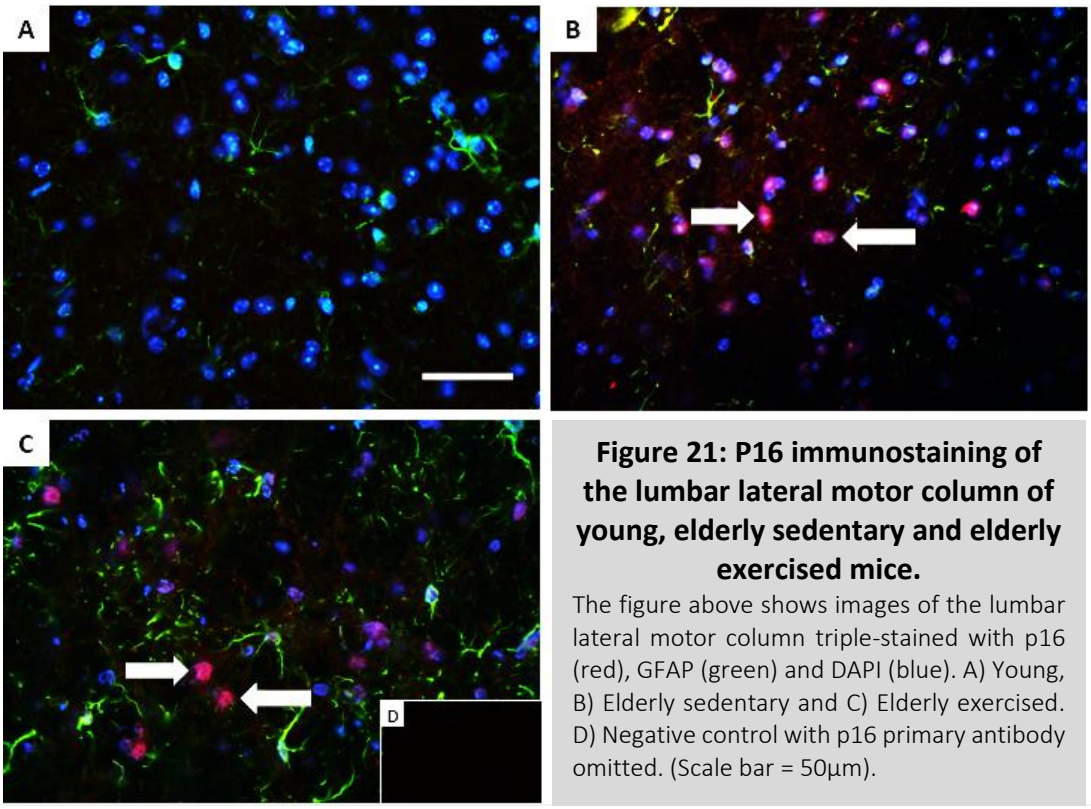

Figure 21: P16 immunostaining of the lumbar lateral motor column of young, elderly sedentary and elderly exercised mice.

The figure above shows images of the lumbar lateral motor column triple-stained with p16 (red), GFAP (green) and DAPI (blue). A) Young, B) Elderly sedentary and C) Elderly exercised. D) Negative control with p16 primary antibody omitted. (Scale bar = 50µm).

5.3.3 P16 positive motoneurons

Due to the incompatibility of the rabbit anti-p16Ink4a antibody and the rabbit anti-ChAT antibody, co-staining of these two proteins was performed but the resulting immunostaining was indistinguishable for the two proteins and therefore was not analysed. Images acquired of p16 co-stained with GFAP show p16-positive nuclei in the lumbar lateral motor column of elderly mice, and diffuse cytoplasmic staining of cell bodies (Fig. 22).

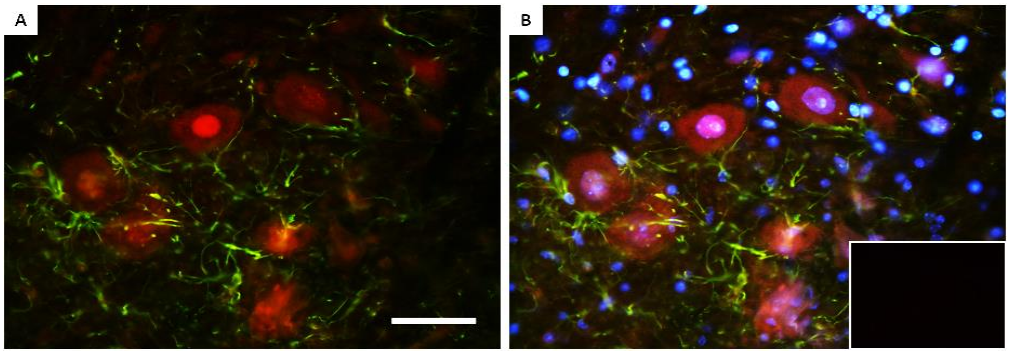

Figure 22: P16 positive staining in motoneurons

A) P16 positive staining overlaid with anti-GFAP staining. Diffuse cytoplasmic staining is visible around the positive nucleus. B) P16, GFAP and DAPI triple-labelling shows p16 appears positive within the nucleus. Negative control bottom right. (Scale bar = 50µm)

Due to the limitation of being unable to co-stain with ChAT to confirm the p16 positive cells are motoneurons, ImageJ was used to measure the diameter of both the longest axis of the cell, and then perpendicular to that axis (orthogonal axis) (Fig. 23). The two values were then averaged to determine a final diameter. Analysis of soma diameter of the cells containing p16 positive staining revealed the diameters of the 4 cells measured to be: 37.3µm, 39.1µm, 35.5µm and 36.2µm, consistent with what is documented in the literature for motoneuron diameter (Ishihara *et al.*, 2001).

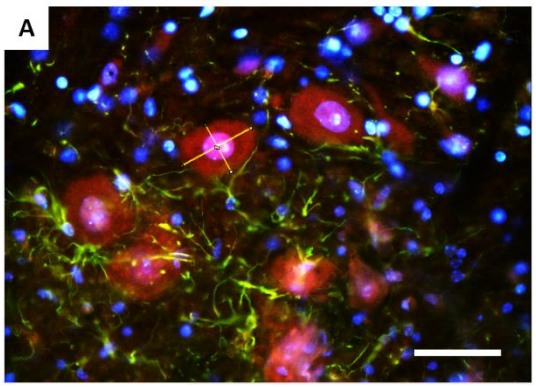

B

	Area	Mean	Min	Max	Angle	Length
1	21.536	97.836	21	250	25.694	43.567
2	16.049	115.254	21	247	-53.267	30.963
3	23.594	88.490	25	228	-29.407	46.767
4	15.775	82.952	16	150	61.928	31.481
5	18.930	23.266	0	54	-60.396	37.486
6	17.284	27.657	0	66	35.981	33.411
7	15.089	21.975	4	84	8.276	41.169
8	11.523	23.795	0	70	-85.236	31.219

Figure 23: Analysis of p16-positive motoneurons

To confirm the p16-positive cells as motoneurons, the diameter of the longest axis of the cell, and perpendicular to that axis (orthogonal axis) were measured to give an average of the two which was used as the actual diameter (unpublished data). (Scale bar = 50µm).

Figure 23B shows the mean greyscale values of 4 cells, each pair of values represents first the longest axis of the cell body, and then perpendicular to that axis. Each pair of means was averaged to calculate diameter of the cells.

5.3.4 Western blot

The western blotting technique was optimized to visualize p16 and allow for quantification of fold-change of p16 expression within young versus elderly sedentary spinal cord tissue. The initial blot was run with varying amounts of protein loaded into the wells: 10, 20, 40 and 80µg. The blot shows bands at 16kDa for the 10 and 20µg with high background, and no distinguishable band for the higher amounts as there was too much protein to be separated out effectively. The white marks indicated by the arrows are the bands of the protein ladder indicating the levels of molecular weights.

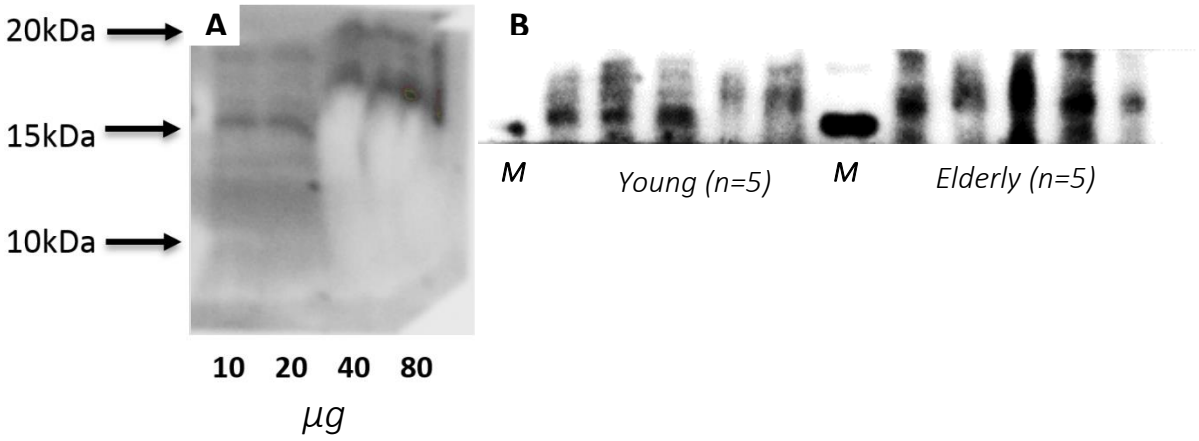

Figure 24: Western blot results

A) Western blot showing bands at 16kDa within the lanes loaded with 10 and 20µg of protein but protein overloading with 40 and 80µg of protein. B) Resultant blot which shows the marker (far left band) at 15kDa and bands of anti p16-staining present at 16kDa, which appear to be thicker in the elderly group. (M = Marker band at 16kDa)

The first western blot performed allowed optimization of protein loading amount for future blots. The optimisation blot shows bands present at 16kDa with high background staining, but no bands clearly visible with 40 and 80µg of loaded protein (Fig. 25A). Due to time restraints and antibody availability, the western blot technique was not optimised to a level which allowed for quantification of fold change in p16 levels between young and elderly spinal cord. A resulting blot shows bands at 16kDa which appear larger in elderly samples, but this is only speculative as staining of the loading control was unsuccessful which is required for reference.

5.4 Glial-Derived Neurotrophic Factor

5.4.1 Immunohistochemistry

Sections of mouse spinal cord were co-stained with sheep anti-GDNF and rabbit anti-ChAT to measure levels of in GDNF within spinal motoneurons. Figure 25 shows immunostaining of ChAT and GDNF, and the result of the two combined images with DAPI to label nuclei. GDNF is located within motoneurons as depicted in figure 25, C.

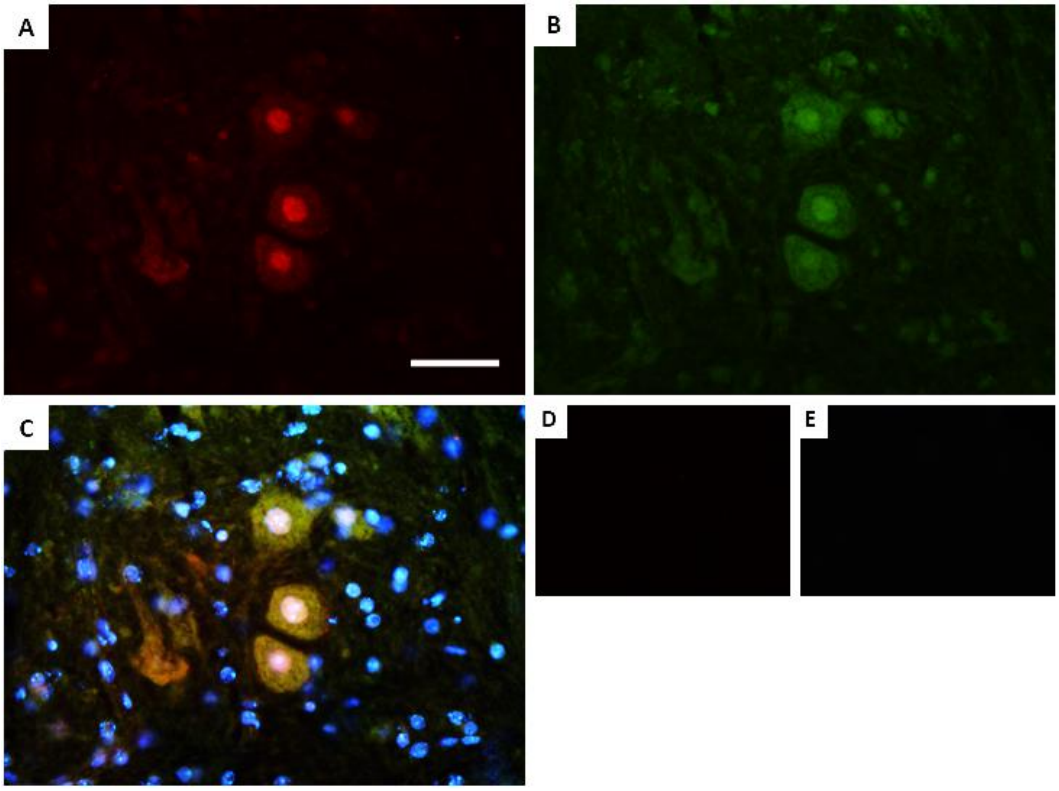

Figure 25: Glial-Derived Neurotrophic Factor (GDNF) triple-labelling
Figure above shows staining of A) Choline-Acetyl Transferase (ChAT) within motoneurons, B) GDNF and C) ChAT overlaid with Glial-Derived Neurotrophic Factor (GDNF) and DAPI. Images D and E are negative control sections of ChAT and GDNF respectively. (Scale bar = 50µm).

Images acquired from the lumbar lateral motor column show motoneurons with GDNF staining within the nucleus and the cytoplasm (Fig. 26). The GDNF staining pattern shows vesicle-like staining around the motoneurons, consistent with what is documented in the literature (McCullough *et al.*, 2013). GDNF staining is visibly brighter in the elderly exercised group compared to both the young, and the elderly sedentary groups. Important to note is that the images acquired for the elderly exercised group were taken at half the gain of the other two groups due to the level of brightness resulting in saturation. This meant that the resulting average greyscale values were doubled to allow them to be compared to the other groups.

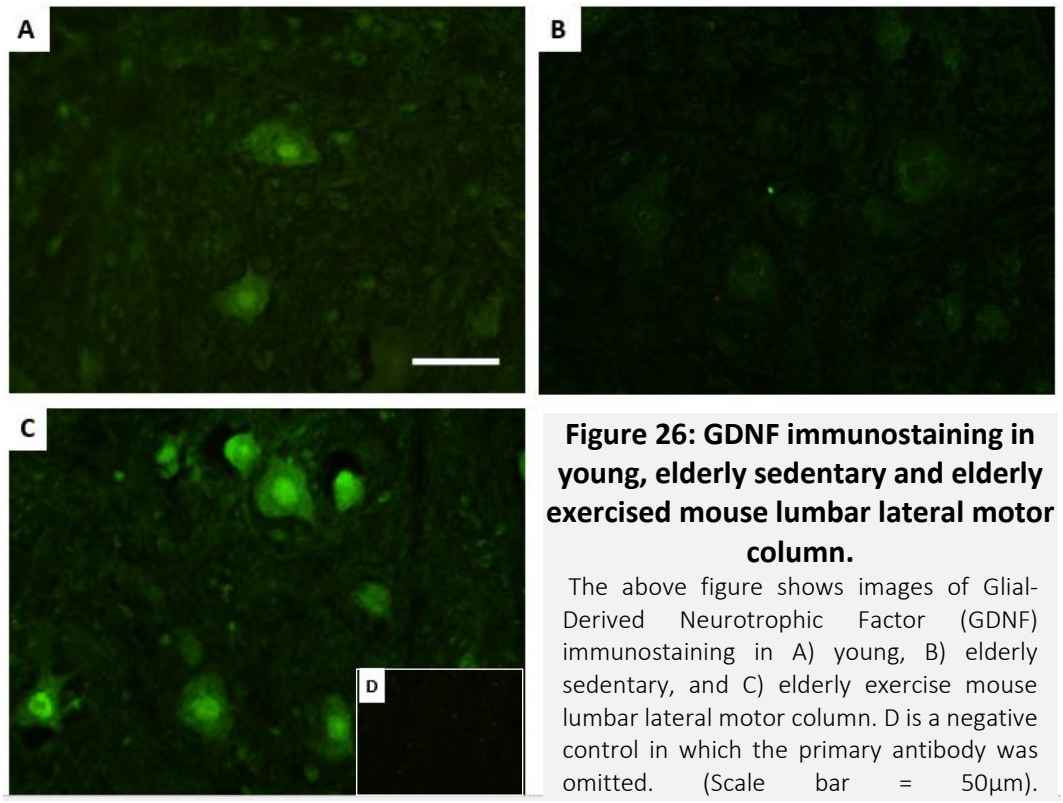

Figure 26: GDNF immunostaining in young, elderly sedentary and elderly exercised mouse lumbar lateral motor column.

The above figure shows images of Glial-Derived Neurotrophic Factor (GDNF) immunostaining in A) young, B) elderly sedentary, and C) elderly exercise mouse lumbar lateral motor column. D is a negative control in which the primary antibody was omitted. (Scale bar = 50µm).

5.4.2 Statistical analysis of GDNF immunostaining of motoneurons

Analysis of the changes in GDNF immunostaining was performed using a linear mixed model (LMM) on R software (R Core Team, 2013). The results showed that there was no change in the level of GDNF between young and elderly sedentary animals, but a significant increase was observed between elderly sedentary and elderly exercised animals ($p<0.0001$). (Fig. 27).

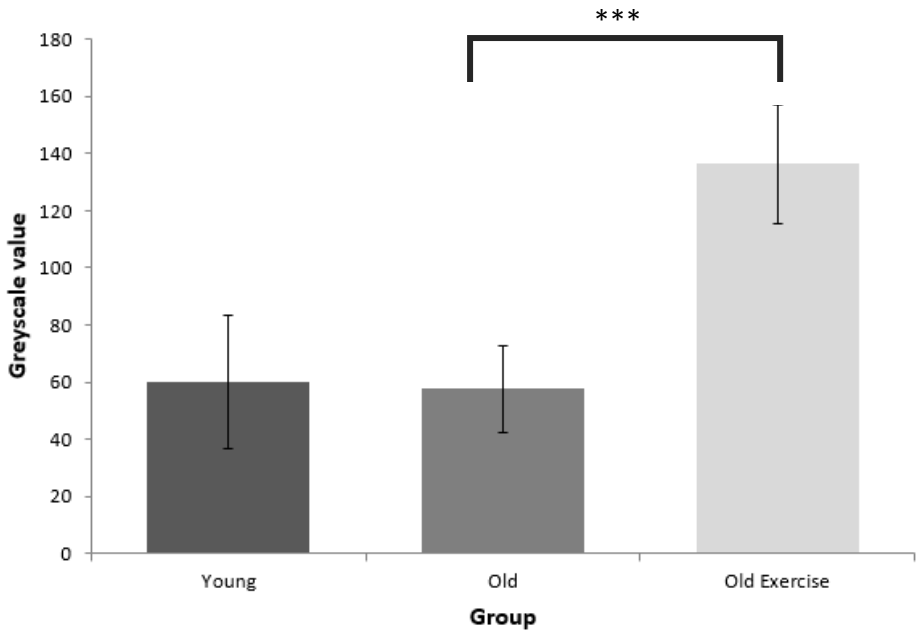

Figure 27: Changes in GDNF staining levels with age and exercise.

The above graph shows average greyscale value of Glial-Derived Neurotrophic Factor (GDNF) immunostaining of motoneurons in young, elderly sedentary and elderly exercised spinal cord. A linear mixed model was used to calculate statistical values. There was no change in average greyscale value between young and elderly sedentary, but a significant increase in GDNF level between elderly sedentary and exercised ($p<0.0001$***). Data expressed as mean ± SEM.

5.4.3 Statistical analysis of GDNF immunostaining within motoneuron cytoplasm

Analysis of the changes in GDNF immunostaining within motoneuron cytoplasm in young, elderly sedentary and elderly exercised spinal cord was performed using a linear mixed model (LMM) on R software (R Core Team, 2013). By excluding the nuclear compartment in the analysis, the average greyscale value of the elderly exercised group was reduced from 136 to 123, whereas the other two groups were unaffected. The observed trends are unchanged, with exercise showing a significant increase in motoneuron GDNF levels ($p<0.0001$). (Fig. 28)

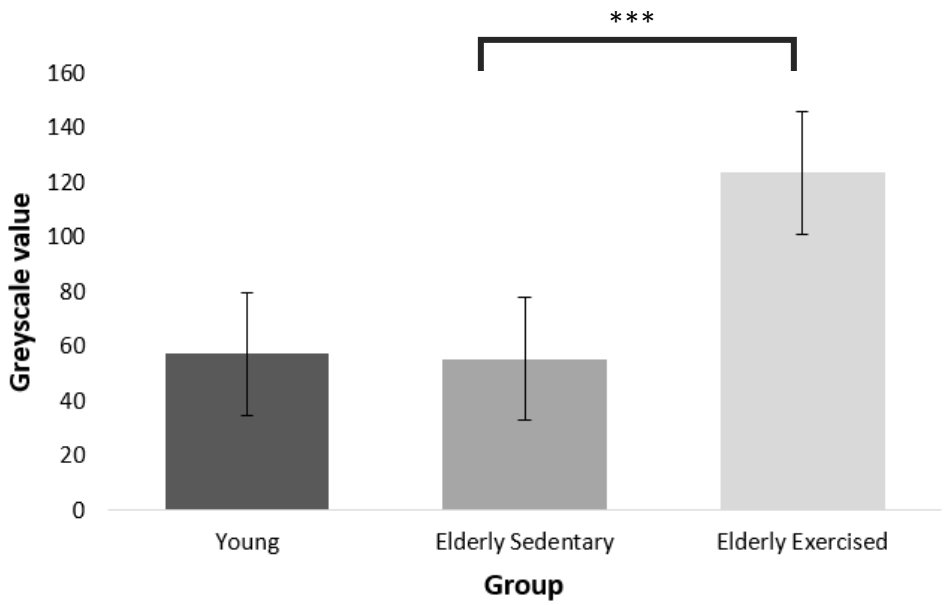

Figure 28: Changes in cytoplasmic GDNF staining levels with age and exercise.
The above graph shows average greyscale value of Glial-Derived Neurotrophic Factor (GDNF) immunostaining of motoneuron cytoplasm within young, elderly sedentary and elderly exercised spinal cord. A linear mixed model was used to calculate statistical values. There was no change in average greyscale value between young and elderly sedentary, but a significant increase in GDNF level between elderly sedentary and exercised ($p<0.0001$***). Data expressed as mean ± SEM.

5.4.4 GDNF staining levels and average distance run by exercised animals

The two data sets of GDNF immunostaining and average distance travelled per day for each animal were plotted together to establish if there was an observed correlation between the two data sets. The results show no observable trend between distance travelled and level of GDNF staining.

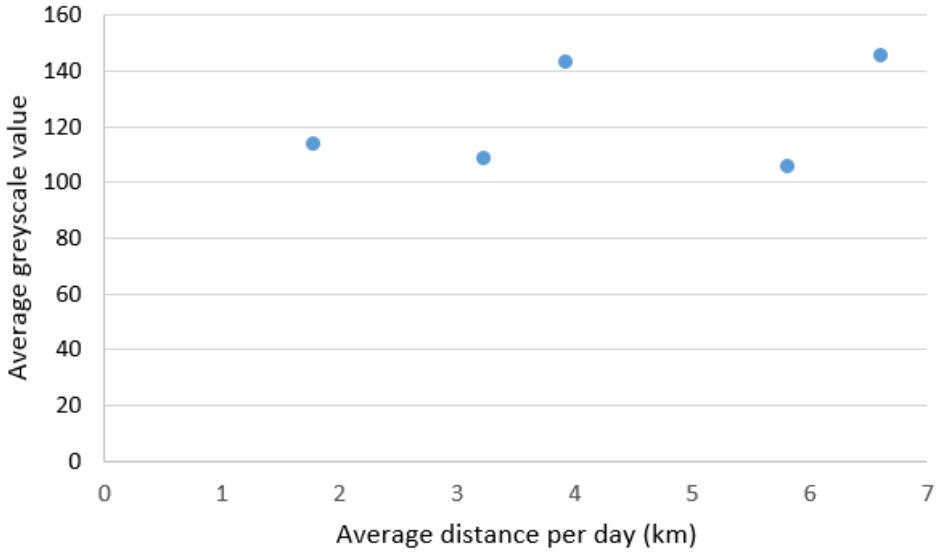

Figure 29: Changes in GDNF staining plotted with average distance run per day
The above graph shows average greyscale value of Glial-Derived Neurotrophic Factor (GDNF) immunostaining elderly exercised animals, plotted with the average distance in kilometres run by each animal. The results demonstrate no relationship between distance travelled and GDNF immunostaining.

5.5 Exercise levels of elderly exercised animals

Table 3: Distance travelled (both total and daily average kilometres) per elderly exercised animal

Animal	1	2	3	4	5
Total distance travelled	805	478	216	393	709
Average distance per day	6.7	3.9	1.8	3.2	5.8

For the exercise protocol, elderly animals were individually housed with free access to a running wheel which was fitted with a device to track the distance travelled by each animal. Table 3 shows the large amount of variance in amount of exercise performed by each animal, varying from <2km - almost 7km per day on average, consistent with what is reported for both the C57Bl/6 breed, and for the 20-month age group (van Praag *et al.*, 1999; Goh & Ladiges, 2015).

Discussion

6 Discussion

This study investigated astrocytes as drivers of motoneuron death and subsequent loss of muscle mass with ageing. The primary aims of the current study were to determine whether astrocytes in the aged mouse lumbar lateral motor column are becoming senescent, and whether the emergence of this phenotype can be prevented or reduced by late-life endurance exercise. This study aimed to investigate changes in GDNF - the most potent neurotrophic factor associated with motoneuron survival (McCullough et al., 2013), with age and exercise, and the potential of this trophic factor to attenuate the senescent or reactive phenotype of astrocytes.

6.1 The rodent model for investigating sarcopenia

It is worth noting that the current study uses a rodent model to investigate the effects of ageing on various parameters of the neuromuscular system. The C57B/6 mouse line was chosen due to the observed similarities in age-related musculoskeletal decline - reflecting both the characteristics and relative age of onset of decline observed in humans (Ballak *et al.*, 2014). Mice age much more rapidly than humans, therefore the effects of ageing are interpreted based on relative lifespan - also expressed as percentage of mean life span (MLS) (24 month-old mice show a similar degree of age-associated decline to a 70 year-old human) (Ballak *et al.*, 2014)(The Jackson Laboratory, 2017).

Despite the fact that rodents are not directly comparable to humans, the mouse model serves as a useful tool in understanding the relative effects of ageing on the muscular system, and provides useful insight into what may be occurring the ageing human neuromuscular system.

6.2 Astrogliosis and astrocyte reactivity

Reactive gliosis describes the process by which astrocytes react to insults of the CNS, either mild such as with ageing, or severe insults such as physical injury (Sofroniew & Vinters, 2010). Consistent with the literature, the current study demonstrated that GFAP levels were low in

young lumbar lateral motor column, with only a few astrocytic processes visible in images taken from this region. This indicates that astrocytes within the young lumbar lateral motor column are functioning normally and show no signs of astrogliosis or reactivity (Fig. 30). GFAP is not essential for the function of healthy astrocytes, therefore is often at low levels or undetectable in nervous tissue from healthy rodents, but is necessary for astrogliosis or glial scar formation (Faulkner *et al.*, 2004; Sofroniew, 2009).

Consistent with the hypothesis, there was a visible increase in anti-GFAP staining levels within elderly sedentary mouse lateral motor column compared to that of young, indicating that astrocytes are undergoing a transition toward a reactive state. The response of increased GFAP levels within astrocytes with ageing relates to the age-associated accumulation of oxidative damage such as lipoperoxidation, and other cellular stresses that drive astrocytes to become reactive (Sofroniew & Vinters, 2010). Astrocytes are sensitive to low levels of H_2O_2, and are therefore more susceptible to the oxidative stresses accumulated with age (Mombach *et al.*, 2015). Although this change in GFAP levels failed to reach statistical significance with my method of quantification ($p=0.052$), the observed trend demonstrates that astrocytes are becoming reactive to some extent.

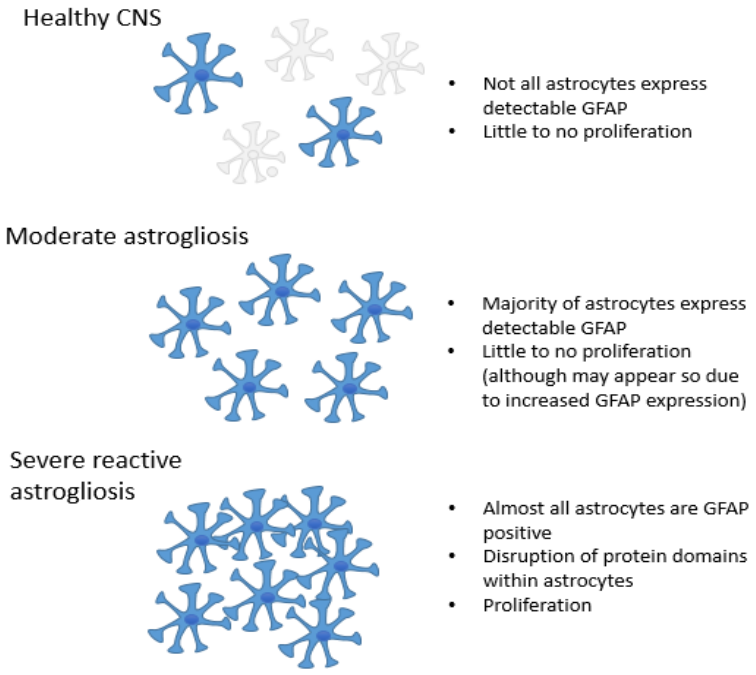

Figure 30: Degrees of astrogliosis

Schematic representation of the gradation of degrees of astrogliosis and their corresponding levels of GFAP expression and cellular proliferation. (Figure adapted from (Sofroniew & Vinters, 2010))

Based on the nature of mild astrogliosis which has been associated with ageing, it is likely that the increased GFAP levels are due to more GFAP per astrocyte, which can often be mistaken for proliferation of astrocytes that occurs as a result of severe CNS insult such as with injury or disease (Sofroniew, 2009). Although to the naked eye, it would appear that there are more astrocytes in an image taken from an elderly lateral motor column compared to a young, this is because GFAP is not present at detectable levels in all astrocytes of a healthy CNS as described above (Sofroniew & Vinters, 2010) (Fig. 30). Therefore, when GFAP is upregulated within astrocytes with their transition to the reactive state, this results in more detectable astrocytes with anti-GFAP immunostaining, but not necessarily more astrocytes. Proliferation of astrocytes is associated with severe trauma or disease of the CNS, which is not comparable to the level of cellular stresses observed with normal ageing (Faulkner *et al.*, 2004).

Due to the extensive nature of astrocytic projections which span up to 40 microns in diameter, the techniques used to evaluate astrocyte reactivity resulted in a limited perspective of astrocyte morphology. Sections were cut at 16 microns to optimise immunostaining of GFAP. To

visualise astrocytes in their entirety and evaluate morphological changes such as hypertrophy of projections, confocal microscopy would be required which would be a useful addition to the current findings. This method would add depth to our understanding of changes in amount of GFAP within an astrocyte with ageing and subsequent morphological changes associated with the reactive phenotype.

A minor limitation of the methods used in this study, was the inability to distinguish whole individual astrocytes within an image. This limitation resulted in the number of data points for analysis being limited to the number of images, instead of number of cells, giving fewer data points per animal and weaker statistical power. Image analysis was performed using Ilastik, an *Interactive Learning and Segmentation software (*Heidelberg Collaboratory for Image Processing (HCI), Germany). *Ilastik* was trained to recognise astrocytic staining and exclude background. By using a computer learning programme to select astrocytic staining, all selection bias was avoided as all regions containing anti-GFAP staining were included in the analysis, regardless of brightness. In addition to this, batch processing ensures that identical selection criteria were applied to every image, so trends in change of GFAP immunostaining are real, but did not reach statistical significance as a consequence of the methods used.

The observed level of astrocytic reactivity is not categorised as severe, but may still hold significance in terms of astrocytic neuroprotective capacity of motoneurons with ageing. Astrogliosis is a graded response, not an all-or-none response, therefore any level of reactivity will negatively impact astrocytic function to an extent (García-Matas *et al.*, 2008; Sofroniew, 2009). Functional alterations of reactive astrocytes include the induction of NF-kB signalling pathways which induce a neuroinflammatory response (Brambilla *et al.*, 2009). This inflammatory phenotype of astrocytes has been implicated in the accelerated death of motoneurons observed in ALS, as well as with normal ageing (Brambilla *et al.*, 2009; Das & Svendsen, 2015; Rodríguez-Arellano *et al.*, 2016). The age-associated reduction in astrocytic function is deleterious to the neurons it supports, which provides a mechanism by which

astrocytes contribute to the death of motoneurons observed with ageing. The observed increase in GFAP, indicative of astrocyte reactivity, supports the initial hypothesis suggesting age-associated astrocyte reactivity as a driver for motoneuron death, and the resulting loss of muscle mass associated as a consequence of denervation.

Exercise was hypothesised to reduce changes in astrocyte reactivity with age, based on the understanding that exercise reduces age-associated oxidative stress and inflammation (Schafer *et al.*, 2016). Interestingly, conflicting results suggest that exercise may have the opposite effect, as rats which were subjected to daily treadmill running demonstrated an increased GFAP expression within the hippocampus (Saur *et al.*, 2014). These findings were suggested to reflect an increase in astrocyte metabolism and protein synthesis, implying a healthy response to increased physiological demand (Saur *et al.*, 2014). Despite these findings, the abundance of literature reports an exercise-induced reduction in GFAP levels in the context of reducing astrogliosis and the associated chronic inflammation observed (Bernardi *et al.*, 2013; Kim *et al.*, 2014).

Results from this study reported no significant change in GFAP levels following 4 months of exercise in late life, which refutes the initial hypothesis. The lack of correlation observed between GFAP levels and amount of exercise also indicates that the level of exercise had no observed effect on GFAP expression. To address the discordance of this finding with current literature, the studies referenced above subjected their animals to walk or run a given distance on a treadmill each day, which may differ in the level of exertion as well as the distance run by mice which run as they choose. In addition to this, there is little data reporting on exercise-associated changes in GFAP within the spinal cord, as the studies referenced above measured GFAP levels of various brain regions which are not necessarily affected by exercise to the same extent. The current findings indicate that the protective mechanism by which exercise reduces the effects of sarcopenia, and protect against motoneuron death with age are not due to a reduction in astrogliosis and astrocyte reactivity.

Astrocytes have been widely implicated as contributors to age-associated neurodegeneration and neurodegenerative conditions in their reactive state (Bhat *et al.*, 2012; Rodríguez-Arellano *et al.*, 2016). Here, we report that astrocytes show an age-related transition toward a more reactive state, and therefore may show reduced support to motoneurons, contributing to their death with ageing. In view of these findings, the next aim of this study was to identify the driver of this astrocytic transition to the reactive state, in particular, cellular senescence which has been suggested as a driver of astrogliosis and neuro-inflammation with ageing (Bitto *et al.*, 2010; Childs *et al.*, 2015).

6.3 A new role for senescence in the ageing neuromuscular system?

A characteristic of ageing is the accumulation of senescent cells in tissues (Hewitt *et al.*, 2012; van Deursen, 2014; Hall *et al.*, 2016). Senescent astrocytes contribute to the observed age-associated inflammation of the CNS via their senescence-associated secretory phenotype (SASP), and have been implicated in the pathology of various neurodegenerative diseases (García-Matas *et al.*, 2008; Das & Svendsen, 2015; Rodríguez-Arellano *et al.*, 2016). This study aimed to find out if the accumulation of senescent astrocytes in the ageing lumbar lateral motor column could be contributing to the loss of motoneurons with age.

Immunohistochemical detection of p16Ink4a, a cyclin-dependent kinase inhibitor and the most commonly used marker of cellular senescence (Serrano *et al.*, 1993; Matjusaitis *et al.*, 2016), revealed the presence of p16-positive nuclei within the lumbar lateral motor column of aged, but not young mice. Surprisingly, these p16-positive nuclei did not coincide with GFAP immunostaining of astrocytes as has been observed in the brain (Bhat *et al.*, 2012). A western blot was performed to attempt to quantify this increase, but due to time restraints this was not optimised to allow for analysis of the blots. Although this was not analysed, it appeared there were larger bands at the level of 16kDa for elderly versus young spinal cord tissue, supporting the immunohistochemistry results that p16 expression is up-regulated in elderly spinal cord

with age. The observed lack of co-localisation of p16-positive nuclei with astrocytic GFAP staining refutes the hypothesis that astrocytes are becoming senescent with age and contributing to the death of motoneurons. This means that the reactive phenotype of astrocytes observed with age may still be implicated in motoneuron death via a reduced neuroprotective capacity, but this is not a consequence of cellular senescence.

The abundance of literature which describes the implications of astrocyte senescence on function of the CNS is based on neurodegenerative diseases of the brain and spinal cord such as Alzheimer's disease and ALS (Bhat *et al.*, 2012; Das & Svendsen, 2015). These conditions differ in their location within the CNS as well as their severity compared to normal ageing. In addition to this, the study which demonstrated the detrimental effect of senescent astrocytes on motoneurons survival, did so in culture conditions which are not necessarily translatable to *in vivo* conditions or in whole tissues (Das & Svendsen, 2015; Sharpless & Sherr, 2015). Astrocyte senescence may be a characteristic of ageing astrocytes within the brain or associated with neurodegenerative disease, but based on current findings; not a characteristic of the ageing neuromuscular system and therefore not a contributor to motor neuron death, refuting the hypothesis.

An important idea to discuss is the abundance of research on senescence performed *in vitro*, and its translation into living tissues and systems. A recent Nature review by (Sharpless & Sherr, 2015) discusses the caveats of applying the findings of *in vitro* investigation to living organisms. In contrast to the conditions in a culture dish, there is a large amount of heterogeneity in cells of whole tissues which makes identifying and characterising senescence *in vivo* a complex task. Studies which investigate senescence *in vitro* often induce this response by administering hydrogen peroxide to mimic the oxidative stress observed in whole tissues with ageing (Bitto *et al.*, 2010). The consequences of direct treatment with peroxide are not necessarily a direct reflection of the mechanisms in which age-associated cumulative oxidative damages affect astrocytes in living tissue. It is for this reason that the role of senescence *in vivo*

may be over-estimated by the methods which are used to conclude its importance, as indicated by the current findings which dismiss senescence as a driver of the reactive transition of astrocytes of the lumbar spinal cord with ageing.

Although astrocytes did not show upregulation of p16 indicative of senescence, anti-p16Ink4a staining was present in larger nuclei of the ageing lateral motor column, some of which contained diffuse, cytoplasmic staining the size of lumbar motoneurons (Ishihara *et al.*, 2001). There is no literature describing the appearance of senescent motoneurons with age, which makes the observed anti-p16-Ink4a staining within motoneuron nuclei an unexpected result. The co-localisation of p16 and motoneuron cell nuclei was unable to be confirmed with Choline Acetyltransferase (ChAT) co-staining, therefore the interpretation of this result remains speculative.

The presence of p16 within nuclei of the lumbar lateral motor column could lead to the assumption that these cells express a SASP which results in a chronic inflammatory microenvironment, as observed in culture of senescent cells (Bitto *et al.*, 2010). It is important to remember that senescence is a mechanism to halt the proliferation of damaged cells, therefore when p16 expression is observed in already terminally differentiated cells, the implications of its expression require further investigation. It has been demonstrated that induction of senescence in human fibroblasts via ectopic expression of p16Ink4a resulted in cell-cycle arrest without a resultant SASP (Coppé *et al.*, 2011). The observation that cell-cycle arrest can occur without a consequent SASP signifies that the SASP is not a result of p16 expression or the senescent phenotype, but a response to damage, independent of growth arrest (Coppé *et al.*, 2011). Therefore, the presence of p16 within the lumbar lateral motor column may not be a contributor to the chronic, low-level inflammatory environment of the CNS observed with ageing.

The resultant changes associated with p16 expression within motoneurons with ageing may not be as a consequence of a SASP, but another downstream pathway. The expression of phosphorylated Rb and E2F (two known downstream targets of p16 in the induction of senescence) (Fig. 4) was observed within ALS-affected motoneurons which stained positive for TUNEL and caspase-3, two known markers of apoptosis (Ranganathan & Bowser, 2010). In view of this finding, the observed increase in p16 expression may be indicative of induction of motoneuron cell death, a proposed driver for atrophy of muscle fibers and sarcopenia.

Further experimentation is needed to investigate this finding in terms of the presence of p16 within motoneurons within the lateral motor column, and the consequences of this expression. It would be useful to measure circulating cytokines and interleukins to determine if there is a SASP associated with the p16 expression observed. Based on the finding that p16 expression co-localises with markers of apoptosis in spinal cord of ALS-affected humans, it would be useful to co-stain the mouse lumbar lateral motor column with p16 and TUNEL or caspase 3, to confirm that motoneurons may be fated to apoptosis. In view of the aims and hypotheses of the current study, in can be concluded that senescence is not a driver for motoneuron death due to the deleterious effects of the SASP. Instead, p16 expression may directly precede motoneuron cell death, which drives the loss of muscle mass via the afore mentioned, disuse atrophy.

6.4 Glial-Derived Neurotrophic Factor increases with exercise: Implications for motoneuron survival

The next aim of this study was to investigate changes in a critical trophic factor for motoneurons: glial-derived neurotrophic factor (GDNF). GDNF is required for the survival and proliferation of motoneurons (Gyorkos *et al.*, 2014). I hypothesised that GDNF would reduce with age, potentially as a result of the reduction in skeletal muscle mass observed with age and consequent loss of retrograde supply to motoneurons. The findings in the current study demonstrated that there was no significant reduction of GDNF in the lumbar lateral motor

column with age, refuting my hypothesis. This finding indicates that an age-associated reduction in GDNF levels within lumbar lateral column motoneurons is not a contributor to motoneuron death with ageing.

Despite the lack of difference in amount of GDNF within the lumbar lateral column of mice with ageing, current findings reported a marked increase in the level of GDNF of elderly exercised compared to elderly sedentary animals, consistent with previous findings (Côté *et al.*, 2011; McCullough *et al.*, 2013). This is an interesting result, as exercise appears to increase levels of GDNF irrespective of an age-associated reduction, implying that exercise may have the same effect on young motoneurons. The increased GDNF levels showed no correlation with amount of exercise which indicates that the ability of skeletal muscle to increase its production of GDNF is not limitless, but has a maximal rate which cannot be exceeded with further exertion.

In the context of sarcopenia, this result demonstrates that the protective effects of exercise against neuromuscular deterioration are observed with even moderate levels of activity. The activity level of the mice in this study was consistent with what has previously been reported for the C57Bl/6 breed, and for the 20-month old age group (van Praag *et al.*, 1999; Goh & Ladiges, 2015). The recorded running levels indicate that one animal ran almost four times that of another animal from the same cohort, yet the observed increase in the trophic factor, GDNF were unaffected by level of exertion. This finding gives a strong indication that low-level exercise is sufficient to increase the skeletal-muscle trophic supply of GDNF to motoneurons, and exert benefits in enhancing motoneuron survival and slowing progression of sarcopenia in late-life.

It would be useful to further characterise the effect of exercise by including a cohort of young exercised animals to determine if the same increase in GDNF level is observed. It would also be beneficial to run animals at varying given levels of exercise, limiting the amount of exercise

for some animals to determine the amount of exercise required to increase GDNF levels, and ascertain the level at which the increase in GDNF plateaus.

Although the effects of an exercise-induced increase in spinal motoneuron GDNF levels were not assessed, in can be incurred from the literature that upregulated GDNF levels have various benefits for motoneuron survival (Henderson *et al.*, 1994). In particular, overexpression of GDNF in skeletal muscle has shown potent effects on neuromuscular remodelling, NMJ innervation, motoneuron survival and motor performance in aged and SOD1 mutant mice (Li *et al.*, 2007; McCullough *et al.*, 2013; Park & Höke, 2014). It would be interesting to further characterise these effects in this mouse model, and investigate whether a correlation is observed between GDNF levels and motoneuron survival, as well as effects on NMJ innervation. These investigations would provide insight as to how GDNF may play a role in attenuating the progression of sarcopenia, by reducing motoneuron loss and subsequent muscle fiber disuse atrophy.

Overall, the reported exercise-induced GDNF increase supports the hypothesis that exercise may induce an activity-dependent increase in skeletal muscle-derived GDNF, which is transported back to motoneuron cell bodies in the lumbar lateral motor column to exert its protective effects. This finding demonstrates the potential protective role of exercise against motoneuron loss with age, irrespective of the age at which exercise was initiated, and irrespective of amount of exercise performed.

As mentioned in the results section, the observed staining pattern of GDNF included bright staining within the nucleus for both GDNF and ChAT, an unexpected result. Previous investigation of the effects of exercise on GDNF levels within motoneurons revealed a staining pattern similar to what was observed in the present study, but staining was absent in the nucleus (McCullough *et al.*, 2013). To account for the potential artefactual staining which could confound the data, motoneuron GDNF levels were measured in only the cytoplasmic

compartment. The resulting trend remained unchanged, but the mean greyscale value of the exercised group was reduced from 136 to 123. This nuclear staining could be attributed to bleed through of the very bright DAPI staining of nuclei, as puncta within some nuclei align directly with what is observed in the blue channel for DAPI staining (Fig. 31).

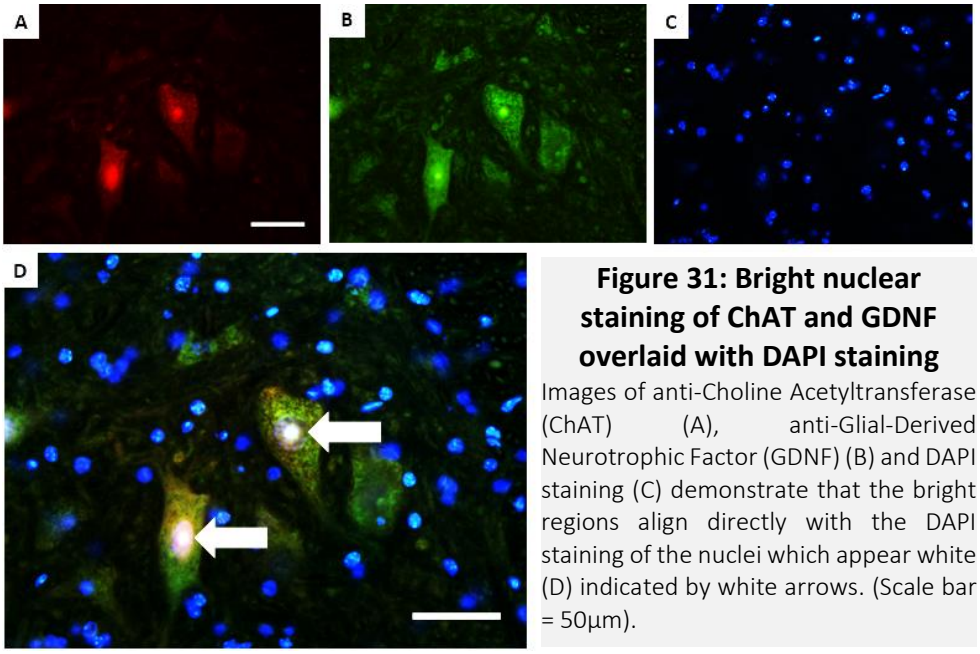

Figure 31: Bright nuclear staining of ChAT and GDNF overlaid with DAPI staining
Images of anti-Choline Acetyltransferase (ChAT) (A), anti-Glial-Derived Neurotrophic Factor (GDNF) (B) and DAPI staining (C) demonstrate that the bright regions align directly with the DAPI staining of the nuclei which appear white (D) indicated by white arrows. (Scale bar = 50µm).

6.5 GDNF: Not sufficient to reduce astrocyte reactivity or cellular senescence

Based on findings which have demonstrated that astrocytes play a role in the death of neurons observed with ageing and neurodegenerative disease via their senescent phenotype (Maragakis & Rothstein, 2006; Das & Svendsen, 2015; Rodríguez-Arellano *et al.*, 2016), this study aimed to investigate whether this astrocyte senescence may be implicated in motoneuron death with age. GDNF has shown promising effects in reducing astrocyte reactivity and senescence (Zhao *et al.*, 2004; Das & Svendsen, 2015), which in turn has benefits for motoneuron survival and viability. Combining the findings of each component of the current investigation, although exercise was able to significantly increase levels of GDNF within motoneurons of the lumbar

lateral motor column, this did not correlate with a reduction in GFAP levels, indicating that astrocyte reactivity was not reduced by the presence of GDNF. In addition to this, GDNF was not sufficient to reduce the presence of p16 positive nuclei within the lumbar lateral column.

The ability of GDNF to act on astrocytes via its receptors GFR-α and RET depends on its ability to exit motoneuron cell bodies and exert its effects on astrocytes. The research which has described the protective effects of GDNF for astrocytic function has failed to demonstrate the mechanism for GDNF to act on astrocytes *in vivo*. One such study cultured astrocytes in GDNF; an approach which has countless limitations when comparing the mode of action of this trophic factor within whole tissues. There is no evidence to suggest the amount of GDNF administered is comparable to that circulating within the spinal cord, which makes it difficult to draw conclusions based on *in vivo* conditions.

Further methods of investigating the relationship between GDNF and astrogliosis involved genetically overexpressing GDNF in skeletal muscle to demonstrate its effects on reducing astrogliosis and increasing astrocyte neuroprotection (Zhao *et al.*, 2004; Li *et al.*, 2007). Again, although these methods demonstrate the potential for GDNF as an exogenous treatment for diseases such as ALS and its benefits for motoneuron survival, they fail to address how *in vivo*, GDNF may act on astrocytes and implicate its protective benefits. In view of current findings, it may be concluded that this mechanism demonstrated *in vitro* is not translated *in vivo*, and that exercise-induced GDNF is unable to exert protective effects against astrocyte reactivity or cellular senescence with ageing.

In summary, these results demonstrate that with ageing; GFAP showed a tendency to increase, p16 appears within cells which appear to be motoneurons, and GDNF showed no change. Exercise showed no effect on the expression of p16 or GFAP, but induced a large increase in GDNF levels within motoneurons. I believe these results demonstrate that astrocytes show a reduced neuroprotective capacity which may contribute to the death of motoneurons observed

with ageing. I also believe that the presence of p16 within motoneurons implicates their fate towards apoptosis, which contributes to loss of muscle mass and thus the progression of sarcopenia with age. (Fig. 32).

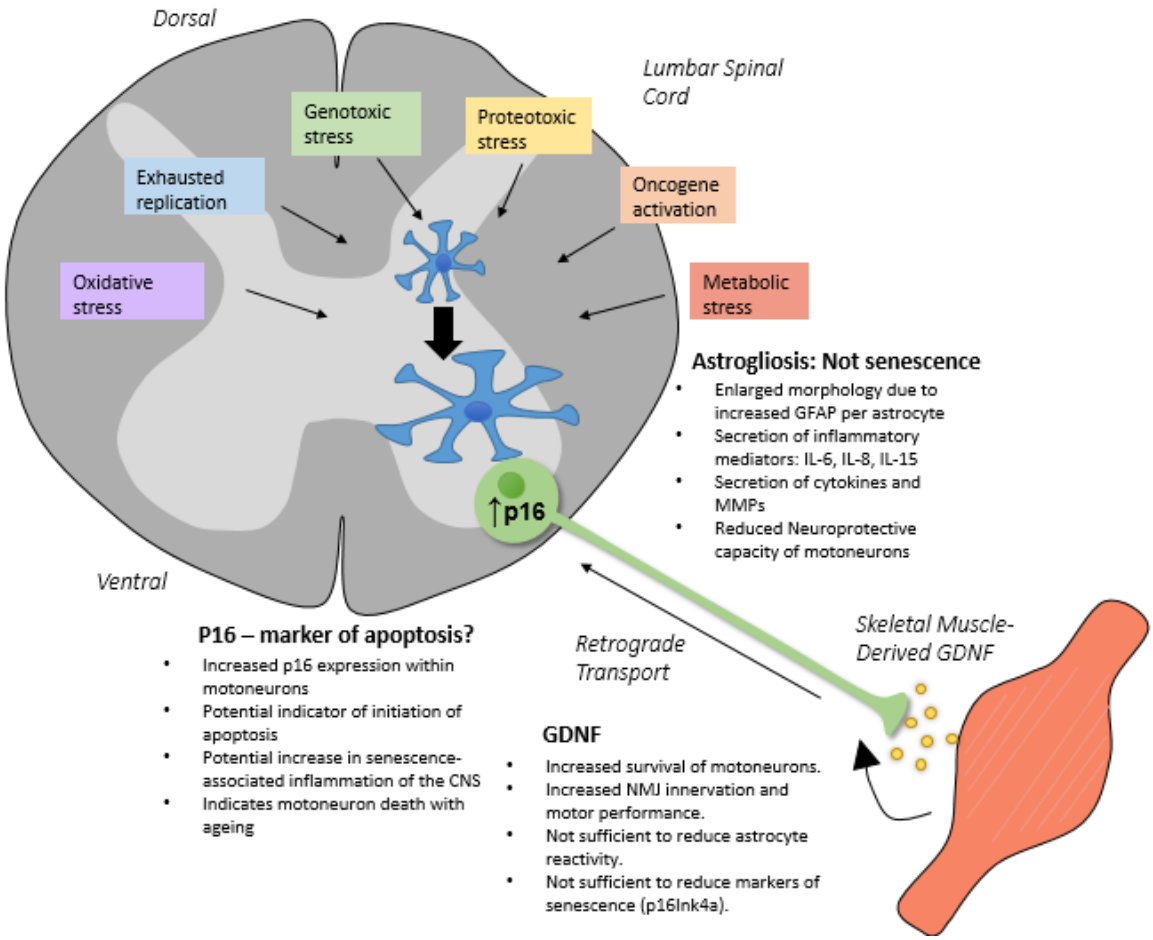

Figure 32: Schematic demonstration of the findings of the current study

This schematic summarises the findings of the current study. Skeletal muscle-derived Glial-Derived Neurotrophic Factor (GDNF) is taken up at the NMJ and exerts its effects directly on motoneurons to increase their survival and innervation of muscle fibers. Astrocytes show a reactive phenotype with age, but do not show markers of senescence: Instead, motoneurons show upregulated p16, which potentially marks them for apoptosis, contributing to denervation-induced atrophy of muscle fibers and sarcopenia.

6.6 Conclusions and future directions

Here we report that astrocytes show an age-associated transition toward a more reactive state, indicating that they may show a reduced neuroprotective capacity of motoneurons, contributing to motoneuron death and subsequent loss of muscle mass with ageing. The dysfunction of astrocytes with ageing was not associated with expression of p16 which refutes my initial hypothesis that advancing age would trigger a senescent phenotype in astrocytes, and that this, in turn, might contribute to the loss of motoneurons and ultimately to sarcopenia. However, the surprising finding that p16 was probably elevated in motoneurons suggests that motoneurons themselves may be affected by p16 expression, in a manner that is not consistent with the senescent phenotype characterised *in vitro*. Instead, this p16 expression within motoneurons may be marking initiation of the apoptotic pathway (Ranganathan & Bowser, 2010), demonstrating that motoneurons are dying with age, driving the progression of sarcopenia.

Exercise was investigated as it is a well-established intervention to slow the progression of sarcopenia via mechanisms which remain unknown. The current findings demonstrate that exercise was not able to reduce the reactive phenotype of astrocytes or the appearance of p16-positive nuclei within the lumbar lateral motor column. Exercise was able to induce a large increase in GDNF levels within spinal motoneurons, which likely increases motoneuron survival, number of motor units, innervation at the NMJ, and motor function, as previously reported (Li *et al.*, 2007; Park & Höke, 2014). It would also be useful to include analysis of parallel changes in neuromuscular status as a result of change in GDNF levels to evaluate the direct benefits of this trophic factor for motoneurons.

It has become apparent during the course of the study that senescence is a very broad term with complex roles and implications in living systems. Future work needs to identify the p16 positive cells present, and to measure other markers of the SASP such as IL-6, IL-8 and TNF-α to evaluate changes in neuroinflammation and whether these are attributable to the presence of p16-positive cells. Based on the findings which implicate the p16-Rb-E2F pathway of

senescence induction in apoptosis, it would be useful to co-stain p16 with apoptotic markers such as TUNEL and caspase-3, to determine if p16 expression precedes motoneuron death - a driver for sarcopenia.

Investigations into mechanisms of sarcopenia have traditionally focused on the muscle where changes are visibly occurring. The direct effects of age could manifest in the muscle, but if cells higher up the chain of command were directly affected, then muscle would surely be impacted as a secondary consequence - such as is observed following the death of motoneurons causing disuse atrophy of orphaned muscle fibers. By understanding that the neuromuscular system consists of a chain of command, and that each component in the chain is necessary to allow maintenance of muscle mass, we can see the diverse nature of the cells involved in maintaining this system.

In this work I have begun to investigate the extent to which changes in the nervous system might impact on muscles, and thereby to evaluate the contribution of non-muscle tissues to sarcopenia. Although my hypotheses were not fully supported by my data, I have described interesting changes in important intercellular signalling factors and processes that potentially point to new avenues to explore for a better understanding of the neuromuscular changes that occur with advancing age. Only when we know why the nervous system and the skeletal muscles undergo age-related degenerative change will be in a position to prevent or delay those changes, and therefore to keep people strong, healthy, and independent further into their old age.

References

7 References

Altman DG & Bland JM. (2011). How to obtain the P value from a confidence interval. *BMJ* **343**.

Anon (2017). Falls in people aged 50 and over. *Health and Quality and Safety Commission New Zealand.*

Anon (2017). Life span as a biomarker. *The Jackson Laboratory*. Available at: https://www.jax.org/research-and-faculty/research-labs/the-harrison-lab/gerontology/life-span-as-a-biomarker [Accessed October 8, 2017].

Baar MP, Brandt RMC, Putavet DA, Klein JDD, Derks KWJ, Bourgeois BRM, Stryeck S, Rijksen Y, van Willigenburg H, Feijtel DA, van der Pluijm I, Essers J, van Cappellen WA, van Ijcken WF, Houtsmuller AB, Pothof J, de Bruin RWF, Madl T, Hoeijmakers JHJ, Campisi J & de Keizer PLJ. Targeted apoptosis of senescent cells restores tissue homeostasis in response to chemotoxicity and aging. *Cell* **169,** 132-147.

Baker DJ, Perez-Terzic C, Jin F, Pitel K, Niederländer NJ, Jeganathan K, Yamada S, Reyes S, Rowe L, Hiddinga HJ, Eberhardt NL, Terzic A & van Deursen JM. (2008). Opposing roles for p16(Ink4a) and p19(Arf) in senescence and ageing caused by BubR1 insufficiency. *Nature Cell Biology* **10,** 825-836.

Baker DJ, Wijshake T, Tchkonia T, LeBrasseur NK, Childs BG, van de Sluis B, Kirkland JL & van Deursen JM. (2011). Clearance of p16Ink4a-positive senescent cells delays ageing-associated disorders. *Nature* **479,** 232-236.

Ballak SB, Degens H, de Haan A & Jaspers RT. (2014). Aging related changes in determinants of muscle force generating capacity: A comparison of muscle aging in men and male rodents. *Ageing Research Reviews* **14,** 43-55.

Barber RP, Phelps PE, Houser CR, Crawford GD, Salvaterra PM & Vaughn JE. (1984). The morphology and distribution of neurons containing choline acetyltransferase in the adult rat spinal cord: An immunocytochemical study. *The Journal of Comparative Neurology* **229,** 329-346.

Bellaver B, Souza DG, Souza DO & Quincozes-Santos A. (2017). Hippocampal astrocyte cultures from adult and aged rats reproduce changes in glial functionality observed in the aging brain. *Molecular Neurobiology* **54,** 2969-2985.

Bernardi C, Tramontina AC, Nardin P, Biasibetti R, Costa AP, Vizueti AF, Batassini C, Tortorelli LS, Wartchow KM, Dutra MF, Bobermin L, Sesterheim P, Quincozes-Santos A, de Souza J & Gonçalves CA. (2013). Treadmill exercise induces hippocampal astroglial alterations in rats. *Neural Plasticity* **2013,** 1-10**.**

Bhat R, Crowe EP, Bitto A, Moh M, Katsetos CD, Garcia FU, Johnson FB, Trojanowski JQ, Sell C & Torres C. (2012). Astrocyte senescence as a component of Alzheimer's Disease. *PLoS ONE* **7**, e45069.

Bitto A, Sell C, Crowe E, Lorenzini A, Malaguti M, Hrelia S & Torres C. (2010). Stress-induced senescence in human and rodent astrocytes. *Experimental Cell Research* **316,** 2961-2968.

Bongers KS, Fox DK, Ebert SM, Kunkel SD, Dyle MC, Bullard SA, Dierdorff JM & Adams CM. (2013). Skeletal muscle denervation causes skeletal muscle atrophy through a pathway that involves both Gadd45a and HDAC4. *American Journal of Physiology - Endocrinology and Metabolism* **305,** 907-915**.**

Brady, J. (2015). Motoneuron NRG and NT-4 in age and exercise (Unpublished doctoral thesis). University of Otago, Dunedin, New Zealand.

Brambilla R, Persaud T, Hu X, Karmally S, Shestopalov V, Dvoriantchikova G, Ivanov D, Nathanson L, Barnum S & Bethea J. (2009). Transgenic inhibition of astroglial NF-κB improves functional outcome in experimental Autoimmune Encephalomyelitis by suppressing chronic central nervous system inflammation. *The Journal of Immunology* **182,** 2628-2640.

Bushong EA, Martone ME & Ellisman MH. (2004). Maturation of astrocyte morphology and the establishment of astrocyte domains during postnatal hippocampal development. *International Journal of Developmental Neuroscience* **22,** 73-86.

Caserotti P, Aagaard P & Puggaard L. (2008). Changes in power and force generation during coupled eccentric–concentric versus concentric muscle contraction with training and aging. *European Journal of Applied Physiology* **103,** 151-161.

Childs BG, Durik M, Baker DJ & van Deursen JM. (2015). Cellular senescence in aging and age-related disease: from mechanisms to therapy. *Nature Medicine* **21,** 1424-1435.

Cirillo G, De Luca D & Papa M. (2012). Calcium imaging of living astrocytes in the mouse spinal cord following sensory stimulation. *Neural Plasticity* **2012,** 1-6.

Coppé J-P, Rodier F, Patil CK, Freund A, Desprez P-Y & Campisi J. (2011). Tumor suppressor and aging biomarker p16(INK4a) induces cellular senescence without the associated inflammatory secretory phenotype. *The Journal of Biological Chemistry* **286,** 36396-36403.

Côté M-P, Azzam GA, Lemay MA, Zhukareva V & Houlé JD. (2011). Activity-dependent increase in neurotrophic factors is associated with an enhanced modulation of spinal reflexes after spinal cord injury. *Journal of Neurotrauma* **28,** 299-309.

Crowe EP, Tuzer F, Gregory BD, Donahue G, Gosai SJ, Cohen J, Leung YY, Yetkin E, Nativio R, Wang L-S, Sell C, Bonini NM, Berger SL, Johnson FB & Torres C. (2016). Changes in the transcriptome of human astrocytes accompanying oxidative stress-induced senescence. *Frontiers in Aging Neuroscience* **8,** 208-221.

Cruz-Jentoft AJ, Baeyens JP, Bauer JM, Boirie Y, Cederholm T, Landi F, Martin FC, Michel J-P, Rolland Y, Schneider SM, Topinková E, Vandewoude M & Zamboni M. (2010). Sarcopenia: European consensus on definition and diagnosis: Report of the European working group on sarcopenia in older people. *Age and Ageing* **39,** 412-423.

Das MM & Svendsen CN. (2015). Astrocytes show reduced support of motor neurons with aging that is accelerated in a rodent model of ALS. *Neurobiology of Aging* **36,** 1130-1139.

Demaria M, Ohtani N, Youssef Sameh A, Rodier F, Toussaint W, Mitchell James R, Laberge R-M, Vijg J, Van Steeg H, Dollé Martijn ET, Hoeijmakers Jan HJ, de Bruin A, Hara E & Campisi J. (2014). An essential role for senescent cells in optimal wound healing through secretion of PDGF-AA. *Developmental Cell* **31,** 722-733.

Dennison EM, Sayer AA & Cooper C. (2017). Epidemiology of sarcopenia and insight into possible therapeutic targets. *Nature Reviews Rheumatology* **13,** 340-347.

Diana V, Ottolina A, Botti F, Fumagalli E, Calcagno E, De Paola M, Cagnotto A, Invernici G, Parati E, Curti D & Mennini T. (2010). Neural precursor-derived astrocytes of wobbler mice induce apoptotic death of motor neurons through reduced glutamate uptake. *Experimental Neurology* **225,** 163-172.

Drachman DA. (1972). Age changes in the neuromuscular system. *Journal of Chronic Diseases* **27,** 427-429.

Edström E, Altun M, Bergman E, Johnson H, Kullberg S, Ramírez-León V & Ulfhake B. (2007). Factors contributing to neuromuscular impairment and sarcopenia during aging. *Physiology & Behavior* **92,** 129-135.

Evangelou K, Bramis* J, Peros I, Zacharatos P, Dasiou-Plakida D, Kalogeropoulos N, Asimacopoulos PJ, Kittas C, Marinos E & Gorgoulis VG. (2004). Electron microscopy

evidence that cytoplasmic localization of the p16INK4A "nuclear" cyclin-dependent kinase inhibitor (CKI) in tumor cells is specific and not an artifact. A study in non-small cell lung carcinomas. *Biotechnic & Histochemistry* **79,** 5-10.

Faulkner JR, Herrmann JE, Woo MJ, Tansey KE, Doan NB & Sofroniew MV. (2004). Reactive Astrocytes protect tissue and preserve function after spinal cord injury. *The Journal of Neuroscience* **24,** 2143-2155.

Funakoshi H, Belluardo N, Arenas E, Yamamoto Y, Casabona A, Persson H & Ibanez CF. (1995). Muscle-derived neurotrophin-4 as an activity-dependent trophic signal for adult motor neurons. *Science* **268,** 1495-1499.

García-Matas S, Gutierrez-Cuesta J, Coto-Montes A, Rubio-Acero R, Díez-Vives C, Camins A, Pallàs M, Sanfeliu C & Cristòfol R. (2008). Dysfunction of astrocytes in senescence-accelerated mice SAMP8 reduces their neuroprotective capacity. *Aging Cell* **7,** 630-640.

Goh J & Ladiges W. (2015). Voluntary wheel running in mice. *Current Protocols in Mouse Biology* **5,** 283-290.

Gould TW, Yonemura S, Oppenheim RW, Ohmori S & Enomoto H. (2008). The Neurotrophic Effects of glial cell line-derived neurotrophic factor on spinal motoneurons are restricted to fusimotor subtypes. *The Journal of Neuroscience* **28,** 2131-2146.

Gyorkos AM, McCullough MJ & Spitsbergen JM. (2014). Glial Cell Line-Derived Neurotrophic Factor (GDNF) expression and NMJ plasticity in skeletal muscle following endurance exercise. *Neuroscience* **257,** 111-118**.**

Hall BM, Balan V, Gleiberman AS, Strom E, Krasnov P, Virtuoso LP, Rydkina E, Vujcic S, Balan K, Gitlin I, Leonova K, Polinsky A, Chernova OB & Gudkov AV. (2016). Aging of mice is associated with p16(Ink4a)- and β-galactosidase-positive macrophage accumulation that can be induced in young mice by senescent cells. *Aging (Albany NY)* **8,** 1294-1311.

Hayflick L & Moorhead PS. (1961). The serial cultivation of human diploid cell strains. *Experimental Cell Research* **25,** 585-621.

Henderson CE, Phillips HS, Pollock RA, Davies AM, Lemeulle C, Armanini M, Simmons L, Moffet B, Vandlen RA, Simpson LC & et a. (1994). GDNF: a potent survival factor for motoneurons present in peripheral nerve and muscle. *Science* **266,** 1062-1064.

Hewitt G, Jurk D, Marques FDM, Correia-Melo C, Hardy T, Gackowska A, Anderson R, Taschuk M, Mann J & Passos JF. (2012). Telomeres are favoured targets of a persistent DNA damage response in ageing and stress-induced senescence. *Nature Communications* **3,** 708-717.

Huang WM, Gibson SJ, Facer P, Gu J & Polak JM. (1983). Improved section adhesion for immunocytochemistry using high molecular weight polymers of l-lysine as a slide coating. *Histochemistry* **77,** 275-279.

Ishihara A, Ohira Y, Tanaka M, Nishikawa W, Ishioka N, Higashibata A, Izumi R, Shimazu T & Ibata Y. (2001). Cell body size and succinate dehydrogenase activity of spinal motoneurons innervating the soleus muscle in mice, rats, and cats. *Neurochemical Research* **26,** 1301-1304.

Janssen I, Shepard DS, Katzmarzyk PT & Roubenoff R. (2004). The healthcare costs of sarcopenia in the United States. *Journal of the American Geriatrics Society* **52,** 80-85.

Khakh BS & Sofroniew MV. (2015). Diversity of astrocyte functions and phenotypes in neural circuits. *Nature Neuroscience* **18,** 942-952.

Kim K, Shin M-S, Cho H-S & Kim Y-P. (2014). Effects of endurance exercise on expressions of glial fibrillary acidic protein and myelin basic protein in developing rats with maternal infection-induced cerebral palsy. *Journal of Exercise Rehabilitation* **10,** 9-14.

Krtolica A & Campisi J. (2002). Cancer and aging: a model for the cancer promoting effects of the aging stroma. *The International Journal of Biochemistry & Cell Biology* **34,** 1401-1414.

Kuilman T, Michaloglou C, Vredeveld LCW, Douma S, van Doorn R, Desmet CJ, Aarden LA, Mooi WJ & Peeper DS. (2008). Oncogene-induced senescence relayed by an interleukin-dependent inflammatory network. *Cell* **133,** 1019-1031.

Latimer CS, Searcy JL, Bridges MT, Brewer LD, Popović J, Blalock EM, Landfield PW, Thibault O & Porter NM. (2011). Reversal of glial and neurovascular markers of unhealthy brain aging by exercise in middle-aged female mice. *PLoS ONE* **6**, e26812,

Lexell J, Taylor CC & Sjöström M. (1988). What is the cause of the ageing atrophy?: Total number, size and proportion of different fiber types studied in whole vastus lateralis muscle from 15- to 83-year-old men. *Journal of the Neurological Sciences* **84,** 275-294.

Li W, Brakefield D, Pan Y, Hunter D, Myckatyn TM & Parsadanian A. (2007). Muscle-derived but not centrally derived transgene GDNF is neuroprotective in G93A-SOD1 mouse model of ALS. *Experimental Neurology* **203,** 457-471.

Lin LF, Doherty DH, Lile JD, Bektesh S & Collins F. (1993). GDNF: a glial cell line-derived neurotrophic factor for midbrain dopaminergic neurons. *Science* **260,** 1130-1132.

Liu X, Wu Z, Hayashi Y & Nakanishi H. (2012). Age-dependent neuroinflammatory responses and deficits in long-term potentiation in the hippocampus during systemic inflammation. *Neuroscience* **216,** 133-142.

Maragakis NJ & Rothstein JD. (2006). Mechanisms of disease: astrocytes in neurodegenerative disease. *Nature Clinical Practice Neurology* **2,** 679-689.

Matjusaitis M, Chin G, Sarnoski EA & Stolzing A. (2016). Biomarkers to identify and isolate senescent cells. *Ageing Research Reviews* **29,** 1-12.

McCullough MJ, Gyorkos AM & Spitsbergen John M. (2013). Short-term exercise increases GDNF protein levels in spinal cord of young and old rats. *Neuroscience* **240,** 258-268.

Mombach JCM, Vendrusculo B & Bugs CA. (2015). A model for p38MAPK-induced astrocyte senescence. *PLoS ONE **10,*** e0125217.

Nakagawa T & Schwartz JP. (2004). Gene expression patterns in in vivo normal adult astrocytes compared with cultured neonatal and normal adult astrocytes. *Neurochemistry International* **45,** 203-242.

Narita M, Nuñez S, Heard E, Narita M, Lin AW, Hearn SA, Spector DL, Hannon GJ & Lowe SW. (2003). Rb-mediated heterochromatin formation and silencing of E2F target genes during cellular senescence. *Cell* **113,** 703-716.

Ohanna M, Giuliano S, Bonet C, Imbert V, Hofman V, Zangari J, Bille K, Robert C, Bressac-de Paillerets B, Hofman P, Rocchi S, Peyron J-F, Lacour J-P, Ballotti R & Bertolotto C. (2011). Senescent cells develop a PARP-1 and nuclear factor-κB-associated secretome (PNAS). *Genes & Development* **25,** 1245-1261.

Olivieri F, Albertini MC, Orciani M, Ceka A, Cricca M, Procopio AD & Bonafè M. (2015). DNA damage response (DDR) and senescence: shuttled inflamma-miRNAs on the stage of inflamm-aging. *Oncotarget* **6,** 35509-35521.

Ortega-de San Luis C & Pascual A. (2016). Simultaneous detection of both GDNF and GFRα1 expression patterns in the mouse central nervous system. *Frontiers in Neuroanatomy* **10,** 73-81**.**

Park J-S & Höke A. (2014). Treadmill exercise induced functional recovery after peripheral nerve repair is associated with increased levels of neurotrophic factors. *PLoS ONE* **9,** e90245.

Pirooznia Sheila K, Dawson Valina L & Dawson Ted M. (2014). Motor neuron death in ALS: programmed by astrocytes? *Neuron* **81,** 961-963.

Ranganathan S & Bowser R. (2010). p53 and cell cycle proteins participate in spinal motor neuron cell death in ALS. *The Open Pathology Journal* **4,** 11-22.

Rodríguez-Arellano JJ, Parpura V, Zorec R & Verkhratsky A. (2016). Astrocytes in physiological aging and Alzheimer's disease. *Neuroscience* **323,** 170-182.

Rowan SL, Rygiel K, Purves-Smith FM, Solbak NM, Turnbull DM & Hepple RT. (2012). Denervation causes fiber atrophy and myosin heavy chain co-expression in senescent skeletal muscle. *PLoS ONE* **7**, e29028

Sacheck JM, Hyatt J-PK, Raffaello A, Jagoe RT, Roy RR, Edgerton VR, Lecker SH & Goldberg AL. (2007). Rapid disuse and denervation atrophy involve transcriptional changes similar to those of muscle wasting during systemic diseases. *The FASEB Journal* **21,** 140-155.

Salminen A, Kauppinen A & Kaarniranta K. (2012). Emerging role of NF-κB signaling in the induction of senescence-associated secretory phenotype (SASP). *Cellular Signalling* **24,** 835-845.

Salminen A, Ojala J, Kaarniranta K, Haapasalo A, Hiltunen M & Soininen H. (2011). Astrocytes in the aging brain express characteristics of senescence-associated secretory phenotype. *European Journal of Neuroscience* **34,** 3-11.

Sasaki M, Kajiya H, Ozeki S, Okabe K & Ikebe T. (2014). Reactive oxygen species promotes cellular senescence in normal human epidermal keratinocytes through epigenetic regulation of p16INK4a. *Biochemical and Biophysical Research Communications* **452,** 622-628.

Saur L, Baptista PPA, de Senna PN, Paim MF, Nascimento Pd, Ilha J, Bagatini PB, Achaval M & Xavier LL. (2014). Physical exercise increases GFAP expression and induces morphological changes in hippocampal astrocytes. *Brain Structure and Function* **219,** 293-302.

Schafer MJ, White TA, Evans G, Tonne JM, Verzosa GC, Stout MB, Mazula DL, Palmer AK, Baker DJ, Jensen MD, Torbenson MS, Miller JD, Ikeda Y, Tchkonia T, van Deursen JM, Kirkland JL & LeBrasseur NK. (2016). Exercise Prevents Diet-induced Cellular Senescence in Adipose Tissue. *Diabetes* ***65*****(6)**, 1606-1615.

Schindelin J, Arganda-Carreras I, Frise E, Kaynig V, Longair M, Pietzsch T, Preibisch S, Rueden C, Saalfeld S, Schmid B, Tinevez J, White D, Hartenstein V, Eliceiri K, Tomancak P & Cardona A (2012). Fiji: an open-source platform for biological-image analysis. *Nature Methods* **9**, 676-682.

Serrano M, Hannon GJ & Beach D. (1993). A new regulatory motif in cell-cycle control causing specific inhibition of cyclin D/CDK4. *Nature* **366,** 704-707.

Shapiro GI, Edwards CD, Kobzik L, Godleski J, Richards W, Sugarbaker DJ & Rollins BJ. (1995). Reciprocal Rb inactivation and p16INK4 expression in primary lung cancers and cell lines. *Cancer Research* **55,** 505-509.

Sharpless NE & Sherr CJ. (2015). Forging a signature of in vivo senescence. *Nature Reviews Cancer* **15,** 397-408.

Soares JP, Silva AM, Oliveira MM, Peixoto F, Gaivão I & Mota MP. (2015). Effects of combined physical exercise training on DNA damage and repair capacity: role of oxidative stress changes. *Age* **37,** 61-73.

Sofroniew MV. (2009). Molecular dissection of reactive astrogliosis and glial scar formation. *Trends in Neurosciences* **32,** 638-647.

Sofroniew MV & Vinters HV. (2010). Astrocytes: biology and pathology. *Acta Neuropathologica* **119,** 7-35.

Souza DG, Bellaver B, Raupp GS, Souza DO & Quincozes-Santos A. (2015). Astrocytes from adult Wistar rats aged in vitro show changes in glial functions. *Neurochemistry International* **90,** 93-97.

Tanimoto Y, Watanabe M, Sun W, Sugiura Y, Hayashida I, Kusabiraki T & Tamaki J. (2014). Sarcopenia and falls in community-dwelling elderly subjects in Japan: Defining

sarcopenia according to criteria of the European working group on sarcopenia in older people. *Archives of Gerontology and Geriatrics* **59,** 295-299.

Tomlinson BE & Irving D. (1977). The numbers of limb motor neurons in the human lumbosacral cord throughout life. *Journal of the Neurological Sciences* **34,** 213-219.

van Deursen JM. (2014). The role of senescent cells in ageing. *Nature* **509,** 439-446.

van Praag H, Christie BR, Sejnowski TJ & Gage FH. (1999). Running enhances neurogenesis, learning, and long-term potentiation in mice. *Proceedings of the National Academy of Sciences of the United States of America* **96,** 13427-13431.

Walters HE, Deneka-Hannemann S & Cox LS. (2016). Reversal of phenotypes of cellular senescence by pan-mTOR inhibition. *Aging* **8,** 231-244.

Ward P, Blanchard R, Bolivar V, Brown M, Chang F, Herman J, Hubrecht R, Lawson D, Maier S, Morton D, Niemi S, Novak M & Zawistowski S (2008.) *Recognition and Alleviation of Distress in Laboratory Animals*. The National Academies Press, Washingon.

Waters DL, Baumgartner RN, Garry PJ & Vellas B. (2010). Advantages of dietary, exercise-related, and therapeutic interventions to prevent and treat sarcopenia in adult patients: an update. *Clinical Interventions in Aging* **5,** 259-270.

Werner C, Fürster T, Widmann T, Pöss J, Roggia C, Hanhoun M, Scharhag J, Büchner N, Meyer T, Kindermann W, Haendeler J, Böhm M & Laufs U. (2009). Physical exercise prevents cellular senescence in circulating leukocytes and in the vessel wall. *Circulation* **120,** 2438-2447.

Witkiewicz AK, Knudsen KE, Dicker AP & Knudsen ES. (2011). The meaning of p16(ink4a) expression in tumors: Functional significance, clinical associations and future developments. *Cell Cycle* **10,** 2497-2503.

Zhao Z, Alam S, Oppenheim RW, Prevette DM, Evenson A & Parsadanian A. (2004). Overexpression of glial cell line-derived neurotrophic factor in the CNS rescues motoneurons from programmed cell death and promotes their long-term survival following axotomy. *Experimental Neurology* **190,** 356-372.

Zhou C, Feng Z & Ko C-P. (2016). Defects in motoneuron–astrocyte interactions in Spinal Muscular Atrophy. *The Journal of Neuroscience* **36,** 2543-2553.

Appendices

8 Appendices

Appendix A: Recipes for immunohistochemistry

Table 4: **20X Tris-Buffered Saline (TBS)***

Component	***Amount***
Tris Xtrapure	1220g
NaCl	1800g
Hydrochloric acid (37%)	pH 7.4
Distilled water	10L

**To make 1L of 1x, add 50mL of 20x to 950L distilled water.*

**To make 1L of 2x, add 100mL of 20x to 900mL distilled water.*

Table 5: Immunodiluent

Component	***Amount***
BSA (1%)	100mL
TritonX-100 (0.1%)	10mL
Tween20 (0.3%)	30mL
Distilled water	860mL
pH balanced	7.3

Table 6: Sodium citrate buffer (pH 6)

Component	***Amount***
Tri-sodium citrate	2.94g
Distilled water	1L
Twen20	0.5mL
Hydrochloric acid (37%)	pH 6

Table 7: Tris buffer for HIER

Component	***Amount***
Tris Xtrapure	1.3g
Distilled water	1L
Tween20	0.5mL
NaOH	pH 10

Table 8: 4',6-diamidino-2-phelylindole (DAPI)/Glycerol mounting medium

Component	***Amount***
4',6-diamidino-2-phelylindole (DAPI)	5ul
1xTBS	1mL
Glycerol	9mL

Table 9: Glycine (0.1M)

Component	***Amount***
Glycine	1.514
Distilled water	200mL

Table 10: Paraformaldehyde fixative solution (1%)

Component	***Amount***
Paraformaldehyde	1g
NaH_2PO_4 (0.2M)	11mL
Na_2HPO_4 (0.2M)	39mL
Distilled water	50mL

Table 11: Sucrose (20%) for cryoprotection

Component	***Amount***
Sucrose	20g
Distilled water	100mL

Table 12: GFAP optimization solution

Component	***Amount***
BSA	0.5mL
Glycine	22.71g
TritonX-100	0.5mL
Tween-20	0.5mL
Sodium Dodecyl Sulphate	0.3g
Tris Xtrapure (1x)	1L

Appendix B: Western blot recipes

Table 13: 10x TBST*

**To make 1L of 1x, add 100mL of 10x to 900mL of distilled water.*

Component	***Amount***
Tris	60.57g
NaCl	87.66g
Tween20 (0.5%)	5mL
pH balanced	7.6

Table 14: 10x Running buffer*

Component	***Amount***
Glycine (1.92M)	144g
Tris (0.25M)	30.2g
Sodium dodecyl sulfate (SDS) (1%)	10g

**To make 1L of 1x, add 100mL of 10x running buffer to 900mL distilled water.*

Table 15: Transfer buffer

Component	***Amount***
Glycine (1.92M)	14.4g
Tris (0.25M)	3.02g
Distilled water	800mL
Methanol	200mL
10% SDS	1mL

Table 16: 5x Sample buffer

Component	*Amount*
Lower tris	2mL
Glycerol	5mL
SDS (10%)	1g
Dithiothreitol (DTT) (0.2M)	0.31g
10% SDS	1mL

Table 17: Loading samples (20µg protein)

Sample	*For 20µg protein (µl)*	*Sample buffer (µl)*	*Distilled water (µl)*
1	3.4	4	12.6
2	4.5	4	11.5
3	5.1	4	10.9
4	6.0	4	10.0
5	5.3	4	10.7
6	3.8	4	12.2
7	5.7	4	10.3
8	4.5	4	11.5
9	3.8	4	12.2
10	4.5	4	11.5

Appendix C: Surgeries

Transcardial perfusion

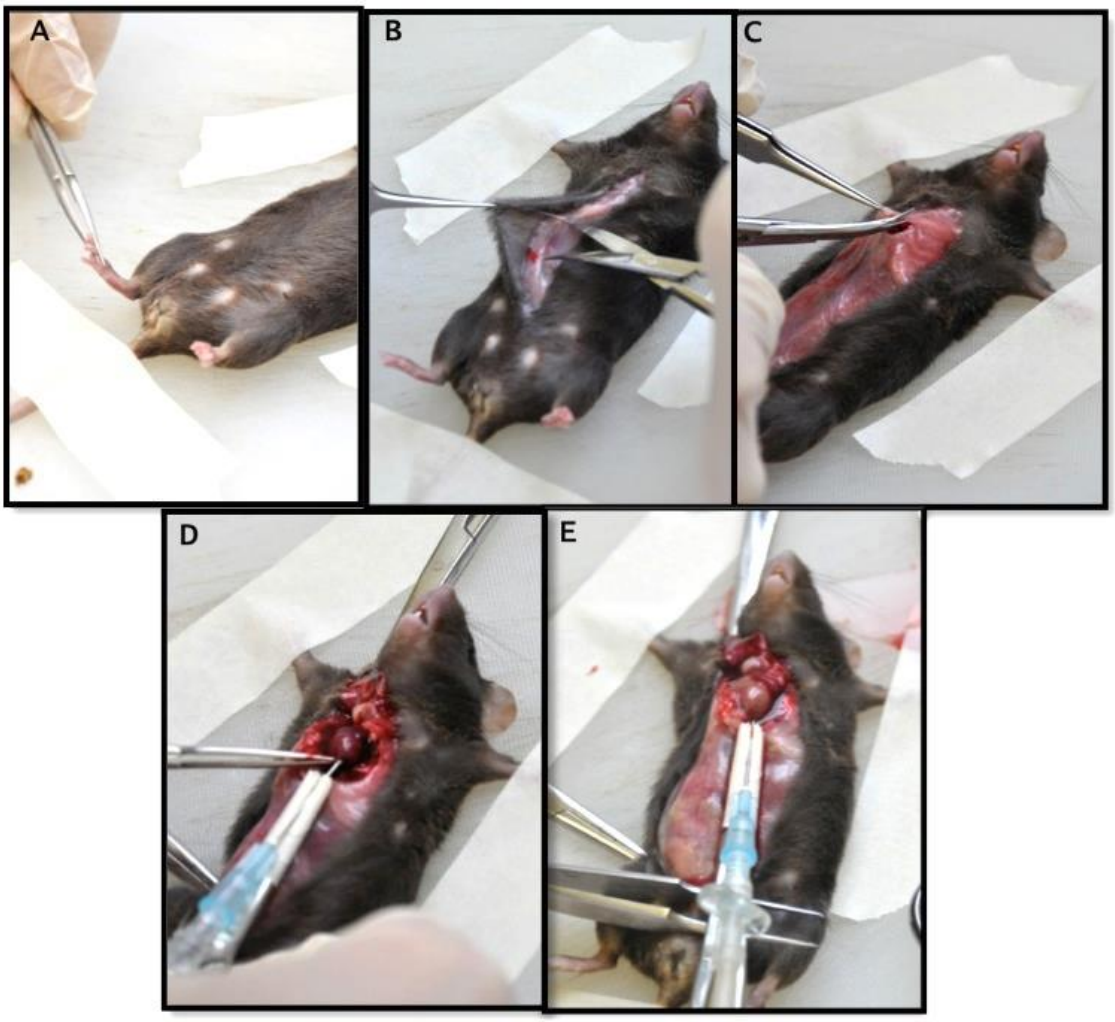

Figure 33: Transcardial perfusion

A) Following anaesthetisation, toes were pinched with forceps to ensure deep anaesthesia was achieved. B) Skin and connective tissue bluntly dissected to expose the ribcage. C) The ribcage was cut twice, once toward each axilla. D) The ribcage was deflected to expose the heart and a needle attached to a peristaltic pump was inserted into the left ventricle. E) The right atrium was cut to allow blood and perfusion solution to be expelled.

Spinal cord removal

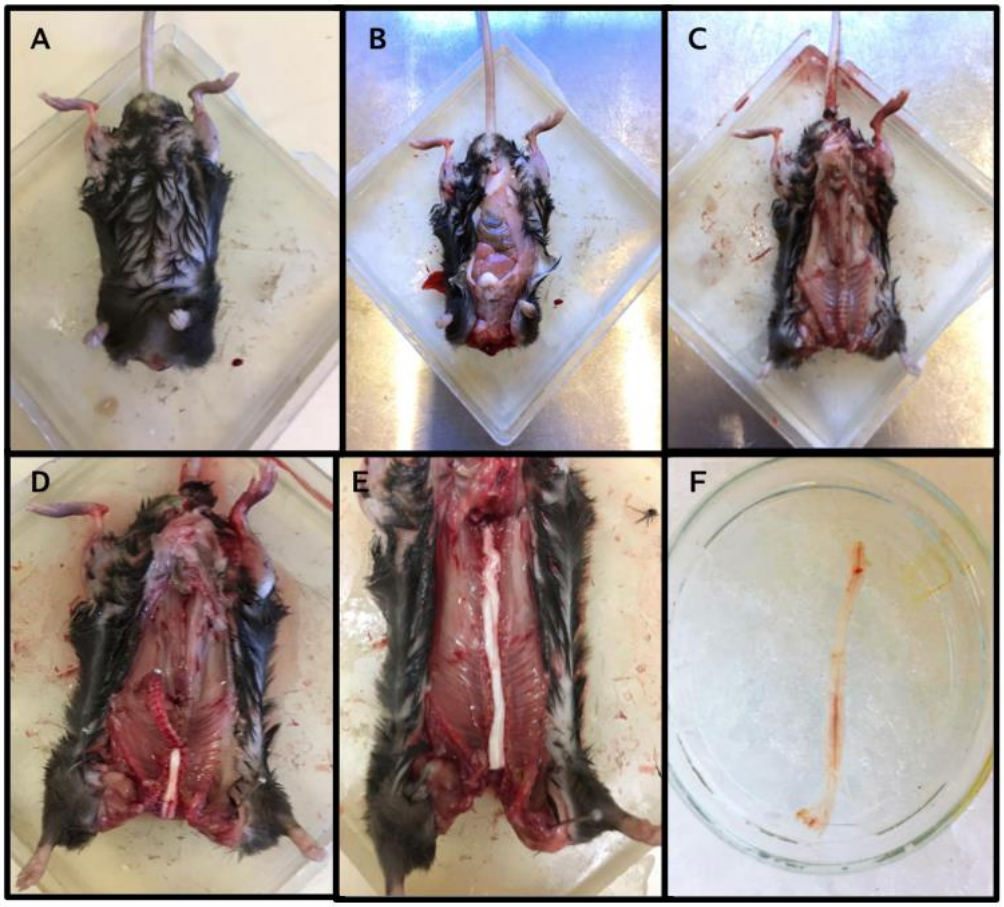

Figure 34: Spinal cord removal

A) The mouse was orientated with the legs facing away. B) The skin and connective tissue was bluntly dissected to expose the underlying abdominal cavity. C) The visceral organs were removed. D) Incisions were made through the ventral spinous processes to expose the central canal and allow excision of the cord in a rostral to caudal direction. E) The cord was exposed until the cauda equina was reached. F) The removed cord was placed in 1xTBS on ice.

Appendix D: Semi-Quantitative Immunohistochemistry (SQI) validation

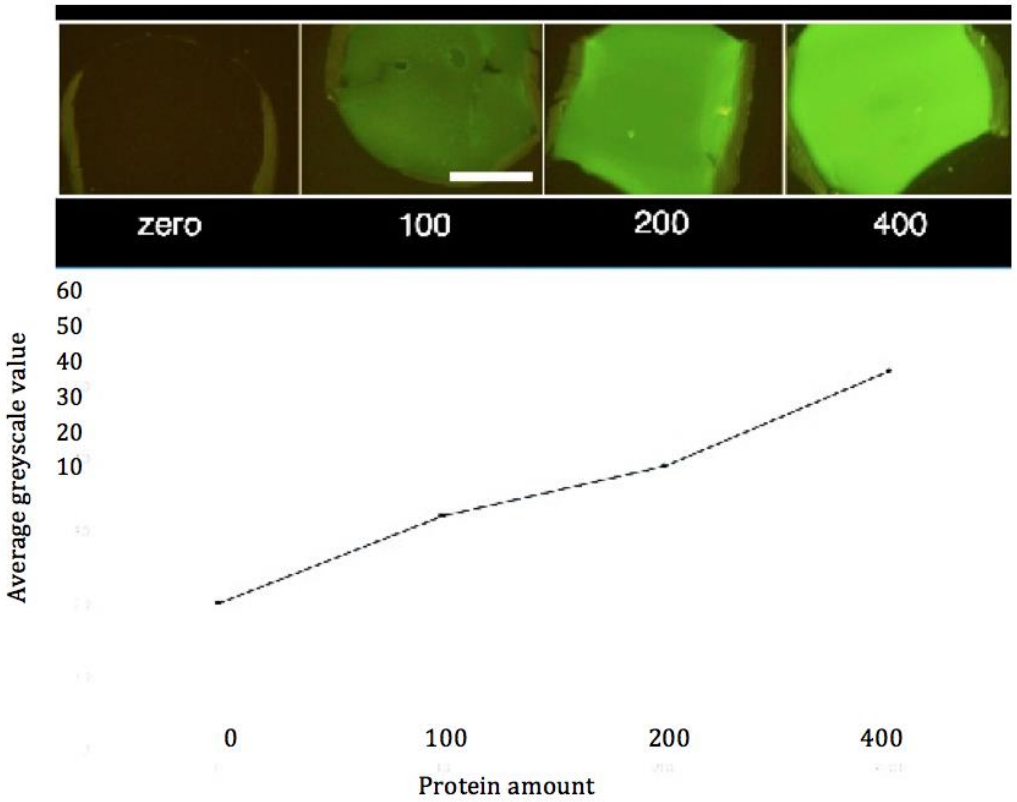

Figure 35: Linear relationship between protein amount and greyscale value.
A reference standard was generated using agarose with known amounts of protein suspended within. The agarose was treated with antibodies and imaged using the fluorescence microscope and average greyscale value was measured.

Appendix E: Western blot optimization

Antibody diluent *Blocking solution*